Recent advances in radiation hardened fiber-based technologies for space applications

1

Recent Advances on Radiation-Hardened Fiber-based Technologies for Space Applications

Sylvain Girard[1,*], Adriana Morana[1], Ayoub Ladaci[1,2,3], Thierry Robin[2], Luciano Mescia[3], Jean-Jacques Bonnefois[4], Mathieu Boutillier[5], Julien Mekki[5], Armelle Paveau[6], Benoît Cadier[2], Emmanuel Marin[1], Youcef Ouerdane[1] and Aziz Boukenter[1]

[1.] Univ Lyon, UJM St Etienne, CNRS, IOGS, Laboratoire Hubert Curien, UMR5516, F-42000 St Etienne, France.
[2.] iXBlue Photonics, Rue Paul Sabatier, F-22300, Lannion, France.
[3.] Polytechnic University of Bari, Via E. Orabona, 4, 70125 Bari, Italy.
[4.] iXblue, 34 Rue de la Croix de Fer, F-78100 Saint-Germain-en-Laye, France.
[5.] CNES, 18 Avenue Edouard Belin, F-31400 Toulouse, France.
[6] Airbus Defense and Space, Toulouse, France.

Outline

2

* Corresponding author: Sylvain Girard, sylvain.girard@univ-st-etienne.fr : Phone: +33 (0)477 915 812

3

***Abstract*:** In this topical review, the recent progresses about radiation-hardened fiber-based technologies are detailed focusing examples on space applications. In the first part of the review, we introduce the operational principles of the various fiber-based technologies considered for use in radiation environments: passive optical fibers for data links, diagnostics; active optical fibers for amplifiers and laser sources as well as the different classes of point and distributed fiber sensors: gyroscopes, Bragg gratings, Rayleigh, Raman or Brillouin-based distributed sensors. Second, we describe the state-of-the-art regarding our knowledge of the radiation effects on the performances of these devices, from the microscopic effects observed in the amorphous silica glass used to design the fiber core and cladding to the macroscopic responses of the fiber-based devices and systems. Third, we present the recent advances regarding the hardening (improvement of the radiation tolerance) of these technologies acting at the material, device or system levels. From this review, the potential of the fiber-based technologies for operation in radiation environments is demonstrated and the future challenges to be overcome in the next years is presented.

* Corresponding author: Sylvain Girard, sylvain.girard@univ-st-etienne.fr : Phone: +33 (0)477 915 812

4

GLOSSARY

AOCS	Altitude and orbit control	**MMF**	Multimode Optical Fiber
ASE	Amplified Spontaneous Emission	**MOF**	Microstructured Optical Fiber
ASPICS	Application Specific Photonic Integrated Circuits	**NASA**	National Aeronautics and Space Administration
BPF	Band Pass Filter	**NBOHC**	Non Bridging-Oxygen Hole Center
BOTDA	Brillouin Optical Time Domain Analyzer	**NIF**	National Ignition Facility
BOTDR	Brillouin OTDR	**NSSDC**	NASA Space Science Data Coordinated Archive
CEA	Commissariat à l'énergie atomique et aux énergies alternatives	**OFDR**	Optical Frequency Domain Reflectometry
CERN	European Organization for Nuclear Research	**OFS**	Optical Fiber Sensor
CL	Cathodoluminescence	**OTDR**	Optical Time Domain Reflectometry
CML	Confocal Microscopy of Luminescence	**PBGF**	Photonic BandGap Fibers
CNES	Centre National d'Etudes Spatiales	**PbP**	Point-by-Point
CW	Continuous Wave	**PCE**	Power Conversion Efficiency
DE	Double-Ended	**PhM**	Phase Mask
DFB	distributed feedback laser	**PIN**	Positive Intrinsic Negative
DOFS	Distributed OFS	**PMF**	Polarization-Maintaining Optical Fiber
EDRS	European Data Relay System	**PM-LMA**	Polarization-Maintaining Large Mode Area
EDFA	Erbium Doped Fiber Amplifier	**PSC**	Pure Silica Core
EDFS	Erbium Doped Fiber Source	**RDTS**	Raman Distributed Temperature Sensor
EDX	Energy Dispersive X-ray	**REDFA**	Rare-Earth Doped Fiber Amplifier
EPR	Electron Paramagnetic Resonance	**RF**	Radio Frequency
ESA	European Space Agency	**RIA**	Radiation-Induced Attenuation
EYDFA	Erbium Ytterbium Doped Fiber Amplifier	**RI-BFS**	Radiation-induced Brillouin Frequency Shift
EYDFS	Erbium Ytterbium Doped Fiber Source	**RI-BWS**	Radiation-induced Bragg Wavelength Shift
FBG	Fiber Bragg Grating	**RIE**	Radiation-Induced Emission
FOG	Fiber Optic Gyroscope	**RIP**	Refractive Index Profile
FUT	Fiber under Test	**RIRIC**	Radiation-Induced Refractive Index Change
GEO	Geostationary Earth Orbit	**RT**	Room Temperature
GLPC	Germanium Lone Pair Center	**SAA**	South Atlantic Anomaly
GCR	Galactic Cosmic Rays	**SBS**	Stimulated Brillouin Scattering
GSFC	Goddard Space Flight Center	**SE**	Single-Ended
IR	Infrared	**SEE**	Single Event Effect
ISS	International Space Station	**SMF**	Single-mode Optical Fiber
LADEE	Lunar Atmosphere and Dust Environment Explorer	**SMOS**	Soil Moisture and Ocean Salinity
LED	Light Emitting Diode	**SNR**	Signal to Noise Ratio
LEO	Low Earth Orbit	**STE**	Self-trapped Excitons
LHC	Large Hadron Collidor	**STH**	Self-Trapped Holes
LIDAR	Light Detection and Ranging	**TID**	Total Ionizing Dose
LLCD	Lunar Laser Communications Demonstration	**TIR**	Total Internal Reflection
LMJ	Laser Mégajoule	**TNID**	Total Non-Ionizing Dose
MCVD	Modified Chemical Vapor Deposition	**UV**	Ultraviolet
MEO	Medium Earth Orbit	**WDM**	Wavelength Division Multiplexed
MIRAS	Microwave Imaging Radiometer with Aperture Synthesis		

* Corresponding author: Sylvain Girard, sylvain.girard@univ-st-etienne.fr : Phone: +33 (0)477 915 812

I. Introduction

There is a growing interest in studying the potential of fiber-based technologies for integration in harsh or severe environments, in particular those associated with radiation constraints. The considered environments can be either natural such as space [1] or man-made such as those associated with fusion-related facilities [2,3,4], nuclear power plants [5] or high energy physics facilities [6]. First studies, from seventies [7,8] were mainly devoted to the characterization of the transmission degradation of optical fibers under irradiation as this effect was limiting their use for data transfer. The origins of this degradation were investigated and radiation-induced attenuation (RIA) phenomenon caused by the generation of optically-active point defects in the silica-based cores and cladding of optical fibers [9,10] was identified. In this topical review paper, an overview of the main parameters influencing the RIA levels and kinetics is given, explaining the observed differences in the radiation responses of the various classes of optical fibers and showing how, by appropriate choices during the fiber design and manufacturing, it has been possible to conceive architectures of radiation tolerant or radiation-hardened optical fibers for almost all targeted applications. Recent results obtained on rare-earth doped optical fibers by coupling theoretical and experimental approaches are detailed as these active fibers play a key role in the radiation response of fiber optic gyroscopes and high power fiber sources that are used and will be more widely exploited for inter and intra-satellite communications in the near future. More recently, radiation vulnerability and hardening studies have been conducted to evaluate the feasibility to use new generations of powerful fiber-based sensors in the various harsh environments. These sensors are either point (*FBGs*) or distributed (*Raman, Rayleigh or Brillouin*) allowing to monitor a wide range of parameters such as temperature, strain, liquid level or dose. An overview of the recently acquired knowledge is given, highlighting the remaining scientific challenges and the increasing impacts of two other radiation-induced phenomena: the radiation-induced emission (RIE) and the radiation-induced refractive-index changes (RIRIC).

A variety of radiation environments exists. The principal ones of interest are listed in Table 1 whereas the main parameters used to define such a harsh environment are listed hereafter:

- *Nature of particles:* depending on the impacting particles, the relative contributions of the ionization and displacement damages processes in silica differ [11,12,9] and so the radiation response of the silica-based optical fibers [13]. Usually for optical fiber-based technologies, ionization processes govern their radiation response [14,15]. However, for environments associated with very high neutron fluences (> 10^{16} n/cm²) or heavy ions, a specific contribution of displacement damages clearly appears in the optical and structural signatures of silica-based fibers and glasses [16,17,18] .

6

- **Total Ionizing Dose (TID):** TID is expressed in Gray (Gy), the dose corresponds to the quantity of energy (1 Gy=1 J/kg) deposited into the considered material. In our case and throughout this review, Gy(SiO$_2$) are then used. An older unit is still widely used by a large fraction of the radiation effect community and especially space engineers: the rad: 1 Gy = 100 rad.

- **Dose rate:** the dose rate corresponds to the speed of dose deposition within the material. It is then expressed in Gy(SiO$_2$)/s for optical fibers. The dose rate strongly varies between the studied harsh environments from 10^{-5} to 10^{-3} Gy/h in the case of space missions [19] up to more than a GGy/h during an ignition shot at a megajoule class laser facility [20].

- **Temperature:** for a number of applications, radiations are not the sole constraint to consider when designing the fiber-based optical system. The temperature of the irradiation will strongly affect the device radiation response too. Temperature ranges from very low temperatures for space missions to high temperatures, especially for the future generation of nuclear power plants for which sensors able to operate at temperatures as high as 800°C are needed for the reactor core monitoring.

- **Other constraints:** many other constraints can also be present. As an example, for the nuclear waste storage facilities, the wastes will release hydrogen in atmosphere [21]. This gas presence has to be taken into account when evaluating the performances of fibers or fiber sensors as hydrogen strongly interacts with the silica-based fibers [22]. Another example is the possible operation in vacuum, water or other liquids instead of air. In case of multiple constraints, the vulnerability study has to be done considering these mixed constraints simultaneously as the interactions between these various parameters are generally too complex to be yet modeled or predicted.

* Corresponding author: Sylvain Girard, sylvain.girard@univ-st-etienne.fr : Phone: +33 (0)477 915 812

Table 1. Main characteristics of the radiation environments and targeted applications for fiber-based systems

Environment of interest	Nature of particles (direct or secondary)	Dose range Gy(SiO$_2$)	Dose rate range	Temperature range	Main applications for fibers	Refs (*and refs herein*)
Space	X-rays, γ-rays, Protons, heavy ions, electrons	Up to 10 kGy (usually < 1 kGy)	10^{-5} to 10^{-3} Gy/h	-200°C to 300°C	Data transfer, fiber lasers, gyroscopes, fiber sensing	[19]
Large Hadron Collider (LHC)	neutral hadrons, photons, electrons and muon	Up to 100 kGy	Up to 0.1 Gy/h	Room Temperature (RT)	Data transfer, distributed sensing (dose, temperature), point sensing (humidity)	[23]
ITER	γ-rays, neutrons	Up to 10MGy, up to 10^{18} n/cm²	1kGy/h and 10^{12}-10^{14} n/(cm².s)	From RT to 400°C	Data transfer, plasma diagnostics, sensing	[24]
LMJ, NIF	γ-rays, X-rays, 14 MeV neutrons	<1kGy	>MGy/s	RT	Data transfer Laser & plasma diagnostics	[20]
Nuclear reactor core	Neutrons, γ-rays	GGy levels up to 10^{20} n/cm²	Up to 10^{15} n/(cm².s)	From RT to up to 800°C	Fiber sensing (temperature)	[25]
Nuclear industries	γ-rays	<10 MGy dose levels	Up to 10kGy/h	From RT to 400°C	Sensing (temperature, liquid level …)	[26]
Nuclear Waste Storage	γ-rays	Up to 10MGy	Up to 10 Gy/h	From RT to 90°C	Data transfer, distributed sensing	[21]
Medicine	X-rays, protons	10mGy to 50Gy	<1Gy/s	RT	Radiotherapy, proton-therapy, beam monitoring, dosimetry	[27]

Describing all these environments is outside the scope of this article. In the next paragraphs, we first remind the advantages of using fiber-based technologies under irradiation and then briefly review their possible space applications as well as the radiation constraints associated to such programs.

I.1. Advantages of fiber-based technologies in such environments

Silica-based optical fibers present a lot of advantages for operation in these harsh environments. Of course, the well-known advantages of optical fibers for telecommunications are also interesting for applications having to operate under irradiation: their low attenuation level, their high bandwidth,

* Corresponding author: Sylvain Girard, sylvain.girard@univ-st-etienne.fr : Phone: +33 (0)477 915 812

8

their multiplexing capability... [28]. In addition to these advantages, others are more specific to an operation in harsh environments. First, optical fibers are quasi-immune to most of the electromagnetic perturbations as their cores and claddings are made of pure- or doped silica glass: a dielectric material. This advantage is crucial for data links or diagnostics operating in megajoule class lasers as during the ignition experiments very high parasitic currents will be generated in coaxial cables [20, 29]. Second, the fiber-based devices are usually lightweight, reliable, crucial advantage for integration into a spacecraft or to reduce the amount of nuclear wastes into nuclear facilities. Third, with appropriate coatings, the optical fibers can resist to high temperatures [30]: Telecom-grade acrylate-coated optical fibers can operate up to 80°C, up to 180 °C with high-temperature acrylate coating, up to 200°C with Ormocer, up to 300°C with polyimide coating. It is also possible to use metal-based coatings, extending the maximal temperature of operation up to 400°C (aluminum, copper) and 800°C for gold-coated fibers.

I.2. Space environment

Spacecrafts are exposed to a complex and aggressive environment having characteristics depending on the targeted mission profile. Several review papers and short-courses were devoted to the description of the space associated constraints [1,31] such as space debris, meteoroids, strong thermal variations, vacuum, energetic particles. Spacecraft and materials, devices and systems within the spacecrafts have to survive to those constraints without degradation of their performances.

As far as missions in Earth's orbits are considered, three different environment profiles are distinguished:

- **Low Earth Orbit (LEO):** altitude below 2 000 km, with polar inclination. LEO is the standard orbit for Earth observation satellites.
- **Medium Earth Orbit (MEO):** altitude between 2 000 km and ~36 000 km at which most of the navigation systems satellites are located.
- **Geostationary Earth Orbit (GEO):** altitude of ~36 000 km, this orbit is mainly used for Telecommunication satellites.

The energetic particles affecting the fiber-based technologies are mainly originating from three sources: galactic and extragalactic cosmic rays (GCR), solar energetic particles and trapped particles. Relative contributions of these different sources to the material or device degradations depend both on the mission orbit characteristics and on the degradation basic mechanisms associated to the tested device technology. The fiber-based devices are mostly degraded through ionizing processes, and

* Corresponding author: Sylvain Girard, sylvain.girard@univ-st-etienne.fr : Phone: +33 (0)477 915 812

therefore, the role of solar particles and trapped particles such as electrons and protons, has been shown to be preponderant.

Indeed GCR, due to their high atomic number and high energy can strongly influence the amplitudes of Single Event Effects (SEE) in microelectronics, but will have a negligible impact on fiber-based systems as their associated flux of ~4 particles/cm²s on average remains low, its intensity being anti-correlated to the solar activity.

Solar energetic particles, originating either from solar flares or coronal mass ejections, as well as trapped particles may damage fiber-based systems. Both events generate protons, electrons, neutrons, γ-rays, X-rays, and heavy ions. Those events are characterized by high fluxes of particles over a short period of time. Event frequency is influenced by the solar activity cycle, with a period of roughly 11 years. Energies of these particles are variable, but are anyway softer than GCR ones.

The Earth's magnetic field keeps trapped electrons and protons around the Earth with the population distributions illustrated in Fig.1 [32].
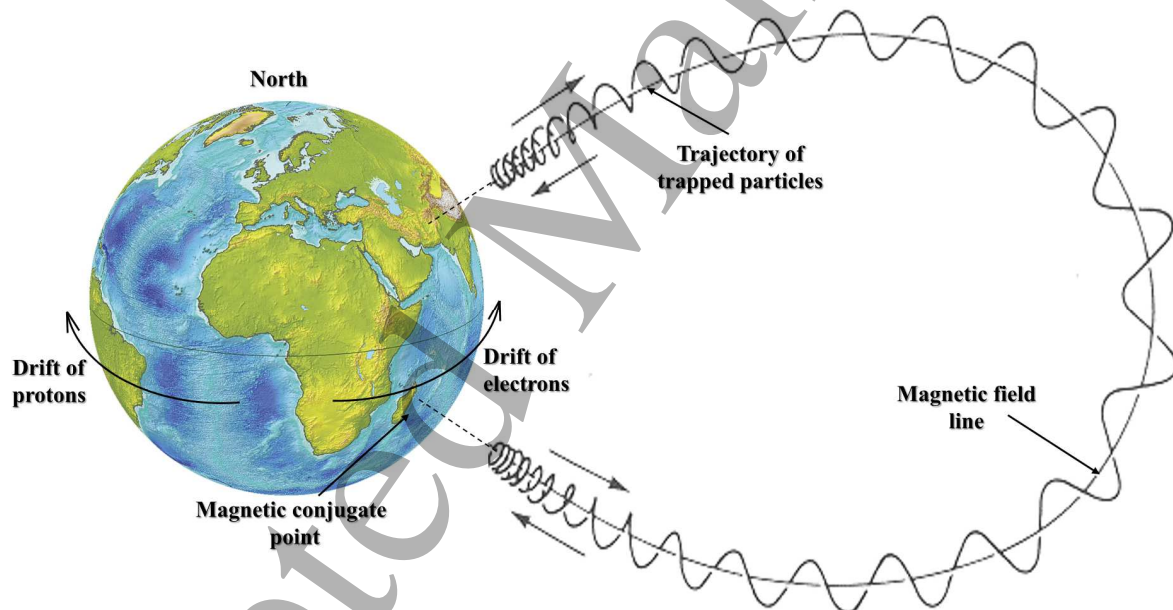
Figure 1: Near-Earth region magnetic field. Electrons and protons populations are trapped in a gyration, bounce and drift movement. More details about the space environment can be found in [32]

The particle movement follows the magnetic lines and is made of various components: drift, gyration and bounce. Protons belt mainly concerns LEO orbits. In this region, main radiation effects are therefore TID and displacement damages. The proton spectrum extends up energies of 500 MeV (larger energies are found in the core of radiation belts), while for MEO and GEO, proton energies remain below 10 MeV and a few MeV, respectively. Higher fluxes of trapped protons are localized at geographic zones associated with weaker magnetic fields: both Earth's poles and at the South Atlantic Anomaly noted SAA. SAA region is associated with a lower magnetic flux due to a tilt by 11° of magnetic

* Corresponding author: Sylvain Girard, sylvain.girard@univ-st-etienne.fr : Phone: +33 (0)477 915 812

10

field with regards to Earth rotation axis, and offset by 500 km towards North Pacific. MEO and GEO orbits are dominated by electron belt making the materials and devices especially exposed to the risks related to ionizing dose and charging effects.

The radiation constraints also evolve with the technology. As an example, recent technical progresses lead to the use of electric propulsion on GEO spacecraft, resulting in an increased duration time to reach the GEO orbit and also a longer stay in radiation belts. This evolution is then accompanied by an increase of the TID received during the satellite on this orbit. Figure 2 presents the fluences of trapped (a) electrons and (b) protons at different orbits and for varying mission profiles [31]:

- Polar orbit (800 km), mission duration of 7 years
- International Space Station (ISS), mission duration of 10 years
- Medium Earth Orbit (MEO), mission duration of 10 years
- Geostationary Earth Orbit (GEO), mission duration of 15 years
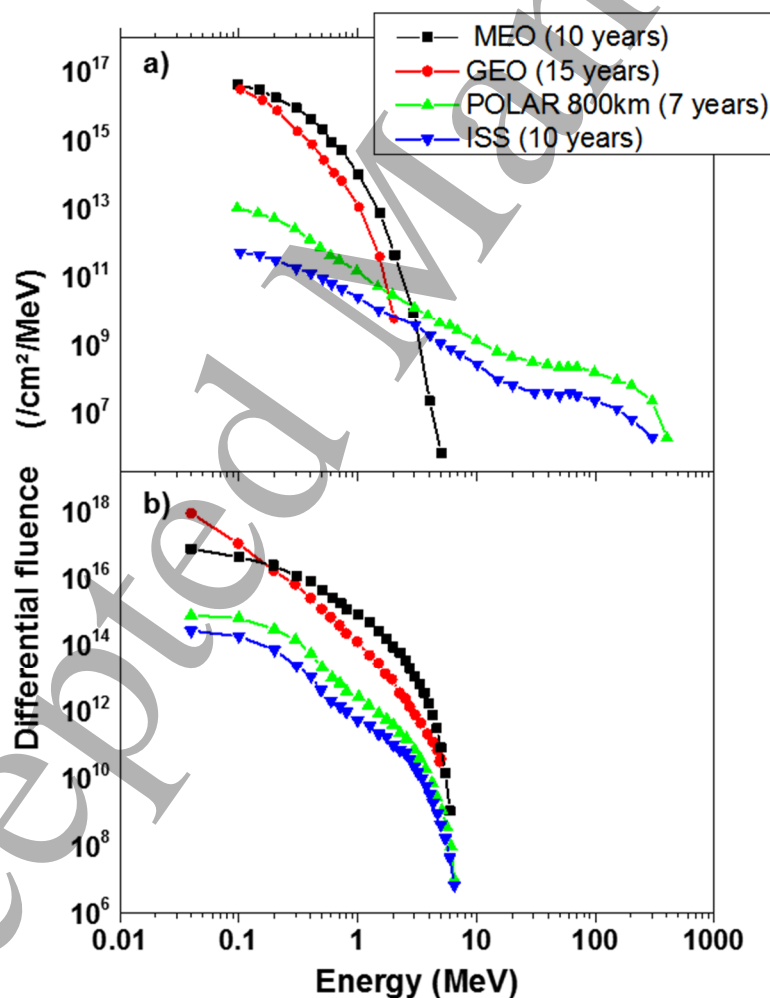
Figure 2. Trapped electrons a) and protons b) fluences for different mission profiles and orbits. Adapted from [31]

* Corresponding author: Sylvain Girard, sylvain.girard@univ-st-etienne.fr : Phone: +33 (0)477 915 812

To estimate the impact of those radiation contributions on the performances of a mission profile, environment models are mandatory. Such models have been developed by space researchers. One can cite AE8 and AP8 models for trapped particles [33,34]. Those models were developed at Aerospace Corporation for the NSSDC at NASA/GSFC, based on data from satellites flown in the 1960s and early 1970s. Improved models, AE9 and AP9, are today under validation [35,36,37,38]. In addition some local models have been developed to cover issues encountered with AE8 and AP8 such as OPAL from ONERA covering high energy protons at low altitudes [39], IGE-2006 as specific models covering electrons in GEO orbit [31]. ESCC-E-ST-10-04 [40] from ESA intends to assist in consistent application of space environment engineering to space products through specification of required or recommended methods, data and models to the problem of ensuring best performance, problem avoidance or survivability of a product in space. Modelling of trapped radiations around other planets within the solar system such as Jupiter is today a major challenge since solar system exploration becomes a strong objective for space agencies [41].

The metrics used to measure the cumulative doses deposited inside a material while exposed to space radiation are TID and Total Non-Ionizing dose (TNID). While TNID effect can be considered as negligible for optical fibers in space, when those waveguides are exposed to TID, their optical absorption increases due to the generation of radiation-induced defects. Figure 3 illustrates the effects of Aluminum shielding on the TID deposited inside Si-based material [42,43,44].

* Corresponding author: Sylvain Girard, sylvain.girard@univ-st-etienne.fr : Phone: +33 (0)477 915 812
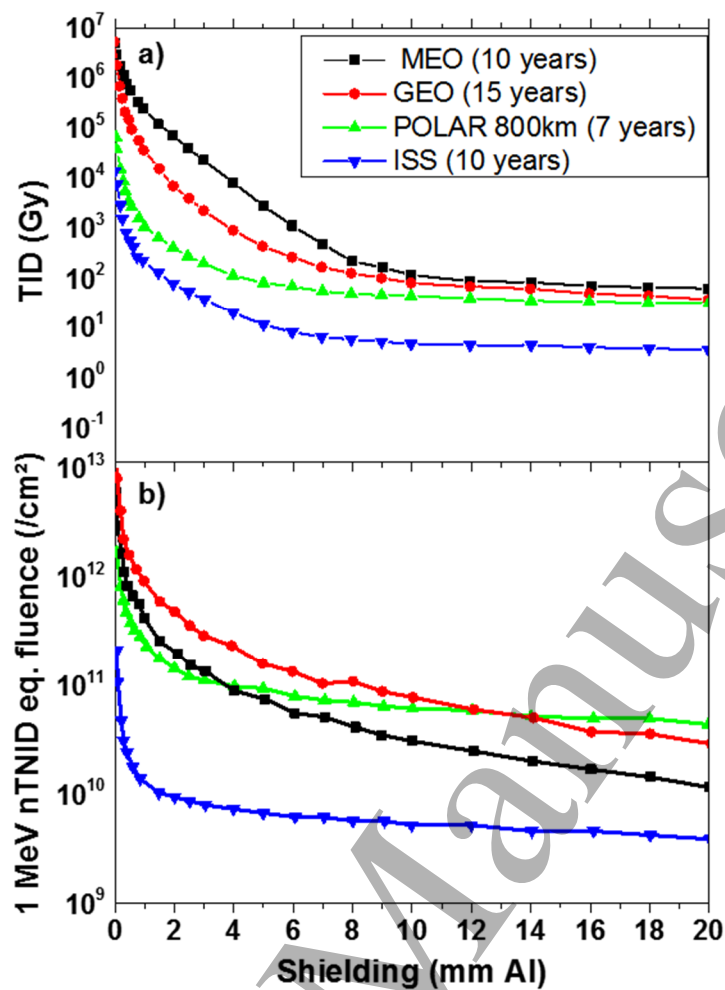
Figure 3: Total Ionizing Dose (TID) and (b) Total Non-Ionizing Dose (TNID) calculated for a simple geometry (solid sphere) as a function of Al shielding thickness for the various mission profiles presented in Figure 2. Adapted from [31].

As shown in Figure 3, spacecraft shielding reduces the TID at component level, however a compromise between additional weight embedded on the spacecraft due to shielding materials and radiation effect on components such as optical fibers has always to be attained.

I.3. Space applications for fiber-based technologies

Various fiber based systems are already embedded in spacecrafts and the potential of many more are today under investigation [45,46]. The needs for these optical technologies concern various applications for different missions. Usually, the systems developed in the framework of space programs are defined as payloads. One example of payload using optical fibers concerns the light detection and ranging (LIDAR) system on the SWARM mission. This LIDAR exploits a fiber laser emitting at 1082.908 nm, single frequency (linewidth <30 kHz) and polarized. This system is used to characterize Earth magnetic fields [41]. We can also notice platform equipments, such as Fiber Optic Gyroscopes (FOGs). Such equipment is based on Sagnac effect that will be detailed later in this review and uses

* Corresponding author: Sylvain Girard, sylvain.girard@univ-st-etienne.fr : Phone: +33 (0)477 915 812

various classes of optical fibers, including rare-earth doped optical fibers (REDFs). Numerous FOGs, such as the Astrix® family, are currently flying and present state-of-the-art performances [47,48].

Another main field of applications concerns optical datalinks, both intra-satellite and inter-satellite (or in-orbit to ground). Concerning intra-satellite datalink, the data could be either analog or digital. Example of first case is the Microwave Imaging Radiometer with Aperture Synthesis (MIRAS) Optical Harness developed for the in soil moisture and ocean salinity (SMOS) mission: it distributes a 56 MHz clock signal to 69L-Band receivers (*carrier wavelength 1300 nm, Corning SMF28 fiber*) [49,50].

Concerning inter-satellites or in-orbit to ground transmissions, we can cite the Lunar Laser Communications demonstration (LLCD) project. The LLCD demonstration consists of a space terminal on the NASA Lunar Atmosphere and Dust Environment Explorer (LADEE) spacecraft and three ground terminals on Earth. Together, they demonstrated the feasibility to transfer up to 622 Mbps of data from the Moon using a space terminal of reduced weight, using less power, and occupying a volume smaller than comparable radio frequency systems [51]. The EDRS (European Data Relay System) accelerates the transmission of data from low-orbiting satellites such as the Sentinels to the end-user on the ground. This is achieved by locking onto the satellites with a laser beam as they pass below, and immediately relaying the information to European ground stations via a high-speed radio beam [52].

Emerging fields of applications mainly concern data transmissions. In telecommunications payloads, introduction of fiber-based systems could lead to some technological breakthroughs. For inter-satellites and orbit to ground transmissions, LLCD demonstrates the concept feasibility and some advantages. However, to take over RF systems, fiber-based systems shall be able to procure higher bandwidth and therefore a good signal-to-noise ratio (SNR). High power emitting laser sources are here required, with a minimum of a few Watts. Development of High Power Erbium-Ytterbium Doped Optical amplifiers (EYDFAs) represents the main challenge for such applications. This aspect will be discussed in more details later in this review.

Other potential field of application for fiber-based technologies is spacecraft monitoring with distributed optical fiber sensors (DOFSs). These sensors can provide cartographies of temperature, radiations, and mechanical constraints during the missions. The huge potential of these DOFSs technology explains that the recent advances and future challenges regarding the radiation vulnerability and hardening are here discussed even if, to the best of our knowledge, these devices are not yet implemented in space missions.

* Corresponding author: Sylvain Girard, sylvain.girard@univ-st-etienne.fr : Phone: +33 (0)477 915 812

II. Fiber-based technologies

In this chapter are described the operational principles and characteristics of the fiber-related technologies that are today characterized under irradiation in view of their integration in harsh environments. We first review the various classes of optical fibers, their main characteristics and specificities necessary to understand their radiation responses. Second, the Fiber Bragg Grating (FBG) technology [53] is introduced as this point temperature and/or strain sensor is today the most studied optical fiber sensor (OFS) under irradiation. Third, we introduce the distributed OFS technologies that exploit one of the light scattering phenomena (*Brillouin, Rayleigh or Raman*) to convert the optical fiber into a sensing element [54]. Combined with a reflectometry technique, these OFSs open the way to distributed measurements of temperature, strain [55,56] or even radiations in harsh environments [57,58]. This part is then followed by a description of the optical devices exploiting the amplification properties of the REDFs to provide optical sources or amplifiers such as the erbium or erbium-ytterbium doped fiber sources (EDFS, EYDFS), or amplifiers (EDFA, EYDFA) [59]. These devices are key elements of FOG that is a major space technology ensuring the inertial navigation of satellites [60]. The operation principles of FOG are then briefly described.

There exists a large variety of optical fibers and all will not be covered by this article that is limited to those having been evaluated under irradiation. In particular we focus the paper on silica-based optical fibers guiding the light by total internal reflection (TIR). This class of fibers represents the quasi totality of the fibers studied in the last decades. However some preliminary results regarding plastic optical fibers (POFs) and infrared-materials based fibers can be found in [61,62] and [63,64,65], respectively. Describing in details the operation principles of optical fibers is outside the scope of the present review (see [28] for more details), but we remind here the main TIR fiber characteristics that will play a role in defining the performances of these waveguides when they are exposed to radiation.

Those components have an optical core, made of pure or doped silica with a refractive-index larger than the one of the surrounding glass called cladding. To ensure the mechanical hardness of the waveguide, the silica material is embedded into a coating, usually a polymer such as acrylate or polyimide, but can also be done in a metal such as copper, aluminum or gold to allow the fiber use at higher temperatures. A typical fiber structure is given in Figure 4a. To modify the glass refractive index and then tune the fiber refractive-index profile (RIP) (*see* Figure 4*b for a typical RIP of a Telecom-grade optical fiber*), the glass is doped with chemical elements – or dopants - allowing to increase (*Germanium, Phosphorus, Aluminum, Nitrogen*) or decrease (*Fluorine, Boron*) the silica index. Figure 4c illustrates the 2D dopant distributions measured in two Telecom-grade fibers by electron microprobe analysis (EMPA). Such compositions allow to define step-index single-mode fibers (SMFs) such as the one of Figure 4b. The control of the fiber guiding properties, meaning the characteristics

* Corresponding author: Sylvain Girard, sylvain.girard@univ-st-etienne.fr : Phone: +33 (0)477 915 812

of the allowed guided modes at the wavelengths of interest, is achieved by defining its RIP. Knowing these profiles, the radial power distributions of the guided modes can be calculated. A 2D illustration of the fundamental LP_{01} mode has been simulated with COMSOL Multiphysics and is given in Figure 4d whereas its radial distribution is compared in Figure 4e with the fiber RIP. An important outcome of this comparison is that for SMFs only a part of the light is guided into the core, an evanescent part of this mode propagates in the fiber cladding. The confinement factor (*ratio of power confined into the core versus the cladding*) depends on the RIP but also strongly on the signal wavelength. As the wavelength decreases, the confinement factor increases up a certain wavelength, the cut-off wavelength, where an additional guided mode of higher order appears and the SMFs then becomes bimodal (*usually around 1.2 µm for Telecom-grade fibers*). Figure 4f illustrates the two guided modes in the same fiber at 980 nm.
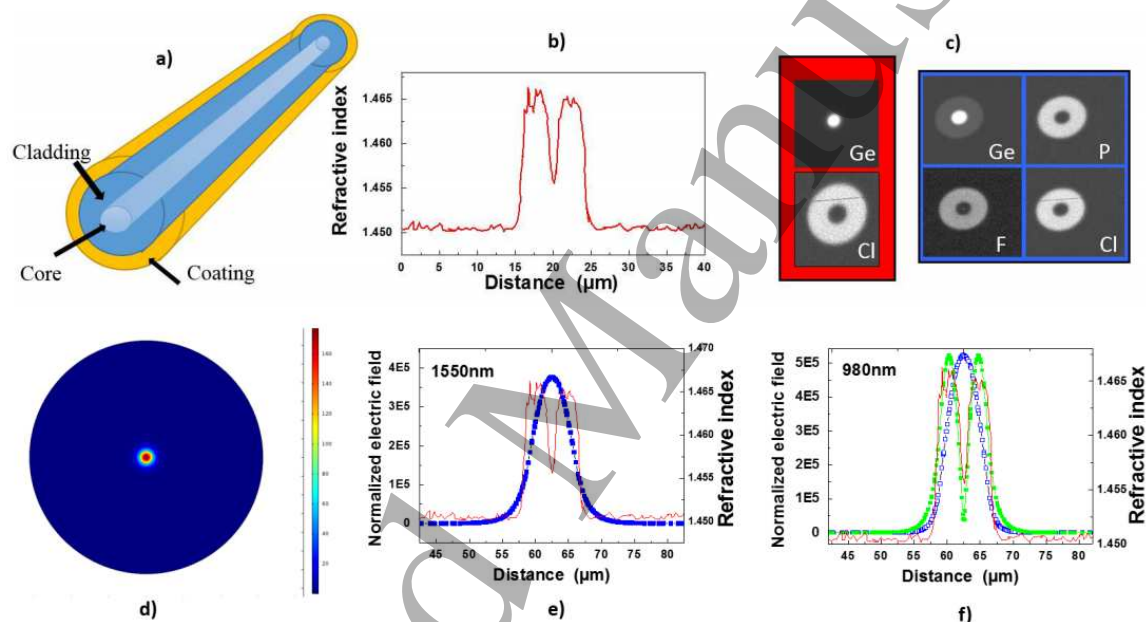
Figure 4. Illustration of a) a Telecom-grade SMF structure b) The RIP of this fiber c) 2D Chemical analysis of this fiber by Electron Microprobe Analysis d) COMSOL simulation of the fundamental mode at 1550nm e) comparison between the RIP and the radial distribution of the LP_{01} mode f) Radial distributions of the allowed LP_{01} and LP_{11} modes at 980 nm.

From Figure 4, it clearly appears that the radiation response of an optical fiber will be complex. Indeed at the material level, the differently doped layers constituting the fiber can have different radiation behaviors and the contribution of each layer to the radiation induced changes of the fiber optical properties will depend of the fiber light guidance properties too.

II.1. Classes of optical fibers and applications
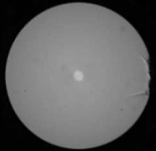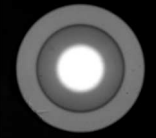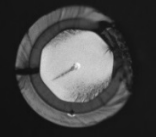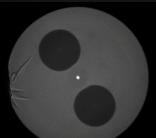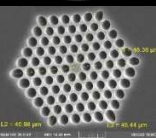
Several classes of optical fibers can be distinguished in terms of their radiation responses and application domains, their main characteristics are listed in Table 2. SMF and Multimode (MMF) optical fibers are of primary importance as they are used for data transfer, diagnostics, and sensing in harsh

* Corresponding author: Sylvain Girard, sylvain.girard@univ-st-etienne.fr : Phone: +33 (0)477 915 812

16

environments. REDFs, or active fibers, are crucial too as they allow to design IR fiber-based lasers or amplifiers. This class of fibers is particularly studied for space applications as RE doped fiber amplifiers and sources (REDFA and REDFs) are developed for a variety of optical functions [66], including the FOGs. The radiation response of polarization maintaining optical fibers (PMFs) is of interest too, especially for space and military applications as they are a key component of FOG Sagnac coil. Since 2000, various architectures of microstructured optical fibers (MOFs) became commercially available. Some of those still guide light by TIR, they are usually consisting in a silica-based core surrounded by a cladding microstructured with longitudinal holes. Interest of this class of optical fibers is that it can be made with a unique glass, e.g. pure-silica, be endlessly single-mode or have large mode area for high power devices [67]. It is also possible to use a photonic band-gap effect to guide the light in a fiber having an air core and a microstructured cladding [68]. In this case, the main interest is to have up to 98% of the light guided in air (or in other gas). If this last fiber appears as very promising for operation under steady state γ-rays [63], the cost of this technology appears still too high and its reliability too low to be considered as the principal candidate for most of the radiation-oriented applications.

Table 2. **Main characteristics of silica-based optical fibers considered for integration in radiation environments**

Fiber categories	Typical Core Diameter	Typical Cladding Diameter	SEM or EDX picture	Key references about their radiation response
Telecom and OFS grade SMF	<10 µm	125 µm		[69], [70], [71], [72], [73], [74], [75], [76], [77], [78]
Telecom and OFS grade MMF	From 50 to 100 µm	125 µm		[69], [71], [72], [73], [74], [76], [77], [78], [79], [80], [81], [87], [82], [83], [84]
REDFs	<10µm	125 µm, ErYb fibers can have a double clad (DC) structure		[85], [86], [87], [88], [89], [90], [91], [92], [93], [94]
PMF	<10 µm	125 µm		[74], [95], [96],[97]
MOF	<20µm	125 µm		[98], [99], [100]

* Corresponding author: Sylvain Girard, sylvain.girard@univ-st-etienne.fr : Phone: +33 (0)477 915 812

PBGF	<10 µm	125 µm		[63], [101], [64]

II.2. Point sensors: Fiber Bragg Gratings

FBGs consist of a periodic perturbation of the core refractive index associated with a period (Λ) of typically from 0.5 µm up to a few µm. Such a structure couples light from a forward-propagating mode to the backward counter-propagating mode. The coupling occurs at specific wavelengths, named Bragg wavelengths. These wavelengths are defined by Eq.1 [102]:

$$\lambda_{Bragg} = \frac{2n_{eff}\Lambda}{m} \qquad \text{(Eq.1)}$$

where n_{eff} is the effective refractive index of the propagating core mode and m is a integer number, called order. So, the transmission and reflection spectra of a FBG show a narrow dip or a narrow peak centered at λ_{Bragg}, respectively, as shown in Figure 5.
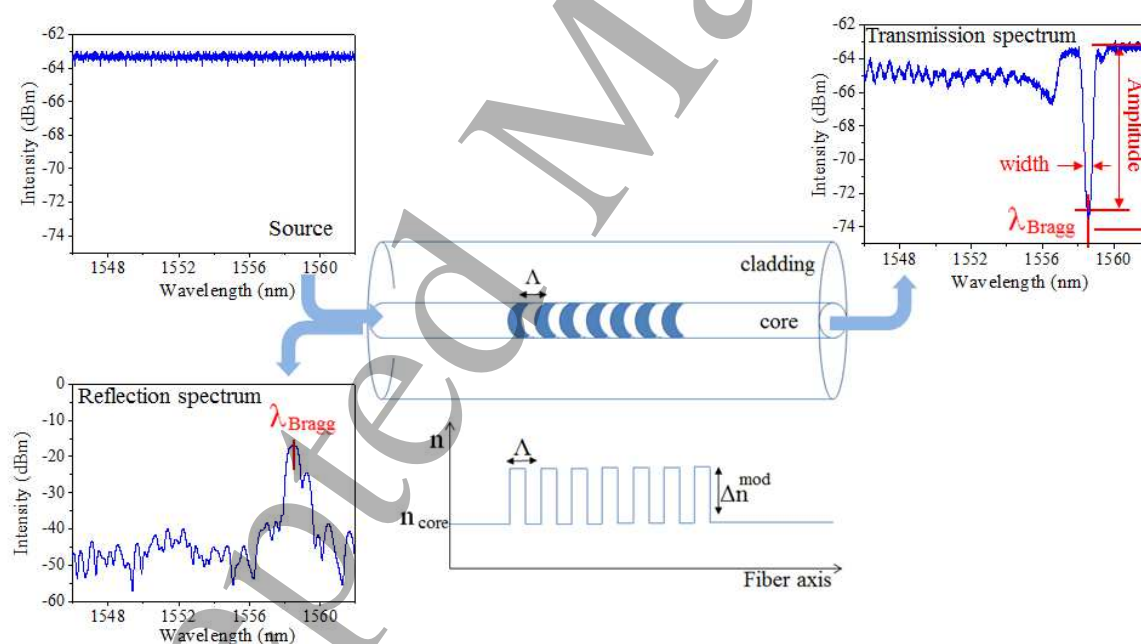
Figure 5. Schema of a FBG written in a SMF. As an example, the white light spectrum of the source injected inside the fiber core and the measured transmission and reflection spectra of the FBG are illustrated. At the center of the figure is schematically represented the FBG as a modulation of the refractive index as a function of the fiber axis. The three main parameters to define a FBG are given: Bragg wavelength, FBG peak amplitude and width.

II.2.1. FBG inscription technique

* Corresponding author: Sylvain Girard, sylvain.girard@univ-st-etienne.fr : Phone: +33 (0)477 915 812

Since the first observation of a FBG in 1978 by Hill *et al.* [103] several techniques have been developed and optimized for the grating fabrication. The most used today are: the point by point (PbP), the phase-mask (PhM) and the free space interferometry technique. The first one was established by Malo *et al.*, in 1993 [104]. The PbP technique consists in generating each grating fringe, one after the other, by focusing the laser light in a point of the core, locally increasing its refractive index and finally by translating the fiber or the laser beam by a distance corresponding to the grating period Λ, parallel to the fiber axis. The other common technique was developed by Hill *et al.* in 1993 [105]. It uses a phase-mask (PhM) made with a material transparent to the laser wavelength and having one-dimensional surface relief. For the FBG inscription, the fiber is placed almost in contact to the PhM with the grating corrugations normal to the fiber axis, while the PhM is perpendicular to laser beam. The PhM spatially modulates the phase and diffracts the laser beam, by forming an interference pattern which causes the refractive index modulation in the fiber core. Indeed, The FBGs written through the PhM technique are highly reproducible but at a well-defined and fixed spatial period, implying to use a specific PhM for each grating architecture. To overcome this last constraint, more flexible methods have been identified to produce the interference patterns, such as Lloyd's Mirror. However the fine reproducibility of the final FBG is somehow difficult to control. For both techniques, the inscription laser beam can emit in the ultraviolet (UV) or infrared (IR) spectral regions. However, whereas the UV light can be continuous wave or pulsed in the time domain of nanosecond or femtosecond, the IR laser pulse duration has to be picosecond or femtosecond to efficiently produce FBGs in silica-based fibers. Due to the small energy of the IR photons, the phenomena originating the gratings can only be multi-photons, and consequently a high power density is required.

II.2.2. FBG based sensors

FBGs are efficient strain and temperature point sensors [106]. Indeed, the Bragg wavelength λ_{Bragg} depends linearly on the axial strain (ε) applied to the waveguide with no evidence of hysteresis effect, as reported in Eq.2 [102]:

$$\lambda_{Bragg}(\varepsilon) = \lambda_{Bragg}^{unstrained} + C_{\varepsilon}.\varepsilon \text{ (Eq. 2)}$$

Typically, the strain sensitivity (C_{ε}) of a grating having a Bragg wavelength peaking at 1550 nm is about 1 pm/µε. The grating temperature response, instead, is linear only on a small range of about 100°C around RT:

$$\lambda_{Bragg}(T) = \lambda_{Bragg}(T_0) + C_T.(T - T_0) \text{ (Eq. 3)}$$

* Corresponding author: Sylvain Girard, sylvain.girard@univ-st-etienne.fr : Phone: +33 (0)477 915 812

The temperature sensitivity C_T is about 10 pm/°C for a bare grating at 1550 nm and is not significantly dependent on the FBG type [107]. However, this coefficient depends on the pre- or post-treatments the FBG undergoes [108] and, above all, on the selected fiber coating and packaging. For example, this sensitivity coefficient C_T can be increased by embedding the FBG in a metal plate or by using a metal coating: the thermal expansion of the metal transfers a strain to the fiber core, which affects the period and also the refractive index through thermo-elastic effect [109].

Consecutive thermal treatments can nevertheless entail hysteresis. As demonstrated by several studies performed above all on the most classical grating type, known as type I UV-FBG, a grating during a thermal treatment can undergo to a degradation, which manifests itself as a reduction in the peak reflectivity and bandwidth and a Bragg wavelength shift towards the blue. During a treatment the decay is first rapid and then the decay rate decreases. Few models [110,111],depending on the pre-treatments performed on the gratings, have been proposed to explain this degradation and allow determining recipes to obtain a stable FBG for the application requirements. If the FBG has to be stable at the temperature T_O for an operating time t_O, after its inscription it has to undergo a treatment at an annealing temperature T_A, higher than T_O, with a duration t_A that depends on the grating type and the parameters T_O, t_O, and T_A [111]. The first model was proposed by Erdogan and applies only to gratings written in H_2-free fibers [110].

II.2.3. FBG classification

The first classification of FBGs separates them in two main groups, known as Type I and Type II, according to the basic mechanisms governing the FBG inscription. This classification is completed by specifying the spectral domain of the inscription laser, either UV or IR, as shown in Figure 6.
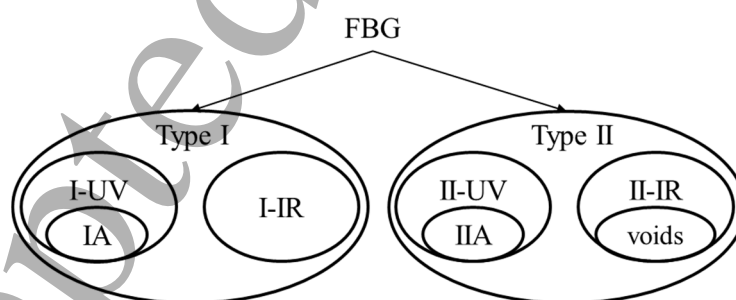
Figure 6. FBG classification

The fabrication of Type I gratings results from color center or point defect formation. These gratings cannot withstand operation temperatures higher than 600°C, since at such temperatures all the defects at the origin of the refractive index periodic modulation Δn^{mod} are bleached. During the inscription, n_{eff} and Δn^{mod} increase and consequently λ_{Bragg} shifts towards the red, while the FBG peak reflectivity and width increase [112,113].

* Corresponding author: Sylvain Girard, sylvain.girard@univ-st-etienne.fr : Phone: +33 (0)477 915 812

Type I-UV FBG inscription is only possible thanks to the photo-sensitivity of the silica-based matrix of the fiber core. To ensure a sufficient photosensitivity, the core has to be doped with specific elements, such as Ge. In germanosilicate fibers, the FBG formation is associated with the generation of some specific Ge-related defects such as the GeE' and GeH centers [114]. To further increase the fiber photosensitivity, a H_2-loading can be performed before the grating inscription. For this, the selected fiber is maintained in a vessel containing the gas and ensuring its diffusion into the silica matrix at kinetics fixed by the fiber geometry, the selected pressure and temperature. The induced refractive index increase ranges between 10^{-5} and 10^{-3} for H_2-free Ge-doped fiber whereas it reaches 10^{-2} for H_2-loaded ones [103].

Type I-IR FBG inscription occurs only for pulse peak intensity beyond a threshold, since the refractive index increase is induced by multi-photon processes. This threshold depends on the fiber composition, the selected writing technique, the laser system alignment accuracy and other laser-related parameters. This threshold is at about 2×10^{13} W/cm² (*femtosecond laser operating at 800 nm*), for a Ge-doped fiber with the PhM technique [115,116]. When the pulse energy, and consequently the pulse peak intensity, increases beyond a threshold, Type II FBGs are written. The growth rate of these FBGs is faster than that of Type I. Moreover, they exhibit higher reflectivity and larger peak width, resulting in a reduction of the effective grating length (typically from a few mm to 2 cm). These Type II gratings are more thermally stable than Type I but have reflection spectra of lower quality [117,118].

The origin of Type II-UV gratings is a laser damage induced at the fiber core-cladding interface [117], whereas for the Type II-IR FBGs, it is assumed to be related to be silica densification induced by femtosecond radiation at high power density. As an example, the pulse peak intensity threshold is at about 5×10^{13} W/cm² (*femtosecond laser operating at 800 nm*) for a Ge-doped fiber and the PhM technique [118].

Concerning the UV-FBGs, two other groups can be highlighted:

- Type IA FBGs are written in highly photosensitive fibers, such as hydrogenated Ge-doped or B/Ge co-doped optical fibers, after a prolonged UV exposure. They exhibit a large red-shift of the central wavelength during the inscription. Such shift can be associated with a large increase of the mean refractive index of the core, of about 2×10^{-2} [119].

- Type IIA FBGs are regenerated gratings written in highly Ge-doped, B/Ge or Sn/Ge co-doped fibers, with or without H_2-loading and characterized by a UV light induced negative refractive index change [120]. By increasing the accumulated laser energy on a pre-existing type I grating [121] or by subjecting this latter to a thermal treatment at high temperature such as 700°C [122], the Type I grating is erased, until the starting point of the regeneration process is reached: a new grating will appear with a blue-shift of the initial central wavelength.

* Corresponding author: Sylvain Girard, sylvain.girard@univ-st-etienne.fr : Phone: +33 (0)477 915 812

Type IA gratings show lower temperature stability than Type I, whereas Type IIA ones have a better stability at high temperatures than Type II gratings. Finally, among Type II-IR gratings, a particular group can be isolated, known as voids-FBGs. They are PbP gratings written by focusing the femtosecond IR laser at successive positions along the fiber. Around the area where the laser is focalized, the silica refractive index increases, whereas in the center it decreases in such a way that it is assumed that a micro-void is formed into the core and that this void is surrounded by high density silica [123]. The voids-gratings exhibit the same high thermal stability of type II FBGs [124].

II.3. Distributed sensors

II.3.1. Operational principles

The laser light injected into a silica-based fiber can be transmitted, absorbed or scattered by the material. Two types of scattering are distinguished [125]:

- Elastic, if the scattered and incident lights have the same wavelength, this is the case for example for Rayleigh scattering and Fresnel reflections [126];
- Inelastic, if a wavelength change is recorded, as it is the case in Raman and Brillouin phenomena. When the scattered photon has a frequency (ν_S) lower than the incident one (ν_0), because this latter gives energy to the system, the scattering is known as Stokes; if the scattered photon absorbs energy from the system, it will have frequency (ν_{AS}) higher than the incident one and in this case the scattering is known as anti-Stokes.
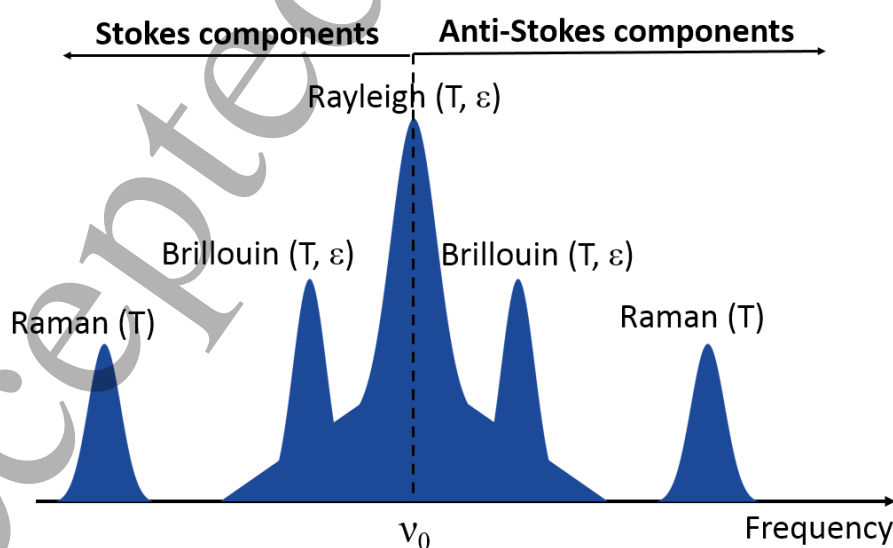
Figure 7. Spectrum of the scattered signal as a function of the frequency. ν_0 is the frequency of the incident light.

* Corresponding author: Sylvain Girard, sylvain.girard@univ-st-etienne.fr : Phone: +33 (0)477 915 812

The silica properties differ when the fiber surrounding environment changes. Local temperature, strain, vibration or acoustic wave changes will affect the scattered signals in a predictable way. Then, by measuring the modifications of the Rayleigh, Raman or Brillouin signatures, the evolution of the external constraints applied to the waveguide can be monitored. DOFSs are able to probe numerous points along the fiber length, by recording the intensities of the signals scattered from different fiber parts. To identify at which position corresponds an acquired scattering trace, most of these sensors are based on reflectometry techniques, such as the Optical Time Domain Reflectometry (OTDR) [127].
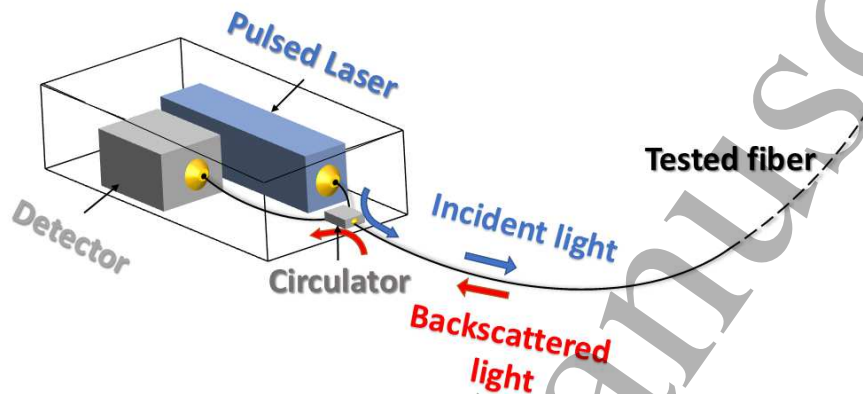
Figure 8.Schema of an OTDR.

A pulsed signal is injected at one end of the fiber and guided along the waveguide. After interaction with the silica material, the backscattered signal is recorded; the time "t" needed by the incident signal to reach a point at a distance z along the fiber and by the backscattered one to go back to the interrogator allows to determine the position z, through:

$$z = \frac{v_g t}{2}$$ (**Eq. 4**)

where v_g is the group velocity of propagated light. Consequently, for this technique, the spatial resolution directly depends on the pulse width duration; i.e. a 10 ns pulse is associated with a spatial resolution of ~1 m.

II.3.2. Rayleigh-based DOFS

Rayleigh scattering is an elastic phenomenon caused by random fluctuations in the RIP, due to small variations in density or dopants concentration. Each fiber is characterized by its own Rayleigh signature or trace, giving the backscattered light amplitude as a function of distance. Such signature is random and static but locally changes when an external stimulus such as temperature or strain is applied. This is the basis of the operation principle of Rayleigh-based DOFS: a temperature and/or strain variation

* Corresponding author: Sylvain Girard, sylvain.girard@univ-st-etienne.fr : Phone: +33 (0)477 915 812

applied to a segment of the fiber length can be measured by comparing the Rayleigh signatures acquired before (reference) and after applying the constraint.

Different techniques to measure the Rayleigh backscattered signal exist:

- The simplest one is the OTDR, which measures the backscattered signal intensity [127]: the external parameter value is obtained by the ratio of the scattered intensity in the new state and in the reference one [128]. For example, for temperature sensors, this ratio linearly depends on temperature with a sensibility of about 0.015 %/°C between RT and 800°C.

- A very efficient technique is the Optical Frequency Domain Reflectometer (OFDR) [129]. In this case, the light of a tunable laser source is injected into the two arms of an interferometer: the reference light is split between the two orthogonal polarization states, while the light in the measurement arm is reflected from the fiber under test (FUT). The analysis of the interference patterns between the measurement light and the two polarization states leads to a complex reflection coefficient of the FUT as a function of wavelength. Finally, the Rayleigh scatter as a function of length is calculated via a Fourier transform.

To measure an external parameter, the two Rayleigh scatter functions recorded on a short fiber segment in two different states, for example at RT and at another temperature, and Fourier transformed in the frequency domain have to undergo a cross-correlation, whose result is a peak. The shift of this peak is proportional to the temperature or strain variation, according to Eq.5:

$$\frac{\Delta \lambda}{\lambda} = -\frac{\Delta \nu}{\nu} = C_T . \Delta T + C_\varepsilon . \Delta \varepsilon \qquad \text{(Eq. 5)}$$

where C_T is the temperature coefficient, of about 6.5×10^{-6} °C^{-1}, C_ε is the strain coefficient, of about 0.8 µε^{-1}, for a germanosilicate fiber, whereas ΔT and $\Delta \varepsilon$ are the temperature and strain variations, respectively.

II.3.3. Brillouin-based DOFS

The Brillouin scattering is the inelastic scattering of a photon from fluctuations in the density of the medium, with the creation (Stokes component) or the annihilation (anti-Stokes component) of an acoustic phonon. The frequency of the scattered light is shifted with respect to the excitation line by a quantity named Brillouin frequency and defined in Eq.6 [130]:

$$\nu_B = \frac{2n_{eff}V_a}{\lambda_0} \qquad \text{(Eq. 6)}$$

where n_{eff} is the the effective refractive index of the propagating mode, V_a is the acoustic speed of silica (about 5800 m/s), that depends on density, and λ_0 is the wavelength of the incident light. The Brillouin frequency of a silica-based fiber ranges from 9 to 13 GHz, depending on its composition and

* Corresponding author: Sylvain Girard, sylvain.girard@univ-st-etienne.fr : Phone: +33 (0)477 915 812

its RIP. Since the acoustic speed depends on temperature and strain, a variation of these external parameters gives rise to a Brillouin Frequency Shift ($\Delta\nu_B$). The relationship between $\Delta\nu_B$ and a temperature variation ΔT or a strain $\Delta\varepsilon$ is linear, indeed:

$$\Delta\nu_B = C_T\Delta T + C_\varepsilon\Delta\varepsilon \quad \text{(Eq. 7)}$$

where C_ε and C_T are the strain and temperature coefficients, of about 0.05 MHz/µε and 1 MHz/°C, respectively, for a germanosilicate fiber.

Different techniques allow measuring the Brillouin frequency. The Brillouin Optical Time-Domain Reflectometry (BOTDR) is a single-ended (SE) device, indeed as all the OTDRs, a laser pulse is injected into a fiber end and the spontaneously backscattered signal is detected from the same fiber end. Another technique is based on the stimulated Brillouin signal and it is called Brillouin Optical Time-Domain Analysis (BOTDA) [131]. This device is double-ended (DE), indeed a pulsed light and a continuous light counter-propagate in the fiber, interact in order to create a beat pattern that causes a periodic fluctuation in the density and consequently an acoustic wave. By scanning one of the two frequencies, one of the beams will be amplified when the difference between the frequencies of the two signals coincides with the Brillouin frequency.

II.3.4. Raman-based DOFS

Raman scattering is an inelastic scattering, due to the interaction of a photon on molecules with the creation and the annihilation of an IR phonon [132]. The phonon that is emitted or absorbed, respectively in the Stokes and anti-Stokes Raman scattering, has frequency $\Delta\nu$ of about 1.3×10^13 Hz for the fused silica.

Raman based DOFSs are not sensitive to strain and measure only temperature. Indeed, the cross sections for Stokes and Anti-Stokes scatterings depend differently on the temperature T. Consequently, this sensor operational principle is based on the intensity ratio of the anti-Stokes signal to the Stokes one, $R(T,z)$, which depends on the position along the fiber length z and on the temperature T in such a point, according to Eq.8 [133]:

$$R(T,z) = \left(\frac{\nu_{AS}}{\nu_S}\right)^4 \cdot \exp\left(-\frac{h\cdot\Delta\nu}{k_B\cdot T}\right) \cdot \exp\left(-\int_0^z (\alpha(\nu_{AS},u) - \alpha(\nu_S,u))du\right) \quad \text{(Eq.8)}$$

where k_B is the Boltzmann's constant. The first factor takes into account the different frequencies of the anti-Stokes and Stokes signals, ν_{AS} and ν_S, respectively; the second one contains the dependence on the temperature, whereas the last one includes the differential losses, due to the different attenuations α at the two frequencies of the two signals. In absence of ionizing radiation, the differential losses are constant, so they can be neglected. Therefore, the temperature can be easily

* Corresponding author: Sylvain Girard, sylvain.girard@univ-st-etienne.fr : Phone: +33 (0)477 915 812

calculated by comparing the ratio $R(T,z)$ in a point z at an unknown temperature T, with that one recorded at a reference temperature (T_0):

$$T(z) = \left(\frac{1}{T_0} - \frac{k_B}{h \cdot \Delta \nu} \cdot \ln\left(-\frac{R(T,z)}{R(T_0,z)} \right) \right)^{-1} \text{ (Eq. 9)}$$

II.3.5. Performances of the various DOFS technologies

Table 3 compares the performances of the different DOFSs in terms of spatial resolution, sensing range, strain and/or temperature measurement accuracies. In this table are given typical values, accessible at the time at which these technologies were evaluated under irradiation, more detailed studies on these performances have been recently published [134,135]. As the development of DOFS is a very active research field, these performances are continuously optimized, thanks to the building of new sensor architectures, or signal processing approaches. An important remark is that for most of the today's applications in harsh environments, it appears as mandatory to combine at least two technologies to simultaneously measure the strain and temperature distributions onto two different fibers [136].

* Corresponding author: Sylvain Girard, sylvain.girard@univ-st-etienne.fr : Phone: +33 (0)477 915 812

26

Table 3. Main characteristics of DOFSs.

Scattered signal	Technique	Spatial resolution	Sensing range	Temperature accuracy	Strain accuracy
Rayleigh	OTDR	1 m	~100 km	15°C	
	OFDR	From 1 cm to 10 µm	From 2 km to 10 m	0.1°C	1µε
Brillouin	BOTDR	1 m	~20-50 km	10°C	60 µε
	BOTDA	<50 cm	~100 km	1°C	20 µε
Raman	OTDR	<50 cm	~100 km	1°C	-

II.4. EDFA and EDFS

II.4.1. Applications for RE-based devices

During the last decade a revolution in the space industry has been observed. New space launch ventures such as Space X, Virgin Galactic and Blue Origin and the advances in nano-satellites, such as the CubeSat, are bringing the focus back to the space industry. This revolution is well underway and private companies, national space agencies, governmental organizations are investing in the design of new satellite constellations that aim to answer specific science questions covering a broad range of sciences including weather and climate on Earth, space weather and cosmic rays, planetary exploration and much more. Moreover, giants such as Virgin, QualComm, Space X, Google, Airbus, Samsung and LeoSat are placing big bets on new mega-constellations into LEO to provide broadband internet service around the world, the internet connectivity in remote or underserved areas, as well as the most secure and high performance data network over Earth [137,138,139,140,141].

Observation and scientific missions will need for larger data transfer capacity. As an example the earth-viewing systems and the planetary probes can generate many image data to exchange between more remote spacecrafts and the ground station on or near to the Earth. Such data transfer has to be done at the appropriate time of request and within brief time slot resulting in high data rate transfer. Moreover, the next fast Internet generation will be based on new satellite systems requiring high-speed inter-satellite links. In this context and considering that the desired data volumes cannot be accomplished using the available radio links, the photonic technologies became of great interest for space payload [142]. In particular, since they enable high-data rate, secure links, decreased mass, size, and electrical power the fiber optic systems are beginning to penetrate satellite technologies and they are expected to play a critical role in next generation space missions bridging the gap addressing different applications including on-board photonic signal handling and processing.

* Corresponding author: Sylvain Girard, sylvain.girard@univ-st-etienne.fr : Phone: +33 (0)477 915 812

Recent and planned developments of spaceborn optical communication systems are based on the eye-safe 1.55 µm telecom wavelength window. This wavelength allows a low-loss transmission through both the fiber and the atmosphere. Moreover, it makes possible the use of suitably designed terrestrial high-bandwidth photonic components as well as it enables the scaling of the link capacities by employing the wavelength division multiplexed (WDM) technology. In order to leverage the significant investment and reliability heritage of terrestrial telecommunication systems, there is a strong motivation to use Er^{3+}-doped (EDFAs) or Er^{3+}/Yb^{3+}-codoped (EYDFAs) fiber amplifiers and sources (EDFS) as integral part of the space optical communication terminals to boost and generate the optical signal and to enable long reach in free-space [143,144,145,146,147,148]. Moreover, optical fiber amplifiers are expected to be used to compensate insertion losses between functional blocks of the payload.

II.4.2. Architecture of REDF amplifiers

In the context of space optical communications, there is no station between transmitting and receiving terminals. So, the transmitter operating at 1.55 µm should be able to provide a stable average output signal power of several watts (>5 W) over a long-term space missions. Figure 9 illustrates the scheme of a high power laser transmitter for space communication [149,150,151]. The seed laser is a high power 1.55 µm distributed feedback laser (DFB) operating in continuous wave (CW) regime [152]. Pulses can be generated using the external intensity modulator (INT mod) having a high extinction ratio. A pulse shape control section is directly connected to the modulator to provide a wide range of pulse position modulation formats with pulse duration typically ranging from 0.5 ns to 8 ns and low duty cycle essential to ensure high pulse energies. Moreover, since at low pulse repetition frequency the pulse energies are near the saturation value, it is important to correct the corresponding pulse energy variation through a pre-pulse shaping function delivered by the control device. A low loss phase modulator (PHS mod) is used for controlling the laser linewidth at values lower than 6 GHz. This signal processing is indispensable to suppress the Stimulated Brillouin Scattering (SBS) occurring at longer pulse durations.

Depending on the mission scenario, the amplifying section could be designed using one or two sub-units in cascade connection. In short range (<2000 km) and high speed LEO to ground downlinks only one mid-power booster amplifier is used to directly amplify the output of the laser transmitter. In long range (> 30000 km) GEO links, the mid-power booster amplifier (AMPL1) is used to pre-amplify the transmitter signal and to saturate the cascaded high power amplifier (AMPL2). The mid-power booster amplifier is typically an EDFA pumped by an uncooled single mode 980 nm pump laser diode (SM-pump1). This amplifier should be designed to achieve a low noise figure (~ 5 dB) and high amplification gain of small signal (> 30 dB) in the wavelength range 1540 - 1560 nm. The polarization independent isolator (Isol1) has to be placed at the input to minimize degradation of the noise figure and to prevent

* Corresponding author: Sylvain Girard, sylvain.girard@univ-st-etienne.fr : Phone: +33 (0)477 915 812

28

optical feedback reflections that could result in lasing. Moreover, a very high inversion level can be accomplished by using a short segment of erbium-doped fiber and the 980 nm pumping.

The high power requirement (output signal power > 5 W) is difficult to satisfy by using EDFA since the various nonlinearity impairments result in serious gain-saturation problems in both C-band and L-band especially when the output power grows up. The co-doping with ytterbium Yb^{3+} sensitizer ions could be an effective way to solve the problem concerning the delivering of high output power. In fact, the presence of Yb^{3+} ions makes possible an efficient indirect pumping mechanism for erbium ions, reduces the formation of Er^{3+} clusters and the cooperative upconversion processes among Er^{3+} ions, extends the range of the possible pump wavelength band between 800 nm and 1100 nm, increases the pump absorption by providing a peak absorption around 975 nm two order of magnitude larger than the non-sensitized one. Moreover, considering that the core pumping is not applicable to multiwatt amplifiers, the double cladding fiber geometry is required (see an illustration in Table 2). Such technique allows the propagation of much larger optical pump powers delivered by low cost multimode pump diodes, without exciting non-linear effects, as well as it reduces the thermal loading density. Starting from these considerations, the high power amplifier (AMPL2) is an Er/Yb polarization maintaining large mode area (PM-LMA) fiber amplifier. The use of PM-LMA fiber is essential to achieve the required very high peak power and SBS free operation. The narrow band pass filter (BPF) is used to suppress the amplified spontaneous emission (ASE) generated in the Stage1 ensuring a clean seeding of the Stage2. The AMPL2 is pumped by a multimode laser diodes (MM-pump2) operating at the wavelength within the range 915 - 940 nm. The high power and low loss multimode pump combiner (MM combiner) is used to launch the pump signal into AMPL2. Moreover, pumping in a backward propagating configuration should enable lower ASE and hence increased signal power in the output. Finally, the low loss high power polarizer collimator (CL) should be designed to ensure an output beam quality $M^2 < 1.1$.
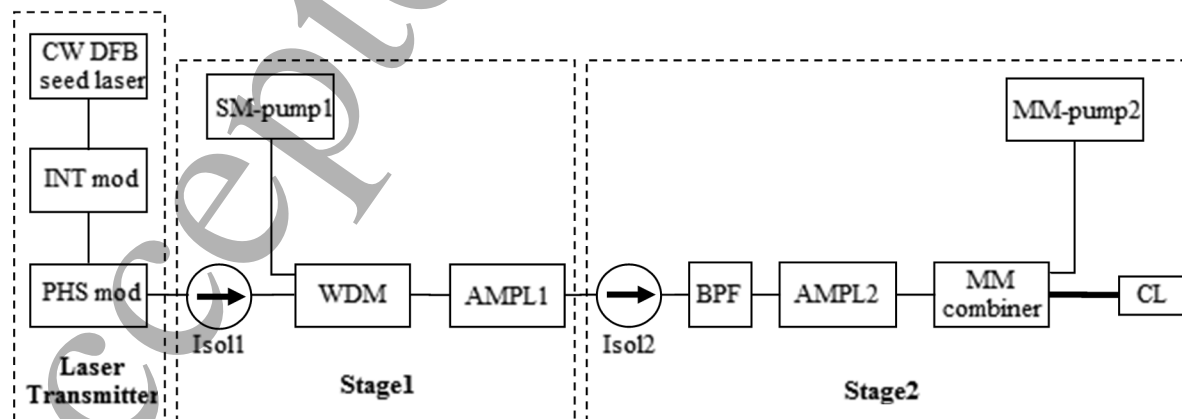

Figure 9. Schematic of the transmitting system based on optical fiber amplifiers.

* Corresponding author: Sylvain Girard, sylvain.girard@univ-st-etienne.fr : Phone: +33 (0)477 915 812

II.4.2. Space constraints on REDF amplifiers

In contrast to terrestrial-based systems, the design and development of components and systems based on rare earth doped fibers for space applications require special treatments to face a number of challenges and performance trade-offs. In fact, because repairs cannot be made in space and the investments are enormous, meticulous analysis, study and testing need to be performed during each phase characterizing the whole construction process. Such activities are essential to eliminate expensive surprises after launch and to ensure that operational performance objectives are met. Very thorough and special tests need to be performed on the individual components and subsystems as well as the complete communication system, both separately and integrated, in the lab and under real-use conditions. It is well known that due to the exposure to ionizing radiation, the long-term EDFA and EYDFA characteristics will be deteriorated when they operate in the space radiation environment. As a result, a number of design challenges including severe attenuation and performance degradation due to radiation have to be taken into account during amplifier design and definition of the optimum parameters (*pump power, fiber length, erbium and/or ytterbium concentration, etc*.). Moreover, in the case of booster and power amplifiers the development of devices having high power conversion efficiency (PCE) is of prime importance. In fact, considering that satellite resources are typically well defined and restricted, the design of fiber amplifiers for space applications has to comply with the spacecraft electrical power resource specifications and component de-rating requirements. In this context, the availability of accurate numerical models is an invaluable tool i) to evaluate the suitable amplifier configuration for controlling unwanted degradation mechanism due to the fiber exposition to ionizing radiation, ii) to correctly predict the amplifier performance in terms of efficiency and power scaling capability, iii) to maximize the PCE through optimization of the amplifier topology, pumping configuration and fiber parameters as numerical aperture, core size, fiber length, cladding geometry, and dopant concentration [144,145,146,147]. Moreover, the amplifier topology has to be engineered according to the wavelength channel plan and noise performance to achieve optimal trade-off between optical performance and electrical power requirements [149,150].

Although radiation can degrade the optical fiber performance, the thermal loading inside the fiber could became a serious problem in booster and power amplifiers. Moreover, since higher optical signal attenuation improves the heat generation, the radiation can further induce dramatic impairments of amplifier in terms of efficiency, gain and noise figure. On the other hand, the quantum defect due to the amplification of the 1550 nm signal using 980 nm pump source generates a further heat accumulation that could became a serious concern especially when high power optical signals transit through short fiber amplifiers. The increased heat load has a number of undesirable consequences resulting in a deterioration of the amplifier performance. As a consequence, the design and

* Corresponding author: Sylvain Girard, sylvain.girard@univ-st-etienne.fr : Phone: +33 (0)477 915 812

30

development of the optical fiber amplifies has to comply with the further constraints due to the heat dissipation. This means that specific functional test validating the unit thermal design have to be defined with the aim to demonstrate stable operation over the required module temperature range. Again, the quantum defect of the mismatch in pump-to-signal wavelength still ultimately limits the potential for higher efficiency in the amplifier, the main power draw in a fiber laser. So, to overcome these drawbacks a new paradigm is required. Recent development of high power fiber-coupled pump diodes at 1480 nm and 1530 nm offer the potential for significantly improving the power efficiency of fiber amplifiers, and hence fiber laser transmitters in general [153]. However, their maturity and reliability has not yet been demonstrated to levels comparable to 980 nm pump diodes.

In conclusion, the requirements of high reliability and robustness make the evaluation of optical fiber booster and power amplifier vulnerability to radiation a crucial point to be considered to ensure the system functionality over the satellite lifetime. To this aim, the End-of-Life performance has to be carefully defined in the context of the mission environmental constraints as well as the mission operational specifications.

II.5. Fiber-optic gyroscopes

FOG provides rotation speed measurements [154,155]. When this technology is associated to accelerometers, FOG can also provide inertial positioning, a crucial parameter in the monitoring of satellites. In space, various grades of gyroscopes are used in a large variety of missions requiring measurement precision ranging from 1°/h to 0.0001°/h. Some FOG usages, sorted by gyroscope precision, are telecommunication satellite spin control, altitude and orbit control (AOCS) for electric propulsion and deep space exploration, AOCS for planetary landing, scientific satellite orientation, science mission, Earth and space observation satellite. FOG exploits the Sagnac effect [156,157]: light travelling along a closed ring path in opposite directions allows one to detect rotation with respect to inertial space (Figure 10). Over one turn as in the original experiment 104 years ago [158], the effect is extremely weak but it can be increased using the numerous loops of a fiber coil as this Sagnac effect is proportional to the apparent surface of the fiber coil. To fully exploit this cumulative behavior, modern commercial FOGs contain up to several fiber kilometers per coil [154].

* Corresponding author: Sylvain Girard, sylvain.girard@univ-st-etienne.fr : Phone: +33 (0)477 915 812
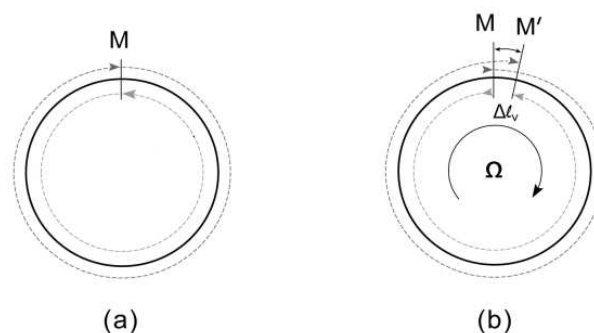
Figure 10. Principle of Sagnac effect: (a)at rest, both opposite paths have equal length (b) rotating at rate Ω, M moves to M' during the transit time, then the corotating path is more than one turn while the counterrotating path is less, yielding a path difference $2\Delta l_v$

The modern FOG's principle of operation is continuous tracking of the interferometric fringe position [155] that evolves with the coil's rotation rate. A modern FOG architecture is displayed in Figure 11 and its basic subparts are listed hereafter:

- A broadband 1550 nm optical amplified spontaneous emission (ASE) source including a 980 nm pumping laser diode and an active Er-doped Fiber [159,160]. For a low to medium FOG performance, a superluminescent semiconductor diode at either 1.5µm or 1.3µm can be used as a cheaper and smaller replacement [161].
- Passive optical components such as couplers and isolators.
- A Lithium Niobate optical phase modulator, in an integrated-optic Y junction form [162,163].
- A polarization-maintaining optical fiber coil of up to several kilometers [164].
- A high quantum efficiency PIN photodiode to convert the optical power returning from the interferometer into an electric signal.
- A digital electronic achieving a servo loop to track the optical fringe [165]

The two following parameters are of particular interest.

- Fiber coil's optical spectrum transfer function and Erbium ASE optical spectrum: any mean wavelength modification at the detector's end linearly affects the FOG scale factor.
- Fiber attenuation as the FOG noise rises as the optical power at detector's end decreases.

* Corresponding author: Sylvain Girard, sylvain.girard@univ-st-etienne.fr : Phone: +33 (0)477 915 812
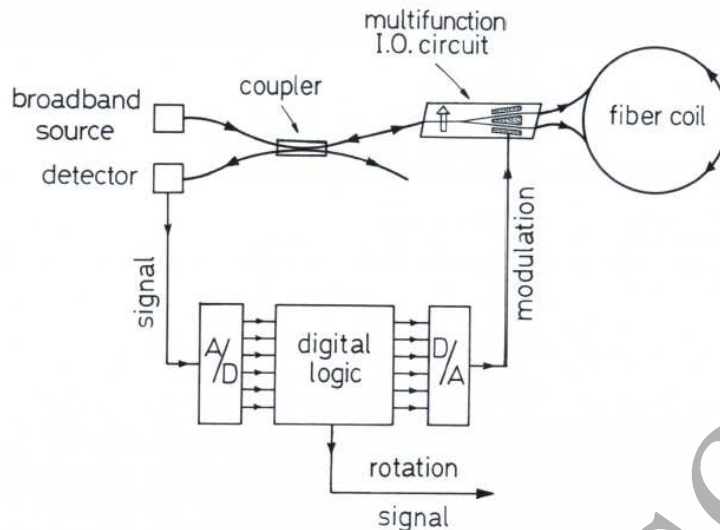
Figure 11. Modern architecture of the FOG

III. Radiation effects on fiber-based technologies

Radiation effects on optical fibers have been investigated since more than 40 years for data transfer applications and an important knowledge has been acquired even if the microscopic mechanisms leading to this degradation are still partially unknown and too complex to be yet predictable by simulation. With the development of more-and-more sophisticated architectures of fiber sensors, new types of degradations have been noticed that are related to changes of the silica-based matrix structure rather than by the evolution of its optical properties. In this part, the multi-scale radiation effects on optical fibers will be first described, reviewing our current knowledge on the main intrinsic and extrinsic parameters affecting their radiation responses.

III.1. Radiation effects on optical fibers

III.1.1. Macroscopic effects: RIA, RIE, RIRIC

Three main radiation effects are observed at the macroscopic scale when a silica-based optical fiber is exposed to radiation:

- The first one is the **Radiation-Induced Attenuation (RIA)**. RIA is an excess of loss that appears during an irradiation, grows with the dose and usually partially recovers after the irradiation stops. Figure 12 illustrates the RIA growth in the spectral range $350 - 900$ nm for a Polymicro FVP-UVMI MMF under γ-rays at a dose rate of 11 Gy/h up to 200 Gy. RIA growth kinetics are illustrated in the inset of Figure 12 at 350 nm, 400 nm and 660 nm.

* Corresponding author: Sylvain Girard, sylvain.girard@univ-st-etienne.fr : Phone: +33 (0)477 915 812

33
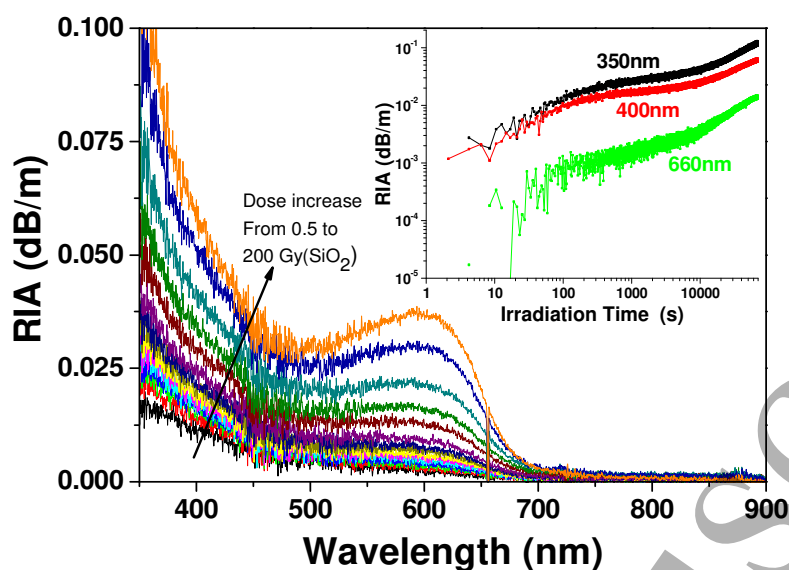
Figure 12. Spectral dependence of the RIA generated during irradiation of a Polymicro FVP-UVMI multimode optical fiber at RT, up to 200 Gy(SiO₂) at a dose rate of 11 Gy/h. In the inset are illustrated the RIA growth kinetics at three particular wavelengths: 350, 400 and 660nm. More details can be found in [166].

This figure illustrates the complex response of an optical fiber, highlighting the strong spectral dependence of these excess losses. Furthermore, for this PSC fiber, a clear absorption band can be seen peaking around 630 nm. In this case, the defect structure associated with this optical absorption band is known: the non-bridging oxygen hole centers (NBOHC) [167]. RIA levels and kinetics depend on numerous parameters that will be detailed in paragraph III.3. RIA is often the main issue to consider when implementing an optical fiber into a harsh environment as it degrades the SNR of optical data links up to, in the worst case, the loss of the guided signal after short distances of propagation. As an example, after a X-ray pulse of a few tens of nanoseconds, RIA levels as high as 2000 dB/km at 1550 nm (*to be compared to the 0.2 dB/km before irradiation*) have been observed for the Corning SMF28 fibers, meaning that 50% of the signal is absorbed in ~1.5 m. For DOFSs, in which the optical fibers are the sensitive element, RIA strongly decreases the available sensing length from kilometers down to a few meters for the most challenging environments. Usually, RIA can be calculated as:

$$\alpha_{RIA}(dB/km) = -\frac{10}{L(km)} \times \log\left(I/I_0 \right) \qquad \textbf{Eq(10)}$$

where I and I_0 are the intensities of the transmitted signal at a given time and before the irradiation starts, respectively. On the fiber market, some optical fibers are sold as radiation-hardened as their composition has been adapted to limit their RIA level for a certain type of irradiation (*usually steady state γ-rays up to MGy dose level*) and a certain range of wavelengths (*usually IR operation within the telecommunication windows*). Generally, this class of optical fibers comprises pure-silica core and fluorine-doped core optical fibers, both types having F-doped claddings. If for most of applications RIA

34

is a limiting issue that has to be mitigated, it should be noted that monitoring of the RIA in radiation-sensitive optical fiber can be exploited for radiation detection or dosimetry applications, for example at DESY facility in Germany [57].

- The second one is the **Radiation-Induced Emission (RIE)**. RIE acts as a parasitic light that superposes to the propagated signal. RIE originates from several sources.

If the energy of the incident particles is sufficient, Cerenkov light can be generated and guided in the optical fibers. This is the case for the example given in Figure 13 with the RIE spectra acquired during and after irradiation of a PSC MMF using a high dose rate X-ray facility, ASTERIX from CEA [168], that allows to reproduce the dose rates encountered during ignition experiments [20]. In addition to Cerenkov, the radiation can also generate some additional luminescence signals from pre-existing defects or new defects created during the irradiation. This is also illustrated in Figure 13 that provides evidence for the excitation of pre-existing or radiation-induced NBOHCs emitting around 650 nm during the first milliseconds following the X-ray pulse.
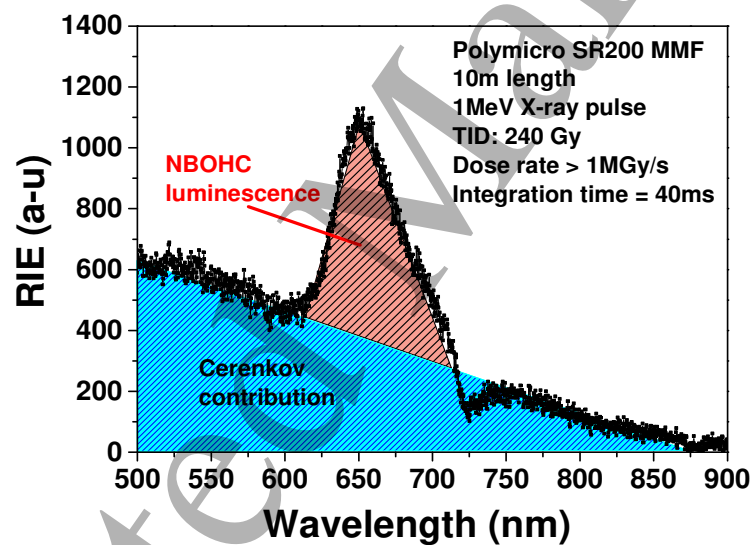
Figure 13. Spectral dependence of the RIE generated in a Polymicro SR200 MMF during and just after (40ms integration time) its irradiation with an X-ray pulse (240 Gy, > 1MGy/s, RT). The fiber length was 10m and the acquired spectrum is not corrected from RIA effect, or by the function transfer of the used HR4000 spectrophotometer from OCEAN Optics.

Regardless of its nature, RIE affects the SNR ratio, especially for systems operating in the visible domain such as diagnostics and in harsh environments associated with high dose rate (this is particularly the case for Megajoule class lasers). As for RIA, in the recent years, several studies have investigated how this luminescence, also called radio-luminescence, can be exploited to provide a real-time monitoring of the dose rate (or particle flux) in high energy physics facilities or for medical applications, radio-[169] or proton-therapy [170].

* Corresponding author: Sylvain Girard, sylvain.girard@univ-st-etienne.fr : Phone: +33 (0)477 915 812

- The third one is **Radiation Induced Refractive Index Change (RIRIC)**.

The observed refractive-index change arising from irradiation probably results from two mechanisms: change in the α-SiO$_2$ glass density and the RIA. The contribution of density ρ change to the refractive-index n can be explained by the Lorentz-Lorenz formula relying the two parameters:

$$\frac{n^2 - 1}{n^2 + 2} = K\rho$$

where the proportionality constant K depends on the glass polarizability. The part of the RIRIC caused by the point defects is described through the Kramers-Kronig relations that define the relation between the refractive index and the absorption. Compaction or swelling leading to glass density modifications was first observed by Primak [171] in bulk pure-silica exposed to high fluences of fast neutrons (> 10^{19} n/cm^2) with a densification of about 3%. It is remarkable to note that, under the same conditions, silica in its α-quartz form exhibits a density decrease of more than 10%. It was observed that neutrons change both types of silica into a common topological structure referred to as the metamict phase [172]. RIRIC affect also the optical fiber waveguide structure, as shown in [25]. For fiber samples exposed to fluences above 10^{19} n/cm^2 at temperatures exceeding 290°C, a linear compaction of 0.25% was observed, furthermore the densification effects of silica can be observed through the evolution of its Raman spectra for fluences above 10^{16}n/cm^2 in bulk silica [173].

III.1.2. Microscopic origins of the fiber degradation

A large number of studies have been conducted since more than 50 years in order to improve our knowledge about the nature of the radiation-induced point defects, also called color centers (RICC) that are generated into pure or doped α-SiO$_2$ glasses under irradiation. Very complete reviews are regularly done, resuming the evolution of our knowledge about this complex subject see for example [9,12,174,175,176] and references therein. The α-SiO$_2$ building unit is the SiO$_4$ tetrahedron, as in the quartz crystalline structure. In this unit, the central silicon (Si) atom is bonded to four oxygen (O) atoms occupying the corners of the tetrahedron. Figure 14a illustrates the 2D continuous random network representation of an ideal pure-silica network whereas Figure 14b illustrates the same glass containing intrinsic and extrinsic point defects such as dangling bonds, oxygen deficiencies. If those defects can exist before irradiation, they are then called precursor sites. The concentration of precursor sites generally decreases through the trapping of radiolytic electrons and holes while the concentration of radiation-induced point defects increases.

* Corresponding author: Sylvain Girard, sylvain.girard@univ-st-etienne.fr : Phone: +33 (0)477 915 812
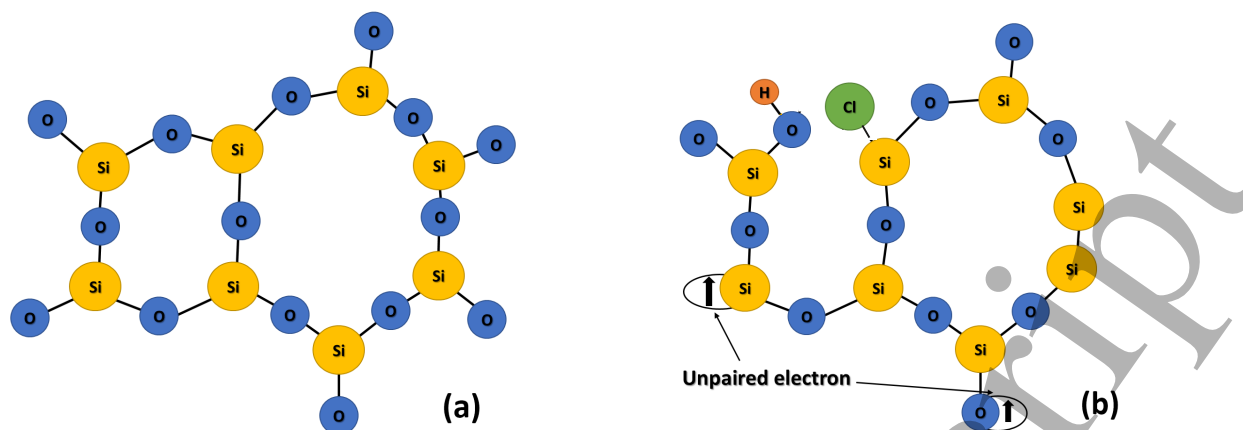
Figure 14. 2D illustration of the silica Continuous Random Network a) Undefected amorphous silica structure b) a-SiO$_2$ structure containing defects (here SiE´ center and NBOHC defects) either created during the fiber manufacturing process or by irradiation as well as chlorine and hydroxyl impurities.

This fundamental research is of primary importance as the identification of the nature and properties of the point defects responsible for the RIA at the wavelength of interest is mandatory in order to imagine radiation hardening approaches. Historically, these studies have been mainly done by combining different experimental tools allowing to associate the optical properties (*absorption, luminescence*) to their structure accessible, for paramagnetic defects, through Electron Paramagnetic Resonance (EPR) measurements. By combining these spectroscopic techniques on samples having been submitted to an external constraint (*radiation, temperature, hydrogen treatment…*) it was possible to correlate the evolutions of the concentration of a particular defect given by EPR with those of observed absorption or luminescence bands. Even if a very deep knowledge has been acquired for a number of defects, such as those related to pure silica, P- or Ge-related defects, this set of experiments presents some limitations that explain that the structures and optical properties of some defects are today still under investigation. As an example, for most of the studies, EPR and luminescence measurements are usually done on irradiated samples, after the end of the irradiation. Then, they are only able to characterize the signatures of point defects that are stable at the temperature of the experiments, all the transient defects that are shortly bleached after the irradiation ends are not measurable by these techniques. Furthermore, EPR and luminescence measurements are only applicable to paramagnetic defects and emitting centers, respectively; limiting the investigation to a reduced fraction of the defects that are absorbing within the silica gap.

Figure 15 gives an overview of the main absorption bands related to pure-silica (Figure 15a), Ge-related defects (Figure 15b) and P-related defects (Figure 15c). It should be emphasized that these bands have been observed in both bulk glasses and optical fibers. From this figure, several statements can be done:

- First, most of the known point defects pre-existing to the irradiation or created during the exposure, are associated with absorption bands peaking in the ultraviolet – visible domain, at

37

wavelengths below 800 nm (E>1.55 eV). As a general rule, the RIA levels are lower in the near-IR part of the spectrum at wavelengths above 800 nm.

- Second, the contribution of the various defects to the measured RIA will also depend on their localization in the fiber cross sections and on the amount of light that travels in this part of the fiber. The concentration of these defects is not always directly related to the dopant concentration, the defect generation or bleaching efficiencies can be affected by other parameters such as the fiber internal stress, or through photobleaching effects. It then appears as crucial to identify spectroscopic techniques allowing to have a spatial information with a resolution permitting to characterize the defect distribution over the fiber cross-section. Confocal microscopy of luminescence (CML) and cathodoluminescence (CL) have been investigated and their potential demonstrated in a series of publications [177,178,179,180]. An example of CL results is given in Figure 16 that illustrates the case of a GeCe-codoped optical fiber. For this fiber, some of the defect distributions are correlated to the internal stress generated at the interfaces between differently-doped parts of the fiber rather than to its composition.

- Origin of the observed RIA levels in the IR is still under investigation. A detailed analysis of the contribution of the described UV-visible absorption bands reveals that the tails of these bands are not able to fully explain the losses in excess. This means that although no clear absorption bands is observable in the IR domain for Ge-doped and pure silica glass, some defects are absorbing in this spectral range and still have to be identified. In addition to this, in the IR domain and for SM optical fibers, it is also mandatory to consider the impact of the fiber guiding properties on its RIA spectral dependence.

* Corresponding author: Sylvain Girard, sylvain.girard@univ-st-etienne.fr : Phone: +33 (0)477 915 812
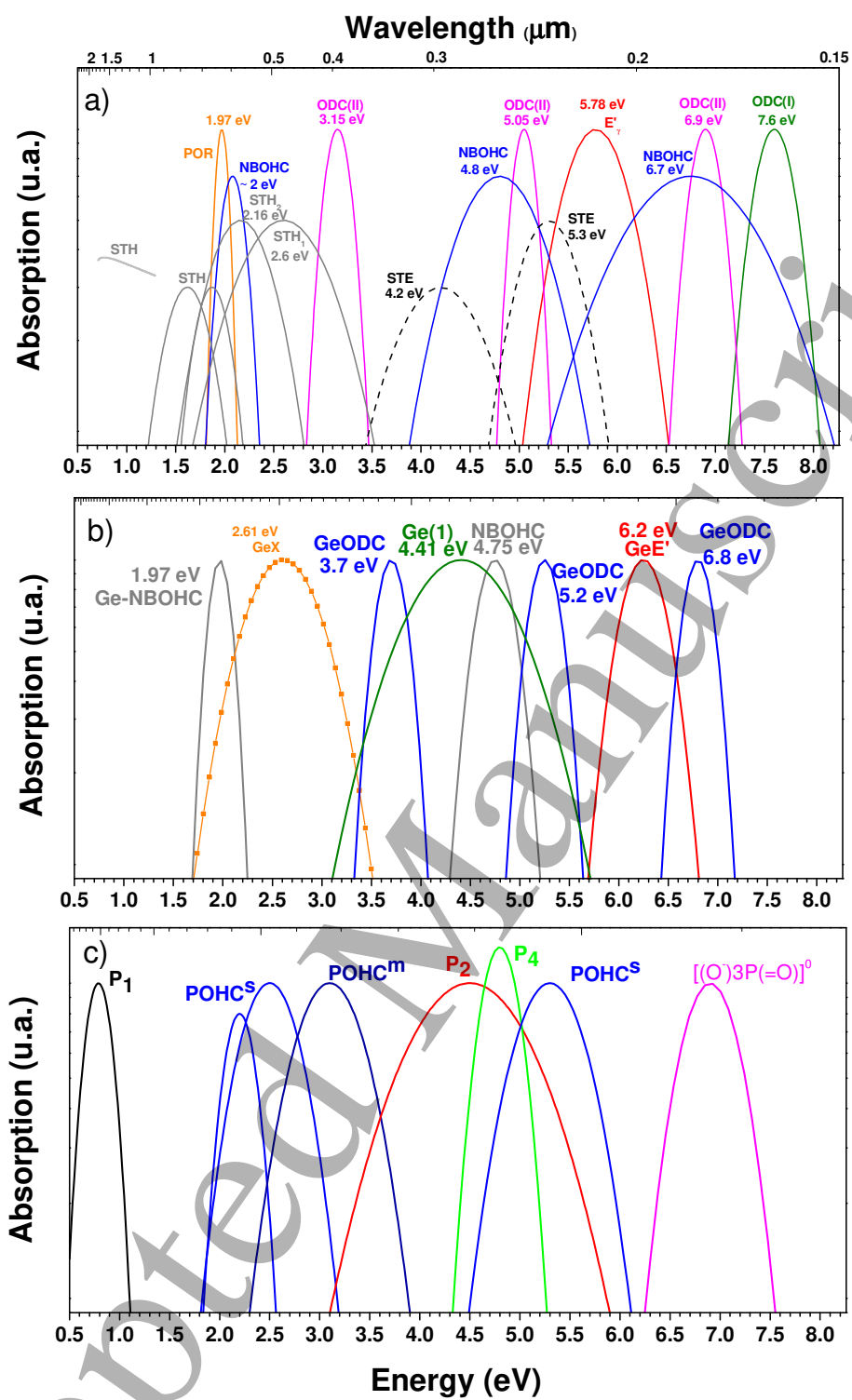
Figure 15. Main absorption bands associated with pure silica, Ge-doped a-SiO$_2$ and P-doped a-SiO$_2$

* Corresponding author: Sylvain Girard, sylvain.girard@univ-st-etienne.fr : Phone: +33 (0)477 915 812
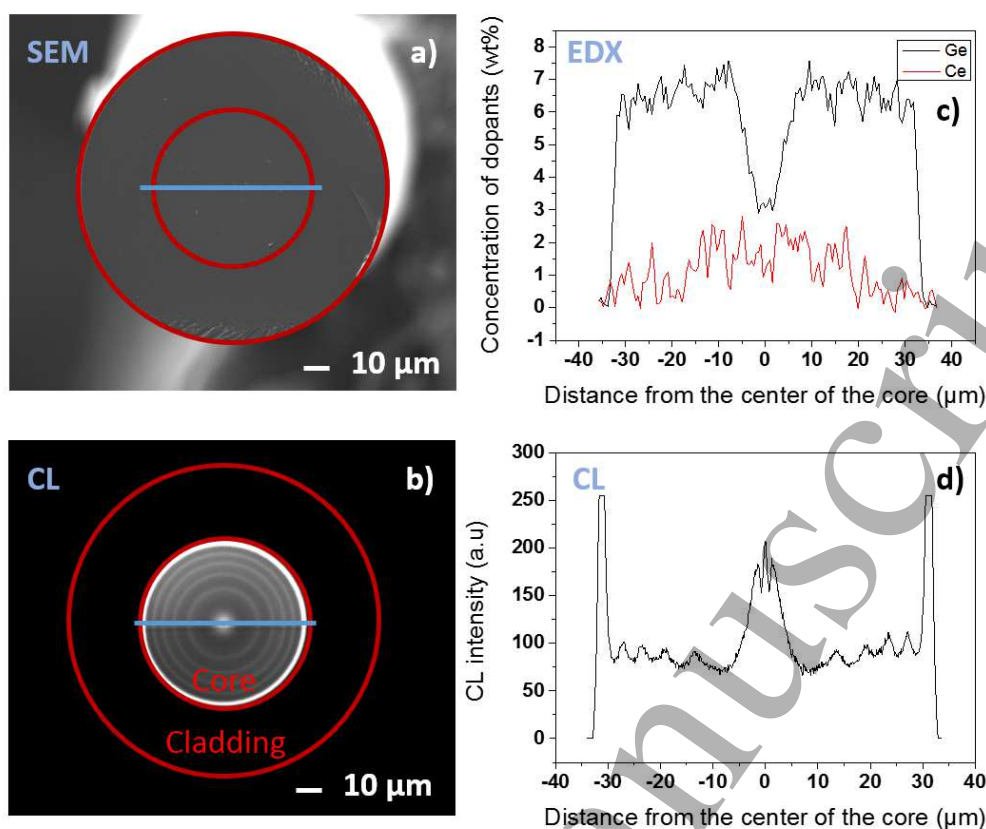
Figure 16. a) SEM image of a GeCe-codoped multimode optical fiber b) Panchromatic image acquired by CL of the same fiber c) EDX analysis of Ge and Ce radial distribution along the blue line of figure b) d) Radial distribution of the emitting centers along the blue line.

III.1.3. Intrinsic and extrinsic parameters affecting the fiber response

Numerous parameters have been shown to influence the radiation response of optical fibers, especially regarding the RIA levels and kinetics. Table 4 reviews those main parameters.

Table 4. Intrinsic and Extrinsic Parameters affecting the fiber response

Fiber Parameters				
Parameters	**Main cases**	**Impact on**	**Remark**	**Refs**
Core composition	Common dopants: Pure-silica, Ge, P, F, B, N, Al, rare-earths,…	Nature & concentration of defects ➜ RIA levels and kinetics	Affects all fiber types, UV to IR domains	[84], [83], [181], [182]
Cladding Composition	Common co-dopants: Pure-silica, Ge, P, F, B	Nature and concentration of defects➜ RIA levels and kinetics	Affects especially SMF	[183],
Impurities	Presence of impurities in core and cladding: OH groups and Cl-species	Nature and concentration of defects➜ RIA levels and kinetics	Affect mainly RIA of pure-silica and F-doped fibers ➜ major for rad-hard fibers	[184], [185], [186]
Fiber stoichiometry	Oxygen-deficient or oxygen-loaded fibers	Nature and concentration of defects➜ RIA levels and kinetics	Affect mainly RIA of pure-silica and F-doped fibers ➜ major for rad-hard fibers	[187],[188]

Drawing conditions	Speed, tension and temperature	Nature and concentration of defects➔ RIA levels and kinetics	Change the observed concentration of defects between preforms and fibers ➔ RIA is not easily changed by varying these parameters in the range used for specialty fibers.	[189],[190], [191], [192]
Irradiation Conditions				
Nature of particles	γ-rays, X-rays, neutrons, protons, electrons, heavy ions	Relative contribution of ionization and displacement effects ➔ Nature & concentration of defects ➔ RIA	Affect all fibers used for data transfer. For distributed fiber-based sensors using reflectometry techniques, the potential RIRIC will impact the sensor performance too.	[14],[193]
Dose (Fluence)	From very low (medical application – a few µGy) to huge (nuclear industry GGy, > 10^{20}n/cm²)	Nature and concentration of defects➔ RIA levels and kinetics Structural changes ➔ point and distributed sensors	Affect all fibers used for data transfer. For distributed fiber-based sensors. The dose dependence of RIA can be very complex, often increasing with dose, with sometimes saturation behaviors or sometimes RIA decrease with dose	[194], [195], [75]
Dose rate (Flux)	From very low (space) to huge (fusion-related facilities	Nature and concentration of defects➔ RIA levels and kinetics Structural changes	Usually RIA increases with the dose rate (rad-hard, Telecom-grade fibers) or RIA is dose-rate insensitive (P-doped fibers). A very few papers related Enhanced Low Dose Rate Sensitivity (ELDRS) effect in fibers	[196],[197], [198]
Temperature	From low (space applications) to high (800°C for nuclear industry°	Nature and concentration of defects➔ RIA levels and kinetics Structural changes	Temperature changes the efficiencies of defect generation and bleaching. It is often assumed that increasing T reduces RIA but this is not always correct.	[199],[200]
Fiber profile of use				
Wavelength	Depends on the application, ranging from UV to the near IR	Operational wavelength will fix the nature of the defect responsible for the RIA and then RIA levels and kinetics	If the application operates in a range of wavelengths (eg. diagnostics), the most affected wavelength has to be considered for the vulnerability study	[201]
Injected power	Depends on the application, ranging from very low (a few µW) to very high (W for high power lasers)	Can increase the bleaching rate of some point defects, could also lead to photodarkening in RE-doped fibers	Photobleaching is very difficult to predict as it is strongly defect-dependent	[202],[203] [204]
Pre-loading with gas	The presence of gas (hydrogen, deuterium) affects strongly the fiber response	Nature and concentration of defects➔ RIA levels and kinetics	Pre-loading sounds an efficient hardening technique ➔ Its efficiency strongly depends on the fiber profile of use	[205],[206], [207]
Pre-irradiation	A pre-irradiation can change the fiber radiation response	Nature and concentration of defects➔ RIA levels and kinetics	The impact of a fiber pre-irradiation is strongly fiber and application-dependent	[208], [209]

A first category of parameters, labeled as intrinsic parameters, are those related to the fiber itself. The main one is the fiber composition. It is important to notice that both the composition of the fiber core

* Corresponding author: Sylvain Girard, sylvain.girard@univ-st-etienne.fr : Phone: +33 (0)477 915 812

41

and cladding play a key role in governing the RIA levels of the fibers. The fibers can be mainly categorized in three sets when considering moderate dose levels of steady state γ-rays (typically up to 100 kGy): radiation sensitive, radiation-hardened and radiation tolerant fibers. This classification strongly depends on the harsh environments of interest and it is important to notice that none of the existing optical fibers has been shown to be radiation resistant for all the studied applications. In particular, this classification is not valid for transient exposures such as those associated with megajoule class lasers or some military applications.

- Among the **radiation sensitive optical fibers** have been identified all the fibers containing phosphorus (P), aluminum (Al) in either their cores or claddings, or more recently Lanthanum (La) or Thulium (Tm) [182]. Usually these fibers are associated with very high RIA levels in both the visible and IR parts of the spectrum and should be avoided for data-transfer. Finally, if these fibers are not suitable for most of the targeted applications in harsh environments, it should be noticed that they are promising candidates for radiation detection or dosimetry systems.

- Among the **radiation tolerant optical fibers** have been identified all the Telecom-grade germanosilicate optical fibers without P in their core and claddings. These fibers are acceptable for a wide range of applications, including for example short length data links in spacecrafts. These fibers are strongly sensitive to dose rate, temperature and photobleaching effects and may not be adapted for applications involving long lengths of optical fibers exposed to radiation.

- Regarding the **radiation hardened optical fibers**, from previous research, pure-silica core, fluorine-doped core (both with F-doped claddings) and nitrogen-doped optical fibers are the most radiation hardened optical fibers up to 100 kGy [210,211,212,213] for steady state irradiations. Optimization of these fibers is still possible to enhance their radiation resistance but implies a fine control of their fabrication process parameters, in particular the glass stoichiometry and fictive temperature, in order to control the nature and concentration of the point defects responsible for their degradation, such as chlorine-related impurities and self-trapped holes and excitons (STEs, STHs) [214],[187]. It should be noted that some of these fibers are today commercially available from manufacturers such as Fujikura [215], IXBlue Photonics [216] or Prysmian [217].

It is well known that part of the precursor sites, such as GLPCs and NBOHCs in germanosilicate and pure optical fibers, respectively, are partially induced during the process of drawing the preform into an optical fiber [84]. This has been clearly shown in [84,218], but numerous studies have reported that changing the drawing conditions (temperature, strain, speed) in the usual range exploited for the

* Corresponding author: Sylvain Girard, sylvain.girard@univ-st-etienne.fr : Phone: +33 (0)477 915 812

design of MCVD specialty optical fibers does not allow to significantly change the fiber radiation response [219,220]. If this limits the development of radiation hardening solutions, it appears as an interesting feature in terms of hardening assurance as it indicates that a fiber radiation response will be quite robust against small process changes during drawing. A complete study of the drawing influence on the radiation response of Telecom-grade optical fibers, drawn at larger speeds and tension has still to be performed to the best of our knowledge. Regarding the coating, it seems to not directly influence the RIA but its nature can impact the hardening approaches for some harsh environments [319] and also influence the response of some of fiber sensors such as those exploiting the FBG [221,222] or OFDR technologies [223].

For a given fiber, its vulnerability will strongly depend on the constraints associated to the application. Among the main constraints that can affect the radiation response, the main ones are the nature of the radiation: X-rays, γ-rays, neutrons, protons, the dose (or fluence), the dose rate (or flux) and also the temperature during the irradiation. For some specific environments such as the one associated with the nuclear waste repositories, other constraints have to be considered such as hydrogen presence [21]. For most of the optoelectronic devices such as image sensors, LEDs, there is a strong influence of the nature of irradiation on the device response, usually neutrons through the displacement damages affect more the devices. In the case of optical fibers, it has been shown that for fission (< 1 MeV) or fusion (14 MeV) neutrons, up to fluence of 10^{15} n/cm², the main degradation mechanism remains ionization [14]. Above this fluence threshold, some effects specific to the displacement damage start to appear, both in terms of optically-active point defects [17,87] and structural modifications [18]. Regarding the dose and dose rate, usually the amount of radiation damages increases with these parameters. The dose dependence of the RIA can follow various kinetics from linear increase, power law dependence or even more complex schemes that are explained by the competition during the irradiation between the generation of point defects and their recovery through thermal- or photo-bleaching processes [195,224,225]. Regarding the temperature impact on fiber response, especially RIA, changing the temperature affects the efficiencies of both the creation and bleaching processes of radiation induced color centers and then strongly affect both the RIA levels and kinetics. An important point is that contrary to what is usually stated in literature, it is not always true that increasing the temperature of irradiation will decrease the RIA levels [199]. This statement is usually deduced from thermal treatments performed after the end of the irradiation that give insights on the temperature effect on the bleaching process efficiencies only. Clearly the combined effects of temperature and radiation should be investigated in more details in the future.

Finally, the fiber operation conditions also clearly impact its radiation response, it is also the main factor to be exploited to improve its radiation tolerance. The main parameter is the selected signal

* Corresponding author: Sylvain Girard, sylvain.girard@univ-st-etienne.fr : Phone: +33 (0)477 915 812

wavelength. Usually, it is more favorable, if possible, to operate in the IR part of the spectrum where less of the point defects are absorbing than in the UV-visible domain [201]. For steady state γ-rays, the minimum of RIA is around 1-1.2μm in most of the classes of optical fibers [72]. It is important to note that the origin of IR-RIA still needs to be fully understood. If in some cases, these IR losses can be explained by the tails of the absorption bands of point defects associated with absorption bands peaking in the visible or near-IR domains (as the STHs [226,227,228]), for most of the fiber types (Ge-doped, P-doped,….), it was shown that this is not the case and that additional unknown absorption bands have to be added to reproduce the RIA spectral dependences [72]. Another phenomenon that can change the fiber behavior under irradiation is the power level of the injected signal through the photobleaching effect. For some optical fibers, it was shown that increasing the light power level in the optical fiber reduces the RIA levels during irradiation and accelerates the recovery processes post-irradiation [204]. The photobleaching efficiency then strongly depends on the radiation induced point defect(s) responsible for the RIA. As a consequence, photobleaching depends on the fiber type and application characteristics (wavelength, temperature…) but can be very efficient for some fibers such as germanosilicate optical fibers [202]. As a consequence of photobleaching, the radiation tests on optical fibers have to be done using a very low light power (typically well below 1μW) to establish the worst case scenario [229, 230]. In case the tests are intended to perform a comparison between the potential of different optical fibers for a given application, the best procedure consists in testing the optical fibers at the targeted light power of the application (for example mW power level) as the fiber ranking done at low power level (< 1μW) may not be representative of the one obtained following the applications requirements.

III.1.4. Modeling of the radiation-induced attenuation

One of the main difficulties regarding the radiation vulnerability study of optical fibers and OFSs concerns the representability of the available irradiation facilities to reproduce the constraints associated to the targeted environments. This is particularly true for space, where the dose rate is very low, the mission duration very long and the temperature varying in a large range. This is also an issue when new facilities or industries are built with environments (dose, dose rate, temperature) not covered by the existing radiation test facilities, eg the megajoule class lasers [20]. The accessible accelerated results have to be associated with models allowing to extrapolate the expected fiber degradation in the conditions of the application from the radiation test data. As it exists for microelectronic components, predictive simulation tools are needed to determine the RIA levels and kinetics of throughout the whole mission duration. Today, several empirical or semi-empirical models have been develop to predict the growth and decay kinetics of RIA versus the dose or time after irradiation basing on a limited set of radiation test results on the chosen optical fiber. Despite their

* Corresponding author: Sylvain Girard, sylvain.girard@univ-st-etienne.fr : Phone: +33 (0)477 915 812

intrinsic limitations, these tools are successfully used for space applications allowing the evaluation of the fiber RIA at low dose rate from high dose rate results. Usually these models are not considering thermal effects and are adapted to the case of Telecom-grade optical fibers or some of the radiation hardened passive and polarization maintaining optical fibers [231]. A selection of some of these models is listed in Table 5. A particular attention was also devoted to the building of models allowing to predict the behaviors of rare-earth optical fibers and related systems for space applications [232] including thermal effects [233].

Table 5. Selection of RIA models

Type of models	Authors	References
Power law	Griscom *et al.*	[194]
Saturating exponentials	Friebele *et al.*	[234]
Stretched exponential fit	Devine	[235]
Series of growth and decay events	Liu *et al.*	[236]
Saturated exponential curves with different other parameters	Kyoto *et al.* Levy	[237,238]
β^{th}-order dispersive kinetic model	Gilard *et al.*	[239,224]
First order fractal kinetics	Maskhov et al.	[225]
First and second order fractal kinetics	Griscom *et al.*	[195]
Kinetic model	Borgermans *et al.*	[79]
Nth order kinetic model	Friebele *et al.*	[240]

III.2. Point sensors: FBG

One key advantage of these point or distributed fiber sensing technologies remains the fact that only their sensitive part, being the sensing fiber, is exposed to radiation, whereas it is possible to install its interrogation part hundredths of meters or kilometers away. As a consequence, in all the performed studies, the performances of these sensors are characterized when only the sensing fiber is irradiated, not the interrogator parts as these electronic-based devices would be for sure more radiation sensitive than the fibers.

III.2.1. Basic mechanisms

As already explained in Section III.1.1, harsh environments, such as space, are characterized by the presence of radiation and particles, which can induce defects and density change through ionization

* Corresponding author: Sylvain Girard, sylvain.girard@univ-st-etienne.fr : Phone: +33 (0)477 915 812

or displacement damage processes. Radiation affects the FBG response in two main ways, as highlighted in the diagram of Figure 17.

First, the absorption bands related to the radiation-induced point defects degrade the optical fiber transmission. Then, even if at the basis of the FBG based sensors there is a wavelength measurement, the RIA degrades the grating performance by decreasing the SNR, until the peak appears undetectable [241]. To avoid this issue, small pieces of photosensitive fiber, with gratings written on them, can be spliced to radiation-hardened optical fibers for the signal transmission [242] or gratings have to be written directly in radiation resistant fibers at the Bragg wavelengths. However, a very important outcome of past studies is that the choice of radiation-hardened optical fibers does not ensure to design radiation tolerant FBGs, as demonstrated in [221].

Second, both the RIA and the density change can cause RIRIC, through the Kramers-Kronig dispersion relation and the Lorentz-Lorenz equation, respectively [243]. Therefore, the effective refractive index, the index modulation amplitude and the period of the grating can change because of the radiation, inducing a reduction of the peak amplitude and a radiation induced Bragg wavelength shift (RI-BWS, $\Delta\lambda_{Bragg}$). The peak amplitude reduction degrades the SNR. The RI-BWS can be defined as the sum of two contributions:

$$\frac{\Delta\lambda_{Bragg}}{\lambda_{Bragg}} = \frac{\Delta n_{eff}}{n_{eff}} + \frac{\Delta\Lambda}{\Lambda}, \qquad \textbf{Eq(11)}$$

and it entails an error on the sensing parameter measurement; i.e., a RI-BWS of 10 pm corresponds to a temperature error of 1°C, for a FBG having a temperature sensitivity coefficient of 10 pm/°C. Figure 18 reports the X-rays induced effects on the Bragg peak of a type I-UV FBG. Figure 18(a) shows the grating reflection spectra recorded during the irradiation; whereas Figure 18(b) highlights the induced peak shift and amplitude reduction.

* Corresponding author: Sylvain Girard, sylvain.girard@univ-st-etienne.fr : Phone: +33 (0)477 915 812

46
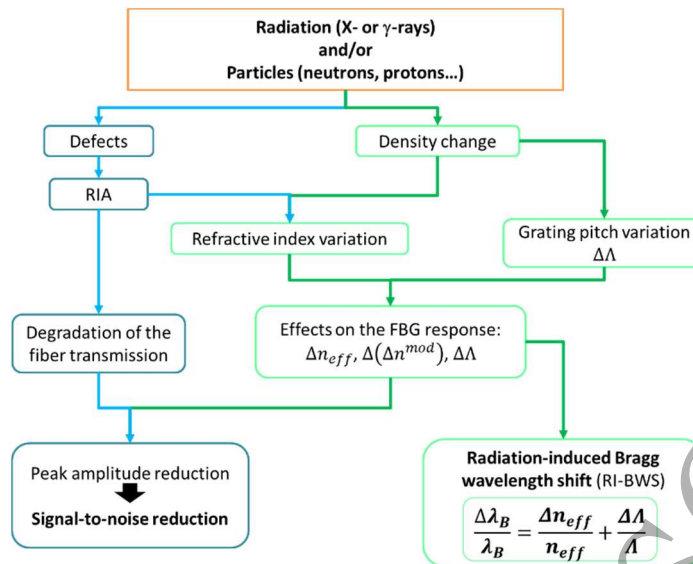
Figure 17. Schema describing how the radiation influences the FBG response.
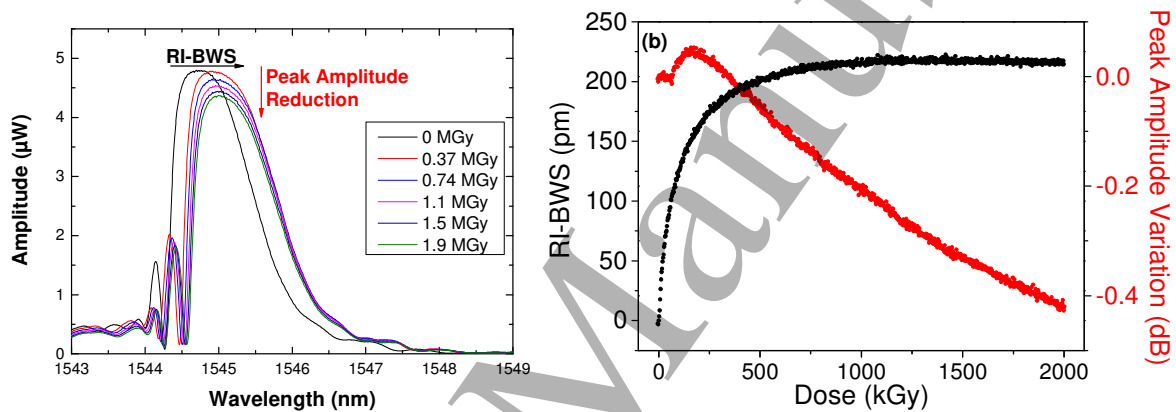
Figure 18. (a) Reflection spectra of a type I-UV FBG recorded under X-rays at RT with 120 Gy/s dose-rate. (b) RI-BWS (black points) and peak amplitude variation (red points) as a function of the accumulated dose.

For most of the cases, above all for type I-UV FBGs, under ionizing radiation the Bragg peak shifts towards the higher wavelengths with a saturating behavior. Neglecting the effects on density and then $\Delta\Lambda$, the red-shift corresponds to an increase of n_{eff}, which could be explained by an increase of absorption at wavelengths shorter than λ_B. The saturating behavior can result from a limited concentration of precursor defects or a competition between defect generation and recovery. In the first case, the saturation level should be dose-rate independent [244, 245].

III.2.2. Parameters affecting the FBG response

The RI-BWS depends on several parameters, as reported in Table 6.

Table 6. Most important parameters affecting the RI-BWS.

Fiber Parameters				
Parameters	**Main cases**	**Impact on BWS**	**Remark**	**Refs**
Fiber composition	Pure-silica, Ge, F, B, Al, N, Ce.	Nature & concentration of defects ➔ photosensitivity	no-correlation between the radiation-hardness of a fiber and that of a grating written in it	[**Erreur ! Signet non défini.**]

* Corresponding author: Sylvain Girard, sylvain.girard@univ-st-etienne.fr : Phone: +33 (0)477 915 812

Pre-treatments	H$_2$-loading	Nature and concentration of other extrinsic defects ➔ photosensitivity	The hydrogen increases the fiber sensitivity to the laser light ➔ it increases also the FBG radiation sensitivity ➔ RI-BWS saturates at higher levels and at higher doses for FBGs written in loaded fibers than in unloaded ones	[246,247]
Irradiation Conditions				
Nature of particles	γ-rays, X-rays, neutrons, protons, electrons, heavy ions	Relative contribution of ionization and displacement effects ➔ Relative contribution of defects and densification	Preliminary results reveal different FBG behaviors at equivalent doses when comparing X-rays, protons and electrons tests.	[222]
Dose (fluence)	From very low (space application – a few Gy) to huge (nuclear industry GGy, > 10^{20}n/cm²)	Concentration of defects and phenomenon of densification	The higher the dose, the larger the induced BWS.	[243]
Dose rate (flux)	From very low (space) to huge (fusion-related facilities	Kinetics of defects➔ competition between defect generation and annealing	For type I FBGs, the larger the dose-rate the larger the induced BWS.

For voids-FBGs, no dependence on the dose-rate. | [248,249] |
| **Temperature** | From low (space applications) to high (800°C for nuclear industry | Kinetics of defects➔ competition between defect generation and annealing | The higher the irradiation temperature, the smaller the induced BWS. | [250] |
| **FBG writing conditions** | | | | |
| **Type of gratings** | Types reported in Figure 6 | Nature of the periodic structure of the refractive index ➔ defect precursors and structural arrangement | Type I-UV gratings are more radiation sensitive than type I-IR ones.
Type IA FBGs are more sensitive than type I. | [107,251] |
Writing laser	Laser wavelength and pulse width	Nature & concentration of defects in the different fringe of the periodic structure of the refractive index	For example, type I gratings written with cw laser at 244 nm are less radiation sensitive than those written with pulsed lased at 248 nm.	[107]
Post-treatments	Annealing	Recombination of defects and precursors & structural relaxation	A post-inscription short thermal treatment at high temperatures (15 minutes at 750°C) reduces significantly the RI-BWS: from 60 pm down to 10 pm for a not-treated and a pre-treated type II-IR FBG.	[108,246]
	Pre-irradiation	Defect precursors depletion.	A pre irradiation will reduce the grating sensitivity.	

III.3. Distributed sensors

Mostly, three classes of DOFSs have been investigated under irradiation, those based on Rayleigh, Brillouin and Raman scattering phenomena, described in section II.3. For each of these technologies, several sensing schemes have been developed allowing to tune the sensing performances with respect to the targeted application in terms of probed length, spatial resolution, sensitivity. In some cases, the

choices made to develop the interrogator part can also modify the sensor vulnerability even by keeping the same optical fiber as the sensitive element, as it will be illustrated with the RDTS example.

III.3.1. Basic mechanisms

For sure, the RIA will affect all the fiber-based technologies reducing the available sensing length as the TID increases. Before irradiation, for most of the described technologies, sensing over kilometers or tens of kilometers is feasible whereas during and after irradiation the available length for sensing will decrease by a factor that depends on the considered harsh environment, the nature of the fiber and its profile of use. As an example, fixing an arbitrary dynamic range of 10 dB for the sensor and basing on the RIA measurements given in [73] for Ge-doped fibers, [252] for P-doped fibers and [73] for pure-silica core or F-doped fibers, Figure 19 illustrates the decrease of the sensing length with the γ-ray dose for OFS operating around 1550 nm either in single-ended (SE) or double-ended (DE) schemes. As it can be seen, at the MGy dose levels, even with radiation-hardened optical fibers, the available sensing length is strongly reduced, being less than one kilometer for all fiber types in these irradiation conditions. The use of DE sensors reduces by a factor of 2 this sensing range. For radiation sensitive optical fibers, such as phosphosilicate ones, the RIA is so important that it prevents their use in DOFSs for doses exceeding 1 kGy. For the given example, the considered fiber presents a RIA of 10 dB/m after a dose smaller than 10 kGy [252].

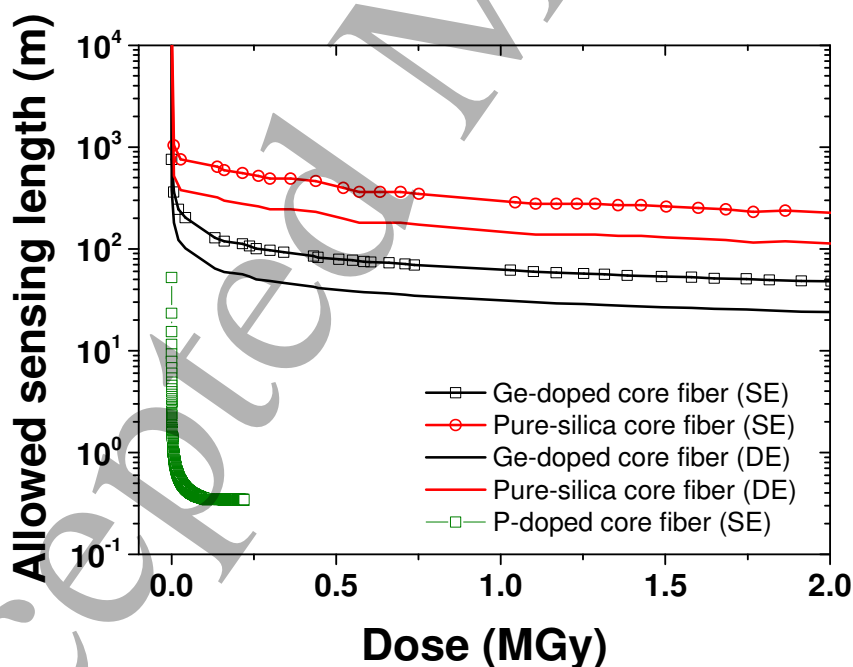**Figure 19. Illustration of the OFS sensing length decrease versus the dose for the main classes of optical fibers and a sensor having a 10 dB dynamic range at 1550 nm: Telecom-grade, radiation hardened and radiation sensitive. RIA data used to build this figure have been extracted from [73] and [252].**

* Corresponding author: Sylvain Girard, sylvain.girard@univ-st-etienne.fr : Phone: +33 (0)477 915 812

In addition to the RIA issues, it has been shown that radiation can change the structure of the pure- or doped amorphous silica glass, this effect being the more obvious at high fluences of neutrons causing displacement damages [16]. By changing the fiber refractive-index, the signature of the scattering mechanisms is affected in a way that usually induce an error in the evaluation of the measurand (temperature, applied strain….), as we have already highlighted for the FBG based sensors.

III.3.2. Macroscopic radiation response of Raman, Rayleigh, Brillouin-based sensors

Raman- based sensors: Several studies have been performed to characterize the RDTS performance under irradiation. The first studies [133,253] provided evidence that in addition to the reduction of the sensing length with the dose, RIA causes a dramatic error in the temperature evaluation done by a SE-RDTS. This error is due to the difference in the RIA values at the Stokes and Anti-stokes wavelengths, also noted differential RIA or ΔRIA. The attenuation spectra before and after a 6 MGy dose are shown in Figure 20a for a radiation hardened pure-silica core optical fiber (PSC-MMF) [82]. The probe wavelength (at 1064 nm) and the associated Stokes and Anti-Stokes signals are indicated, highlighting that these different signals are differently affected by radiation [82]. This differential RIA, ΔRIA, causes an error in the evaluation of the ratio between the Stokes and Anti-Stokes intensities, exploited to calculate the temperature. Its impact is shown in Figure 20b: when the 6 MGy irradiated optical fiber is used as the sensitive element of a SE-RDTS, the ΔRIA causes a direct error on the temperature estimation, the amplitude of this error increases with the fiber distance, reaching 30°C after a short length of about 100 m. Even if this error can be reduced by an appropriate choice of the fiber [254] or by applying some correction procedure [255], standard SE-RDTS are not adapted to operate in radiation-rich environments.
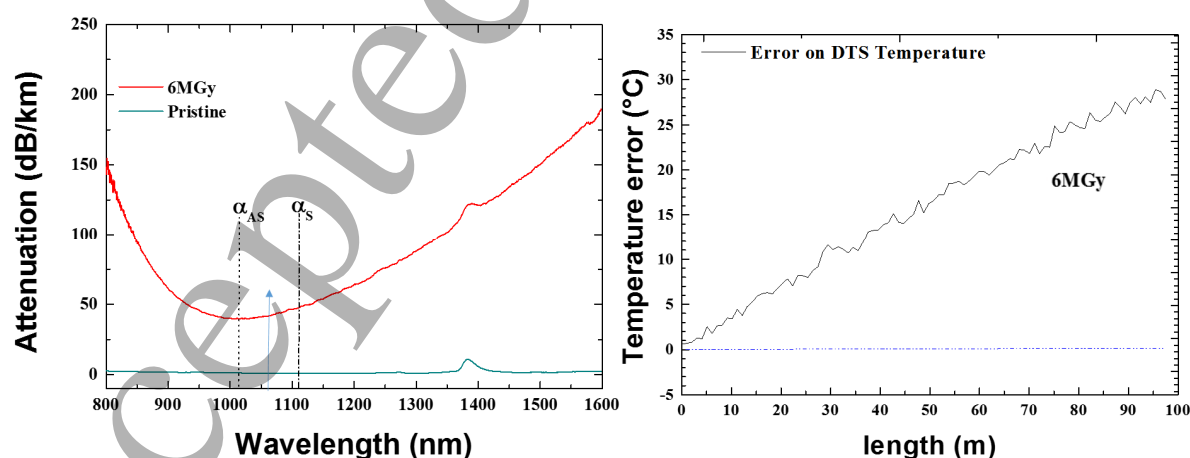
Figure 20. a) RIA spectra before and after irradiation at 6MGy in a PSC MMF. The Stokes and Anti-Stokes wavelengths as well as the probe laser light wavelength of used SE-RDTS are highlighted b) illustration of the error in the temperature measurement by this SE-RDTS using the PSC MMF pre-irradiated at 6 MGy. From [82].

* Corresponding author: Sylvain Girard, sylvain.girard@univ-st-etienne.fr : Phone: +33 (0)477 915 812

50

For the sensors exploiting a DE scheme, the negative impact of the ΔRIA can be avoided at the cost of doubling the RIA impact on the sensing length [253]. A recent work has been published, demonstrating that such a DE-RDTS can be used to monitor the temperature around 350°C in a nuclear facility at doses of a few kGy using metal coated PSC optical fibers [256].

Brillouin-based sensors: Several studies have been performed to characterize the radiation performance of Brillouin-based sensors [257], [258]. Here again the RIA limits the possible sensing range, for example from several kilometers down to a few hundredths of meters for doses exceeding 1 MGy using a radiation hardened optical fiber. Figure 21.a) illustrates the decrease of the Brillouin peak amplitude of a radiation hardened pure-silica core SMF during a γ-ray irradiation at a dose rate of ~1kGy/h, when using a BOTDA [82]. Although the irradiation run was carried out for 160 h, the signal was no more exploitable after ~ 80 h due to a too small SNR. An analysis of the Brillouin signature after ~53 h of irradiation reveals that the peak amplitude value was reduced by more than 90%. Another radiation effect on the Brillouin based sensor performances is a shift of the Brillouin frequency, hereafter named RI-BFS. This is due to the radiation induced effects on the acoustic speed, through the density, and to the RIRIC. Figure 21b) reports the RI-BFS as a function of the fiber length for these specific irradiation conditions (53 h). A RI-BFS toward lower frequencies is observed during the γ-ray exposure at 1 kGy/h up to 53 h; its value remains almost constant along the fiber and is equal to $(-1.8 \pm 0.4)MHz$. This RI-BFS cannot be distinguished from shifts caused by the measurands of interest (temperature, strain) and then causes a direct error of 1.5°C , for example, in case of temperature monitoring.

Figure 21. a) Normalized Brillouin peak amplitude response versus the irradiation time for a radiation-hardened pure-silica core single-mode optical fiber b) Radiation-induced Brillouin Frequency Shift (RI-BFS) as a function of the same fiber length after an irradiation dose of 53 kGy. From [82].

* Corresponding author: Sylvain Girard, sylvain.girard@univ-st-etienne.fr : Phone: +33 (0)477 915 812

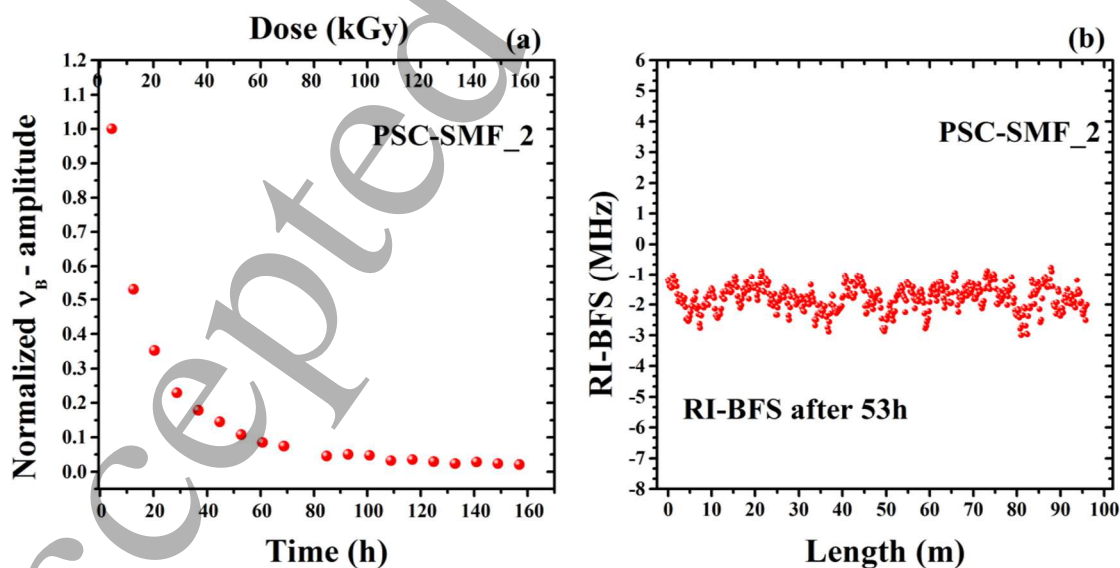The amplitudes and the kinetics of this RI-BFS depend on many parameters such as the fiber composition, the irradiation conditions. Today, the best identified optical fibers for Brillouin sensing at the MGy dose range are those with pure-silica or fluorine-doped cores. In addition to be associated with the lowest RIA levels in the near-IR range of wavelengths, these fibers also present the lowest RI-BFS, of a few MHz (equivalent to a few °C error) [82,258].

Rayleigh- based sensors: Several studies have been performed to characterize the performance of Rayleigh-based sensors in radiation-rich environments. The two main categories of sensors are those based on the OTDR technique, and those operating in the frequency domain, OFDR [57,259,260,261,262]. From the available results, it seems that except for some very specific environments such as those associated with very high neutron fluences, the Rayleigh signature remains almost unaffected by radiation and that RIA reducing the fiber sensing length remains the main degradation parameter to be followed. Exploiting this interesting radiation tolerance of Rayleigh sensing, several sensors have been investigated: some of them use radiation sensitive optical fibers for radiation detection and dosimetry while others exploit radiation tolerant or radiation hardened optical fibers for distributed sensing:

- *OTDR/OFDR radiation sensors*: associating these technologies with a radiation sensitive optical fiber such as Phosphorus, Aluminum or REDFs, it is possible to make distributed radiation detector with ODTR or OFDR sensors. OTDR are efficient tools to design dosimetry systems while OFDR are associated with a more complex response to RIA [57,263,264,265,252]. For distributed dose measurements, the RIA is measured all along the fiber and knowing its dose dependence, the dose profile along the fiber is deduced with typically one-meter resolution. First demonstration of such approach was a dosimetry system deployed at the Tesla Test Facility (TTF) using an OTDR probing a multimode phosphosilicate optical fiber at 850nm [266]. Today, another use of the OTDR based-systems is under qualification at CERN, in view of its deployment at the LHC [252,267].

- *OFDR temperature sensors*: For temperature sensing, the OFDR sensors associated with radiation hardened optical fibers are able to operate up to very high doses of γ-rays [261,262,268] and neutron fluences up to 10^{17} n/cm² [17].

- *OFDR liquid level sensor:* in the context of the post-Fukushima researches, a recent architecture for a water-level sensor to be implemented in nuclear pools has been demonstrated in [269] allowing to measure the liquid level with a spatial resolution better than 1 cm or 3 cm in the targeted normal and in accidental conditions, respectively.

* Corresponding author: Sylvain Girard, sylvain.girard@univ-st-etienne.fr : Phone: +33 (0)477 915 812

III.4. Rare-Earth doped fibers, EDFA and EDFS

Considering the interest of researchers for employing EDFAs and EDFSs in space missions, most of the radiation studies were performed at low γ-ray or X-ray doses (<1 kGy(SiO$_2$)) or low fluences of protons since the end of seventies. The first important outcome of these studies is that the REDF-based components are quite sensitive to radiation. An important decrease of the amplifier optical gain and an alteration of the noise figure are observed. These effects were sufficiently large to limit the EDFA integration in space. Furthermore, these studies demonstrate that the few meters (typically less than 20 m) of the selected active REDF explain the high EDFA radiation vulnerability. As a consequence, most of the past studies were then devoted to the RE-doped fiber characterization in order first to identify the best fiber types to increase the tolerance of EDFA or EDFS, second to understand the basic mechanisms at the origin of the high radiation sensitivities of REDFs compared to Telecom-grade passive optical fibers. Among the different types of RE-doped fibers, Erbium (Er) and Er/Ytterbium (Er/Yb)-doped fibers are the most studied ones [270,271,272,273,274] but other RE elements have also been considered in the past [92,275] or are today investigated as promising technologies for future applications [276]. Characterizing the radiation response of REDFs appears to be more complex than the characterization of the transmission degradation of passive optical fibers. Indeed, the response of REDFs can be investigated under passive configurations (white light source and spectrophotometer, the configuration called P$_{MIN}$ in part IV.4) similar to the ones used for passive fibers. However, as most of the applications used these waveguides in an active scheme in which the rare-earth ions are pumped in the near-IR to generate amplified signals in the IR, the most representative results are the ones obtained in active configurations [277,278,279,280]. These studies first reveal a high sensitivity of commercial RE-doped optical fibers at both pump and signal wavelengths. This excess of losses clearly limits their use as laser or amplifiers but their high radiation sensitivity could be exploited for dosimetry applications [152].

III.4.1. Basic mechanisms

Spectroscopic measurements revealed that the excess losses measured at the pump and signal wavelengths in REDFs are better explained by the nature of the matrix co-dopants (Al, P) added to facilitate RE incorporation rather than by the presence of the RE ions [281]. These co-dopants are added to facilitate the rare-earth incorporation while reducing the quenching effects. In the case of the Er-Yb-coped optical fibers, phosphorus is often used to increase the transfer efficiency from Yb^{3+} ions to Er^{3+} ions [281]. However, both Al and P dopants are associated with point defects responsible for an important RIA increase at both the pump and signal wavelengths [282,283]. Furthermore, radiation, at space levels, seems to be associated with limited changes in the RE ions spectroscopic

* Corresponding author: Sylvain Girard, sylvain.girard@univ-st-etienne.fr : Phone: +33 (0)477 915 812

properties [85] whereas at larger doses (> MGy), changes of the ion spectroscopic properties have also to be considered to fully understand the properties of the RE-doped glass [284,285].

III.4.2. EDFA macroscopic response

Under irradiation, the EDFAs designed without hardening strategies suffer from a strong gain degradation even at low doses. Figure 22 illustrates the gain decrease measured for an EDFA under X-rays at RT. For the used irradiation conditions, the EDFA gain decreases from 24 dB down to 14 dB after a dose of 3 kGy. The noise figure is also altered by irradiation, simulation shows an increase from 6.5 dB up to 10 dB after the same dose. In the same figure are also illustrated the RIA spectra of the Er-doped fiber measured at different doses, highlighting very high RIA levels at both the pump and signal wavelengths, exceeding 1 dB/m. These excess losses are mainly responsible for the EDFA and EYDFA gain and noise figure degradations.
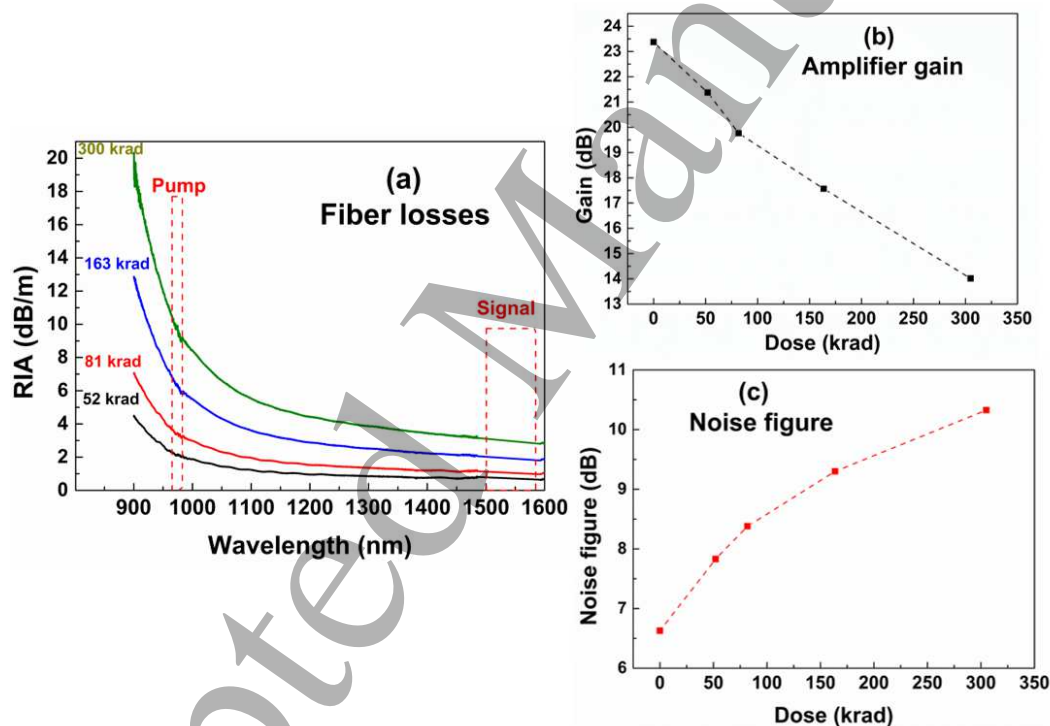
Figure 22. a) Illustration of the radiation-induced attenuation (RIA) spectra measured in a Erbium-doped optical fiber at different doses: 0.5, 0.8, 1.6 and 3kGy b) Evolution of the EDFA gain versus the deposited dose (experimental results) c) Evolution of the EDFA noise figure vs deposited dose (simulation results [90].

III.4.3. Parameters affecting the EDF response

Numerous parameters can affect the response of the EDFA or EDFS. Among them, all those previously described in section III.1.3 that affect the RIA levels in passive optical fibers are also impacting the induced losses in RE-doped fibers. They are summarized in Figure 23.

* Corresponding author: Sylvain Girard, sylvain.girard@univ-st-etienne.fr : Phone: +33 (0)477 915 812
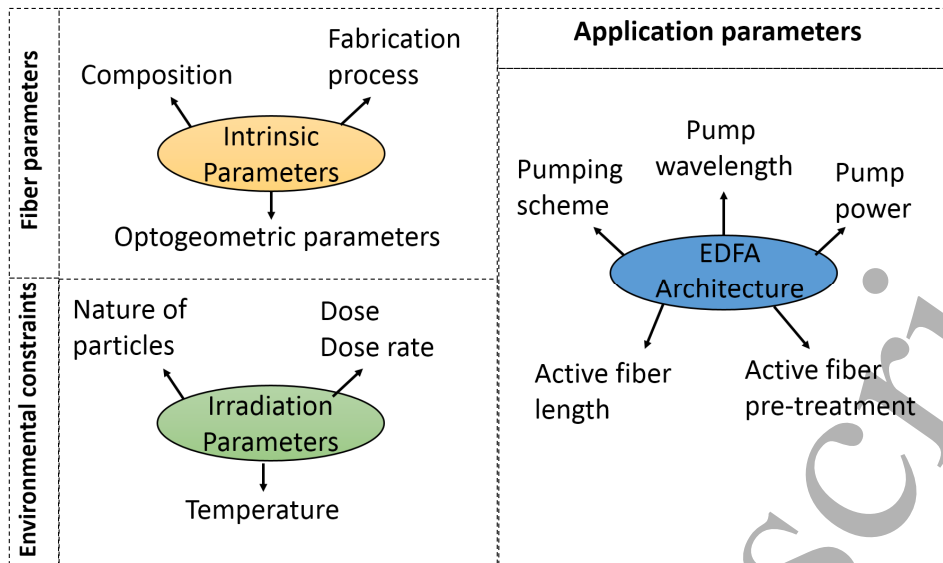
Figure 23. Illustration of the main parameters affecting the gain degradation of an EDFA or EYDFA under irradiation

Of primary importance is the REDF composition with a clear impact of the nature of codopants or additional RE ions (such as Cerium) used to optimize the amplification process. In addition to the fabrication process, the opto-geometric parameters have a strong influence too. As an example, for an ErYb-doped optical fiber, the double clad where the pump signal is propagating before being absorbed by the rare-earth ions can strongly contribute to the gain degradation if it appears to be too radiation sensitive and absorb the pump before its interaction with the RE ions embedded in the fiber core. Conditions of irradiation (*dose, dose rate, temperature*) influence the nature and growth and decay kinetics of point defects and then RIA at the wavelengths of interest. From the available literature, it seems that ionization processes govern the fiber degradation, as a consequence equivalent low doses of γ-rays, X-rays or protons seem to lead to the same degradation levels [273]. In the case of EDFA (or EFDS), the architecture choices also greatly impact the device radiation response:

- The EDFA radiation response depends on the **pumping wavelength**. It may appear advantageous to use 1480 nm pump wavelength as the RIA around this wavelength is lower than at 980 nm [286] and then the gain reduction is minimized. However, to the best of our knowledge, no space-qualified diodes exist at 1480 nm at the contrary of 980 nm, explaining that all current architectures of EDFA intended for space operate at 980 nm.

- The **EDFA pumping scheme** also influences its radiation response. Depending on the selected architecture (*backward, forward, bidirectional*), the pump and signal wavelengths present different RIA levels and kinetics and are also differently affected by the additional phenomena such as photobleaching. The EDFA optimization will depend on each application case and will for sure benefit from new simulation tools [146].

55

- The **active fiber length** is of primary importance. Without considering radiation, this length is optimized to obtain the best gain, usually by simulation, for a given optical fiber. Fibers with higher concentration of rare-earth ions allow to design EDFA with smaller length of active fiber, but can present quenching effects that limit the application process. As a general rule, as shown by Gusarov *et al.* [287], shorter is the fiber length, better is the amplifier radiation response. Recently a more systematic study about possible broadband radiation-resistant EDFA has been performed in [288].

- The **pump power** also strongly affects the relative contributions of point defect generation and bleaching mechanisms. Pump at a sufficient power level can induce both a darkening of the glass by creating point defects and simultaneously favor the bleaching of absorbing species through photobleaching [289]. Competition between these phenomena is complex but was studied in details in [93]. At the device level, the observed gain degradation can then be pump power dependent rendering mandatory to perform the radiation tests in conditions representative of the application.

- **Active fiber pre-treatments:** As it will be discussed in more details in section IV.1.2 about hardening techniques, it is possible to change the active fiber radiation response and then the EDFA response by pre-treating the waveguide, with gas loading as an example. Every pre-treatment allowing to change the nature, concentration and kinetics of the point defects responsible for the RIA around the pump and signal wavelengths will affect the EDFA radiation response either in a positive or negative way.

III.5. Gyroscopes

Commercial Space FOGs have to deal with radiation at doses up to 1 kGy for 2 to 20 years missions with a strong variability due to different orbits and shielding configurations. The various FOG subassemblies react differently to radiation as detailed hereafter:

- **Electronics:** Radiation effects are obviously very important for the design of the digital part of the FOG servo loop. They are outside the scope of the present review.

- **Laser diode and PIN photodiode:** Although the pump laser diode includes both a semiconductor laser and a FBG, neither the laser nor the photodiode display any significant degradation under proton and/or gamma exposures. The radiation induced threshold current variation of the laser diode [290] remains negligible for the FOG design. Regarding space needs, those components are considered as radiation insensitive [291].

- **The lithium niobate modulator:** is immune to radiation too. No transparency variation is observed at space relevant doses [290,292,293]. Hypothetical variations of its electro-optic

56

response are not an issue too as the FOG's servo loop continuously adapts itself to the modulator.

- **Passive optical components:** such as couplers and isolators do react to irradiation (through RIA) as they each contain a few meters of optical fiber [294,295]. Their transmission properties are then affected but the involved fiber length in those components remains sufficiently small to be neglected if the selected fiber is a Telecom grade fiber such as the Corning SMF28. For the cases where the FOG design imposes an exotic optical fiber associated with higher RIA levels than SMF-28 fiber, the radiation response of those components would then become of importance. The transparency is not the only affected parameter during irradiation: spectral variations of those components due to RIA are detectable for relevant space dose but not strong enough to restrict the FOG design of even for high precision ones. With the continuous improvements of FOG performances, this could still become an interesting topic in the future.

- **Optical coil:** The Sagnac coil contains a length of PM fiber ranging from a few hundreds of meter to several kilometers according to the aimed FOG performance. With such a fiber length, any RIA phenomenon quickly becomes a problem as the available optical power takes a hit and the FOG rotation noise rises. This excess of optical losses cannot be entirely mitigated by increasing the optical source power implying the use of radiation resistant optical fiber for the Sagnac coil. The fiber transmission is not the only affected parameter during irradiation: spectral variation occurs and affects the FOG scale factor performance. This spectral effect is negligible nowadays with radiation resistant fibers and current high end FOG performance but as the FOG performances are still increasing, this could still become an interesting topic too in the next years. Radiation induced birefringence variation could also theoretically affect the FOG but this has not been observed today in existing commercial systems.

- **Erbium doped optical fiber:** High performance FOGs use EDFs as an ASE optical source. The fiber length ranges between 1 and 10 meters while the power extracted at 1550 nm is in the 10 to 100 mW range. As already discussed, EDF is much more sensitive to RIA than passive optical fiber. As a consequence, this subpart of the FOG, albeit being far shorter in length than the Sagnac coil, is an important contributor to global FOG's radiation degradation and use of radiation hardened optical fiber appears mandatory. Radiation induced optical spectrum change is inevitable, as the RIA change the operating point of the ASE source, but does not limit today the FOG scale factor performance.

* Corresponding author: Sylvain Girard, sylvain.girard@univ-st-etienne.fr : Phone: +33 (0)477 915 812

IV. Recent advances on radiation hardening

As more and more applications are envisaged for optical fibers in harsh environments, strongly extending their use to sensing, new approaches have to be followed to improve the radiation tolerance of optical fibers and fiber-based devices and to extend their lifetimes in harsh environments. In this part of the review, the recent advances regarding the hardening of optical fibers, FBG and distributed sensors are given, with a particular focus on the technologies already evaluated for space programs.

IV.1. Optical fibers

Improving the radiation tolerance of optical fibers is possible by controlling the nature and concentrations of point defects in order to limit the RIA at the wavelengths of interest. For this, different approaches have been followed. The first one, called hardening-by-component, consists in tuning the fiber composition in order to decrease the RIA levels in the spectral domain of interest for a given environment while maintaining the requested optical performances. The second one corresponds to pre-treatments of the fibers in order to change (decrease) its number of precursor sites, reducing as a consequence the number of radiation-induced point defects. It is important to mention that today there exists no optimal composition allowing the design of an optical fiber with reduced RIA for all environments of interest. As an example, the so-called radiation hardened pure-silica core and fluorine-doped core fibers present the best radiation response in the infrared part of the spectrum under steady state γ-rays (*high energy physics facilities, nuclear power plants,…*) [75] whereas these fibers show the highest transient RIA after an X-ray shot (*fusion by inertial confinement*) [181].

IV.1.1. Hardening-by-component

Up to now, most of the research has been devoted to the identification of the best classes of optical fibers for operation either in the visible domain or in the infrared part of the spectrum and up to doses of a few MGy. This first class of fibers is of interest for the plasma diagnostics of the ITER facility that require large core MMFs (above 100 µm) able to transmit light in the visible. Numerous studies have been conducted in Europe [296], Russia [297] and Japan [298] allowing to identify the best candidates for this application that appear to be pure-silica core (PSC) or fluorine doped optical fibers. After that, several studies focused on the hardening of these fibers to reduce the RIA levels in the visible domain. First attempts were done to reduce the impurity levels in the fiber core and cladding. Two main classes of silica were available; the first one also called "dry silica" contains low levels (>1 ppm) but this is achieved by increasing the amount of chlorine into the glass. As a result, this kind of fiber presents high transmission level in the IR but lower transmission in the UV range compared to the second class of

* Corresponding author: Sylvain Girard, sylvain.girard@univ-st-etienne.fr : Phone: +33 (0)477 915 812

58

silica, the "wet silica" that contains high hydroxyls amounts (>100ppm) and low Chlorine concentration (< 1ppm). For ITER needs, the wet silica is better adapted but under irradiation these fibers are characterized by a strong RIA around 600-650nm that is related to the NBOHC, see Figure 12. The NBOHC high concentration is related to the presence of hydroxyls groups that act as precursor sites:

$$Si\text{-}OH \rightarrow 2\ Si\text{-}O^{\cdot} + H_2 \qquad\qquad Eq(12)$$

To overcome this limitation, new class of glasses were made, mainly in Russia, combining both low hydroxyl groups content (<1 ppm) and low chlorine impurity (< 1ppm) content. Radiation tests reveal that for these fibers, the strong diminution of precursor sites opens channels for the generation of less-studied room temperature unstable defects: the self-trapped holes (STHs). These defects have been studied in details in [227] and are associated with absorption bands in the visible (see Figure 15), making these fibers difficult to qualify for the targeted applications. Another efficient way to minimize the NBOHC concentration is to slightly dope the glass with fluorine. Adding this element does not induce the appearance of F-related defects whereas it has the demonstrated ability to passivate some point defects such as the NBOHCs. In addition to the ITER studies, a very complete investigation was performed by CERN to select the best optical fibers for the Large Hadron Collider (LHC) data links operating at 1310 nm. For these applications too, the most tolerant fibers to the considered dose of 100 kGy(SiO_2) are fluorine-doped optical fibers from Fujikura [215]. These fibers present quite complex RIA growth kinetics at this wavelength but the RIA levels remains below 5 dB/km at 100 kGy dose for the IR wavelengths: 1310 nm and 1550 nm.

IV.1.2. Hardening by pre-treatment

Another very efficient approach to reduce RIA due to NBOHC consists in loading the fiber core with gas, this gas being able to quickly react with the radiation induced point defects and passivate them. Hydrogen and deuterium are the most investigated as fibers can be easily loaded with these gas. This treatment was deeply studied by the fiber community in order to enhance the photosensitivity of the germanosilicate optical fibers in view of their functionalization with FBGs. Several studies reported that the hydrogen presence strongly changes the fiber radiation response, regardless of its composition [299,300]. For PSC or F-doped optical fibers, the hydrogen presence improves their radiation hardness in the visible domain thanks to the passivation of the NBOHCs [301], the drawback being that these defects are converted into hydroxyls groups absorbing in the IR part of the spectrum and in other defects causing an increase of induced losses in the UV part of the spectrum. The process at stake is the following:

$$2 \times Si\text{-}O^{\cdot} + H_2 \rightarrow 2 \times Si\text{-}O\text{-}H \qquad\qquad Eq(13)$$

* Corresponding author: Sylvain Girard, sylvain.girard@univ-st-etienne.fr : Phone: +33 (0)477 915 812

This example clearly shows that the efficiency of this hardening technique strongly depends on the application needs as the hydrogen presence will enhance the concentration of some defects such as H(I), H(II) centers absorbing in the ultraviolet while passivating other defect structures. Using deuterium provides globally the same effect, one difference concerns the spectral positions of the related D2 species that differ from those of hydrogen species, allowing for some applications to less impact the signal propagation [22]. One of the main concerns with this hardening solution is that the hydrogen diffuses out easily from the fiber at RT and that without specific mitigation solutions, it is not possible to keep the gas inside the waveguide for more than a few days. This is of particular concern for long duration space missions or long lifetime's facilities and existing solutions will be detailed in paragraph IV.4. More recent studies investigates the potential of adding an excess of oxygen into the optical fibers, varying the manufacturing process or by direct O_2 loading of the fiber at high temperature and high pressure [187,188,302]. Contrary to hydrogen, oxygen is not mobile at RT and its concentration will remain constant during the fiber lifetime. Such treatment also strongly changes the defect equilibrium under irradiation, with positive or negative impact on the RIA levels and kinetics depending on the considered signal wavelength. In [302], a larger RIA is reported in the UV and visible domain whereas in [187] and [188], the authors reported a positive impact of an excess oxygen on the RIA levels in the IR part of the spectrum for PSC optical fibers. In addition to gas, other pre-treatments can change the nature and concentrations of point defects generated under irradiation. This is for example the case of a pre-irradiation treatment that can be used to convert the existing precursor sites into optically-active point defects. If it is possible, e.g. by a thermal treatment, to bleach these defects, the treated fiber can present a better radiation response when exposed to a second irradiation as it contains a lower amount of precursor sites. Such effect was patented [209] and its efficiency on the response of PSC optical fibers was demonstrated in [208].

IV.2. FBG

FBGS are affected by radiation through two phenomena: the decrease of the FBG peak reflectivity and the Radiation-Induced Bragg Wavelength Shift (RI-BWS). The first one can be quite easily mitigated using several types of inscription methods. For the RI-BWS, since its amplitude and kinetics depend on so many parameters, the usual identification approach of the most tolerant FBG for a given application consists in testing each FBG technology at facilities reproducing the radiation constraints associated to the aimed application (*see the 2013 review [243]*).

Grobnic *et al.* showed that the gratings, of type I and II, written with femtosecond IR laser in unloaded Ge-doped or PSC fibers are among the most radiation resistant under γ-rays at RT [303]. RI-BWSs of less than 15 pm were observed at the accumulated dose of 100 kGy. Even the type I-IR FBGs are more radiation tolerant than type I-UV ones. This may be explained by the fact that the high laser peak power

* Corresponding author: Sylvain Girard, sylvain.girard@univ-st-etienne.fr : Phone: +33 (0)477 915 812

density values used to write the FBGs probably convert all the precursor sites into point defects during the grating inscription, reaching a stable state maintained during irradiation [107].

Morana *et al.* recently patented a method for fabricating FBGs resistant to very harsh environments mixing high doses and high temperatures [304,108]. These gratings are written in radiation hardened optical fibers (PSC or F-doped fibers), to ensure the signal transmission, with a femtosecond IR laser (i.e. at 800 nm) and then subjected to a thermal annealing treatment at 750°C lasting at least 15 minutes. The laser power density has to be higher than the threshold needed to generate type II gratings, since the thermal treatment at 750°C will erase all the type I component, only the type II one resists to such high temperature. It is the post-thermal annealing performed on the gratings before the irradiation that makes the FBGs more resistant. The robustness of these gratings has already been confirmed in several radiation environments, involving X-rays (up to 3 MGy dose) or γ-rays (up to 200 kGy) and operating temperatures as high as 350°C [305,306], a total fast neutron fluence of $\sim 5 \cdot 10^{19}$ n/cm² and a total gamma-dose of ~5 GGy [25], and high energy protons (63 MeV) up to fluences of about 10^{13} p/cm² [307]. Figure 24a reports the response of such rad-hard gratings under X-rays at three different temperatures: low (-20°C), room (30°C) and high (230°C) temperatures. Independently of the irradiation temperature, the induced error on the temperature measurements is always lower than ±1°C. Figure 24b compares the responses of a classical type I-UV grating and of a rad-hard FBG under flux of about 3×10^{12} protons/(cm²·h) at RT, up to a fluence of 10^{13} protons/cm², which corresponds to an equivalent TID of about 9 kGy(SiO₂). The Bragg peak of the classical FBG shifts of about 18 pm at the maximum TID, whereas the response of the rad-hard grating is not influenced by protons. As a consequence, such rad-hard FBGs will be efficient temperature and/or strain sensors in space, since they are insensitive to ionizing radiation at low and high temperatures and insensitive to TNID related to protons.

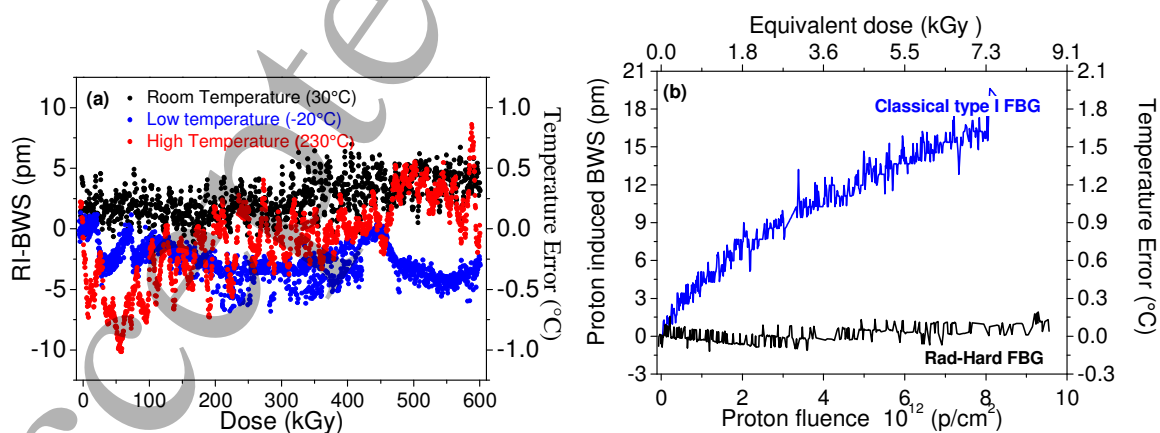**Figure 24. (a) BWS induced on rad-hard FBG by X-rays at different temperatures (30°C – black points; -20°C – blue points; 230°C – red points), as a function of the TID, up to 600 kGy. (b) Proton-induced BWS of a classical type I-UV FBG (blue curve) and a rad-hard FBG (black curve) as a function of the proton fluence.**

* Corresponding author: Sylvain Girard, sylvain.girard@univ-st-etienne.fr : Phone: +33 (0)477 915 812

Recent studies [308,107,249] were focused on the radiation response of the voids-gratings. They show a complex behavior under radiation: when the exposure is performed at RT, these gratings are as resistant as the Type II gratings (RI-BWS less than 5 pm at 1 MGy dose, for a voids-FBG written in a F-doped fiber [249]); however, when these FBGs are exposed to combined effects of radiation and temperature, the Bragg wavelength of the voids-FBGs blue-shifts, without showing a saturating behavior with the accumulated dose [107, 249].

IV.3. Distributed sensors

In this section, we discuss how the radiation tolerance of distributed sensors can be improved by appropriate choices at the component (fiber) or at the interrogation system levels. Today, these different technologies are not directly considered for use in space to the best of our knowledge. Their integration remains limited by the interrogator parts of the sensors that are not yet sufficiently miniaturized and radiation tolerant. In the near future, this limitation will probably be overcome thanks to the new generation of miniaturized integrators based on ASPICs (Application Specific Photonic Integrated Circuits). Such an on-chip interrogator already exists for FBG strain or temperature sensing [309]. However DOF technologies are today of major interest for the Ground environments associated with nuclear power plants, high energy physics facilities or radioactive waste repositories. For all these environments, the acquisition units can be stored in radiation-free zones and the sole sensing fiber be exposed to the harsh radiation constraints.

IV.3.1. Rayleigh DOFS

Several papers demonstrated that the fiber Rayleigh signature used by OFDR sensing technology is robust against radiation [310]. However, radiation affects the acrylate coating properties and that, by stabilizing the coating through pre-thermal treatments, the precision of the OFDR measurements is increased [223]. The only remaining parameter to consider is then RIA that limits the available sensing length. As these sensors operate at Telecom wavelengths, in the IR, the best fibers are usually PSC optical fibers or F-doped optical fibers, as shown in Figure 20, allowing to use fiber lengths exceeding 100 m under irradiation. In the future, the capabilities of Rayleigh based sensors may be enhanced thanks to the development of a new generation of fibers, the so-called All Grating Fibers [311]. These fibers contain densely spaced low reflective (R<0.1%) Draw Tower Gratings (DTG®s) [311]. Combined with an OFDR interrogator, these fibers should greatly improve the measurement dynamics and then increase the tolerance to RIA effects. By combining the OFDR technology with a radiation sensitive optical fiber, it appears possible to detect radiation and maybe to perform spatially-resolved dose

* Corresponding author: Sylvain Girard, sylvain.girard@univ-st-etienne.fr : Phone: +33 (0)477 915 812

measurements with resolution of 15 cm but with a more difficult calibration phase of the sensor than for OTDR-based dosimetry systems [259].

IV.3.2. Brillouin DOFS

For the Brillouin-based sensing, two radiation effects have been observed that reduce the sensor performances: the RIA the radiation-induced Brillouin Frequency Shift (RI-BFS). Although the microscopic origin of the RI-BFS is still not fully understood, the amplitude and growth kinetics of the RI-BFS with the dose clearly depend on the fiber composition. As a consequence, optimizing the fiber for sensing in harsh environments implies to simultaneously reduce the RIA and RI-BFS levels. From today's knowledge, the fluorine-doped fibers are the best candidates for such applications, having limited RIA levels at MGy dose levels (below 50 dB/km at 1550 nm) and limited RI-BFS of a few MHz (equivalent to a temperature error of a few Celsius degrees). Regarding the RIA issues, some architectures of Brillouin sensors allow to achieve a greater dynamic of measurements than others, allowing to partially mitigate the RIA effects and to consider higher sensing distances at MGy dose levels [312].

IV.3.3. Raman DOFS

For the Raman-based sensing, two phenomena reduce the sensor performances: the RIA and the differential RIA (ΔRIA). If an appropriate choice of the fiber allows to reduce the RIA-related constraints, it appears very difficult to overcome the ΔRIA issue by tuning the fiber composition or its fabrication process. For this sensor, it is however possible to improve its radiation hardness by working on the architecture of the interrogator.

The first solution is to use a double-ended architecture that allows to compensate for the ΔRIA but at the cost of doubling the RIA issues. With such architecture and as demonstrated in [82, 133,253], it is possible to maintain the quality of the temperature measurements thanks to the correction made possible by probing the sensing fiber from its two ends. Using this scheme, in [256], the authors show that temperature measurements along a PSC optical fiber with a gold coating at 260°C are possible thanks to a positive combined effect of temperature and radiation on the fiber RIA.

Another solution, recently published in [313], allows to keep a single-ended scheme (and then a reduced RIA impact) while avoiding the ΔRIA negative impact. This architecture of SE-RDTS exploits two probing lasers at given wavelengths allowing to record simultaneously the OTDR traces at the Stokes and Anti-Stokes wavelengths in addition to the Stokes and Anti-Stokes traces. By this way, it is possible to correct these last traces for ΔRIA caused by radiation or the appearance of bending losses and keep the temperature measurement precision. Associated with a radiation sensitive optical fiber,

* Corresponding author: Sylvain Girard, sylvain.girard@univ-st-etienne.fr : Phone: +33 (0)477 915 812

63

this system could allow to simultaneously record the dose (through RIA) and temperature distributions along a unique optical fiber [313].

IV.4. Rare-Earth Doped Fiber Amplifiers and Sources

As previously discussed in III.4, the high radiation sensitivity of EDFA, EYDFA or sources is mainly explained by the high sensitivity of the REDFs, either Erbium doped (EDF) or Erbium-Ytterbium-doped (EYDF). To improve the hardness of these amplifying systems, the first investigated solution was to enhance the radiation tolerance of these active fibers to decrease the observed RIA levels at the pump (around 900nm – 1 μm) and signal wavelengths (around 1550 nm). Since 2010, several techniques have been described in literature to achieve this goal and they are schematically summarized in Fig.25. In addition to these hardening-by-component approaches, it also appears possible to optimize the amplifier architecture (hardening-by-system) to reduce its radiation vulnerability, regardless of the fiber behavior. Finally by combining these two hardening approaches, it is today possible to conceive EDFAs and EYDFAs with optimized performances and reliability for a given space mission profile rather than for on-Ground testing.
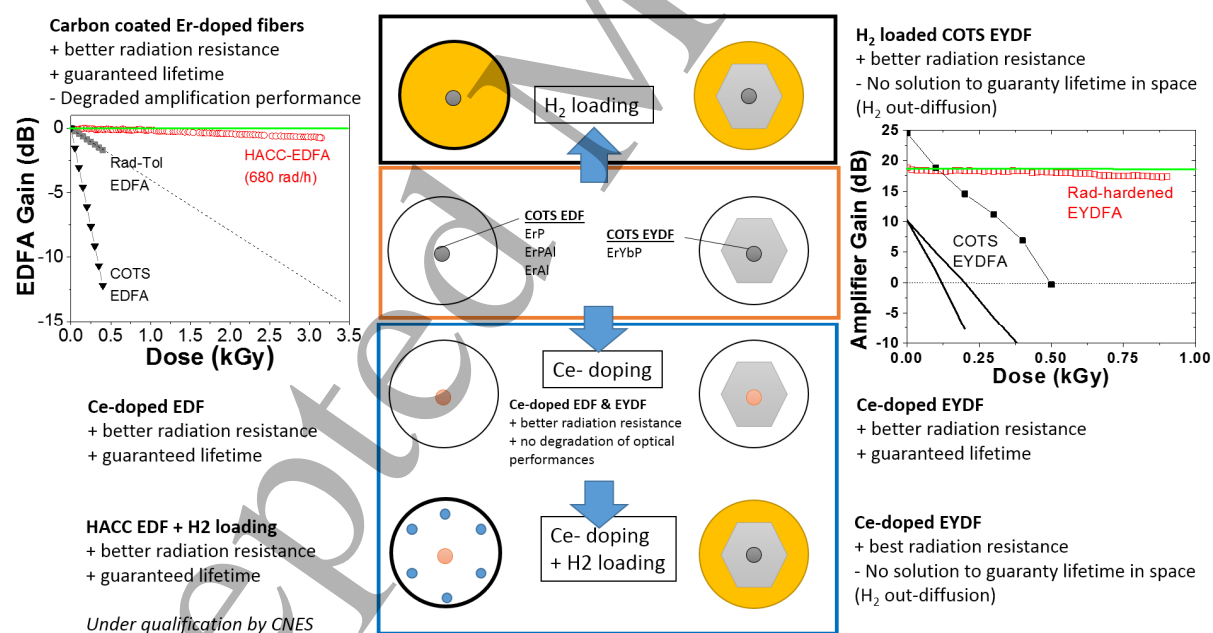
Figure 25 Illustration of the variety of hardening by components solutions proposed in literature to enhance the radiation tolerance of EDF and EYDFs. a) comparison between the gain degradation measured for a variety of EDFAs based on different generations of EDFs, more details can be found in [314]. b) comparison between the gain degradation measured for a variety of EYDFAs based on different generations of EYDFs, more details can be found in [315].

* Corresponding author: Sylvain Girard, sylvain.girard@univ-st-etienne.fr : Phone: +33 (0)477 915 812

IV.4.1. Hardening by component

As for the hardening of passive optical fibers for data transfer, several approaches have been followed to reduce the RIA in active optical fibers caused by the P and/or Al-related defects. The first solution relies on a manufacturing process change allowing to design active fibers without using these dopants and still maintaining high amplification efficiency. Another approach could be to control the equilibrium between the various point defects created in silica under irradiation, trying to reduce the concentrations of those absorbing at pump and signal wavelengths. Such defect control can be achieved by appropriate codoping of the fiber core or by pre-treatments.

The first approach was followed by Draka Comteq in 2012 that showed that active Erbium-doped optical fibers with reduced amount of Al through can be produced through their patented nanoparticules doping process [316,317]. This approach improves noticeably the radiation resistance of the fiber without degrading too much its amplification performances through quenching effects [318]. To the best of our knowledge, such manufacturing process is not yet transposable to EYDFs. In Fig.25a, the advantage of using this technology is highlighted by comparing the performances of EDFA based on this fiber and on a conventional Al and/or P-doped fiber and tested under γ-rays in an OFF configuration (pumping only during the gain measurements), the conventional EDFA gain decrease is of about 100% after 500Gy dose whereas it remains below 15% for the EDFA based on the nanoparticles EDF [319].

The same year, the efficiency of codoping the active fibers (EDF or EYDF) with cerium was demonstrated and patented by iXBlue Photonics [320]. Adding Cerium to the fiber core does not modify the spectroscopic properties of the Erbium and Ytterbium ions [321] or the EDFA performances but strongly improves the fiber and EYDFA radiation resistance [315]. This can be explained by the positive impact of Ce^{3+} ions on the POHC and P1 defects that are less efficiently produced in presence of this element [83]. Such positive impact of the Ce-codoping on the radiation hardness of bulk optical materials was known from years [322,323] and exploited to manufacture radiation hardened glasses for the space optical systems. This is also the case for Er-doped optical fiber and EDFA even if the Ce positive impact seems less important than in the Er-Yb case from the published results [314]. The data of Fig.25a shows that a Ce-doped EDF allows to build an EDFA with better radiation response than the nanoparticles EDF, with a gain decrease limited to 10% after 500 Gy. Fig.25b shows the strong positive impact of the Ce-codoping of the EYDF on the EYDFA performances. For this optimized EYDFA, the gain
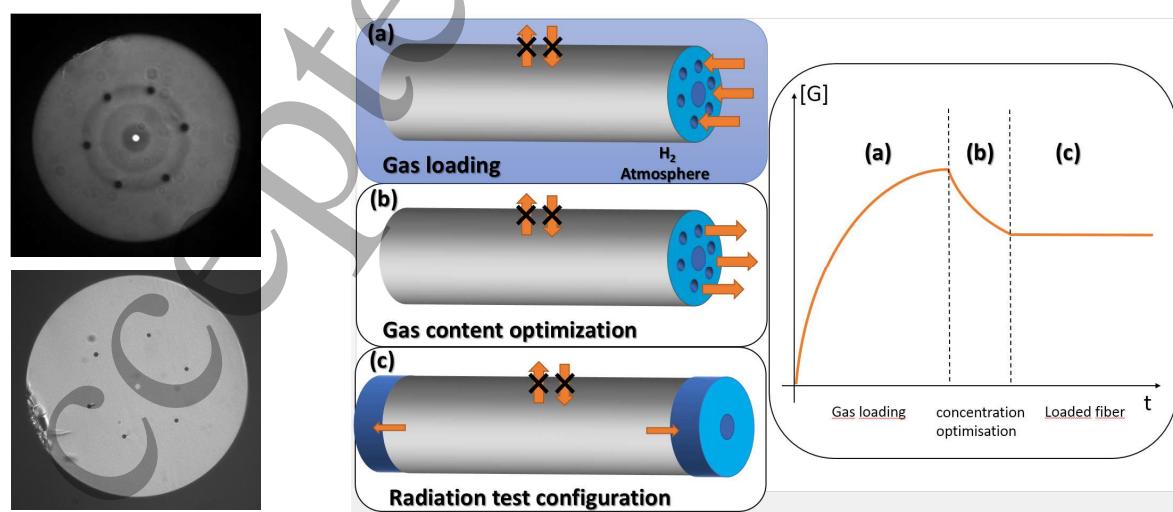
* Corresponding author: Sylvain Girard, sylvain.girard@univ-st-etienne.fr : Phone: +33 (0)477 915 812

decrease is of less than 5% after 500 Gy of γ-rays whereas it reaches about 35% with a conventional EYDF [315].

In addition to these techniques, several authors demonstrated that if the active fiber contains hydrogen in its core, its radiation resistance and the corresponding EDFA or EYDFA is strongly increased [86, 315, 319,324], with an almost complete bleaching of the Al and P-related absorption. By combining the two mitigation solutions (Ce codoping and H_2-loading), it was demonstrated that both EDFA [319] and EYDFA [315] became very radiation resistant at high doses exceeding those expected for future challenging space missions. This is also illustrated in Fig.25 for the EDFA and EYDFA, the systems using gas loaded fibers present almost no degradation of their gains (less than a few %) after 500 Gy dose.

One of the difficulties with the practical use of an active fiber loaded with gas is that this gas will easily diffuse out the fiber core at RT for a conventional fiber structure. Another challenge is that if the gas concentration is too high, the amplification properties of the active fiber are affected too, with a decrease of the achievable gain for the EDFA or EYDFA [145]. One solution to keep the gas inside the fiber is to use a waveguide having a carbon layer of a few tens of nanometers between the fiber cladding and its coating [324]. Mobile hydrogen cannot go through this layer at normal conditions but the loading of this carbon-coated fiber with hydrogen remains possible at elevated temperatures [325]. This solution is interesting but the loading procedure is complex, the amount of gas difficult to control and usually the performances of the fibers are degraded by the high temperature treatment. An alternative approach was proposed in 2014 [319, 314] to overcome the observed limitation: the hole-assisted carbon coated (HACC) optical fibers. These fibers have holes in their claddings (see Figure 26a); these holes have no impact on the fiber guiding properties (at the contrary of MOFs) but allow their gas loading having access only to one fiber end according to the procedure described in Figure 26b.

* Corresponding author: Sylvain Girard, sylvain.girard@univ-st-etienne.fr : Phone: +33 (0)477 915 812

a)   b)

Figure 26 a) Illustration of two different HACC fiber structures manufactured by iXBlue Photonics with holes of different sizes b) Principle of gas loading into these fibers, more details can be found in [319, 314]. During the first phase the gas is injected into the fiber through the holes at one of its ends whereas the second end is closed. The gas diffuses into the fiber up to a certain concentration. The gas level is controlled in a second phase to ensure the best compromise between radiation hardness and amplifier gain. When the targeted amount is achieved, the fiber is spliced, the out-diffusion kinetics of gas at room temperature is decreased by a factor of more than 100, allowing to guaranty the hydrogen presence during the lifetime of a space mission.

Through this procedure, it is possible to control the amount of gas to achieve the best compromise between the radiation hardness and the optical performances of the optical system. By this approach, an EDFA based on this HACC fiber has been characterized under γ-ray doses up to 3.15 kGy(SiO_2) in an ON configuration where the active fiber is pumped during the whole irradiation test. The 31 dB amplifier is practically radiation insensitive, with a gain change of merely -2.2×10^{-4} dB/Gy [319]. Irradiation of the same generation of EDFA with 63 MeV protons up to a fluence of 7.5×10^{11} p/cm² (equivalent dose of 1 kGy) confirms the excellent tolerance of this HACC-EDFA component that showed a limited decrease of ~0.6dB of its ~27dB gain [314].

IV.4.2. Hardening-by-system approach

Various architectures of EDFA can be done to tune the amplifier performances (gain, noise figure) with respect to the targeted applications requirements. For example, different pumping schemes can be used: forward, backward, double pumping… Different pumping wavelengths can be selected (eg. for EDFA 980 nm or 1480 nm), the active fiber length needs to be optimized. All this optimization is usually performed by simulation as the physics of the light amplification, the spectroscopy of the various rare-earth ions is today well-known. State-of-the-art tools allow to optimize the amplifier architecture to obtain the targeted performance. Recently, studies have been initiated to implement the radiation effects in the code in order to optimize the system not only for in-lab testing but rather for its operation during the space mission. Particularly, the results of the optimization process will change by considering the radiation effects and their impact on the system characteristics and the resulting selected architecture will differ. The objective of such a modeling is to optimize the full system for its operation profile-of-use in regards to the environmental constraints and not for the on-Ground tests before launch.

For the radiation effects module the RIA at the pump and signal wavelengths have to be considered since they are known to greatly affect the gain. However, the impact of radiation on the rare-earth ions is less studied and more difficult to experimentally investigate. To identify those parameters that could significantly modify the amplifier behavior if they evolve under irradiation, a parametric simulation study was recently performed, varying each parameter by +/- 20% and evaluating its impact

* Corresponding author: Sylvain Girard, sylvain.girard@univ-st-etienne.fr : Phone: +33 (0)477 915 812

on the gain and noise figure of the system [90]. The outcomes of this study are that the energy transfer coefficient from Yb^{3+} to Er^{3+} ions could influence the EYDFA amplifier gain if radiation changes their value by +/- 20% whereas upper levels lifetimes and up-conversion coefficient are not expected to affect the amplifier gain and noise figure [90]. At this time, two different categories of amplifiers have been investigated through the coupled experiment/simulation approaches:

- The first category concerns EYDFA with moderate output power (< 2W) [315]. In this case, it was shown that the measurements of the RIA at 915 nm and 1550 nm through a classical measurements setup (white light source + spectrophotometer, PMIN configuration of Figure 27) can be used as input parameters in the simulation tools and allow to reproduce with a good confidence the observed EYDFA gain decrease under irradiation. As a consequence, it was deduced that for such ErYb doped fibers, the photobleaching effects are negligible as it was assumed by the limited gain recovery at the end of the -ray exposure and that all other radiation effects (on RE ions,…) can be neglected at the first order. It should be noted that the modeling becomes more complex for high power EYDFA (>10W) for which combined photo and thermal issues will affect the RIA levels and kinetics.

- The second category concerns EDFA with output power on the order of 1W. In this case, a recent work [145] reveals that a more complex approach has to be followed to evaluate the RIA levels at the pump (980 nm) and signal (1550 nm) wavelengths in order to reproduce the experimentally-observed degradation of their gains with the dose. This is explained by the fact that for such optical fibers, there is a strong photobleaching effect of the pump on the RIA at both the pump and signal wavelengths and that with the PMIN configuration, the RIA levels are overestimated compared to those occurring in the pumped fiber of the EDFA. To reduce the error, the RIA measurements have to be done in conditions representative of the application. Today, the best solution (configuration PMAX) consists in pumping the fiber 80% of the time while the 20% of remaining time are used to measure the RIA values in a passive-mode. In Fig we illustrate the different dose dependences of the RIA at 980 nm and 1550 nm measured with the two configurations: PMAX and PMIN. In the PMAX mode, the induced losses at 980 nm are reduced from 10 dB/m at 3.5 kGy (350 krad; PMIN down) to less than 6 dB/m, while at 1550 nm, the losses decrease from 3.5 dB/m to about 1 dB/m. Considering these new values for the RIA into the codes, it can be seen that the gain degradation is more efficiently reproduced, almost perfectly for the EDFA based on a COTS fiber, the error is larger for the EDFA based on the rad-hard fiber, especially at higher doses, it is assumed that this is due to the fact that even if the PMAX configuration allows to better take into account the positive impact of the photobleaching, its impact still remains underestimated due to the 20%

* Corresponding author: Sylvain Girard, sylvain.girard@univ-st-etienne.fr : Phone: +33 (0)477 915 812

68

of time where the active fiber is not pumped. From these results, it clearly appears that for future missions, a model of the RIA dependence on dose, on injected power will have to be built to design prediction tools able to cover the variety of mission profiles of use.
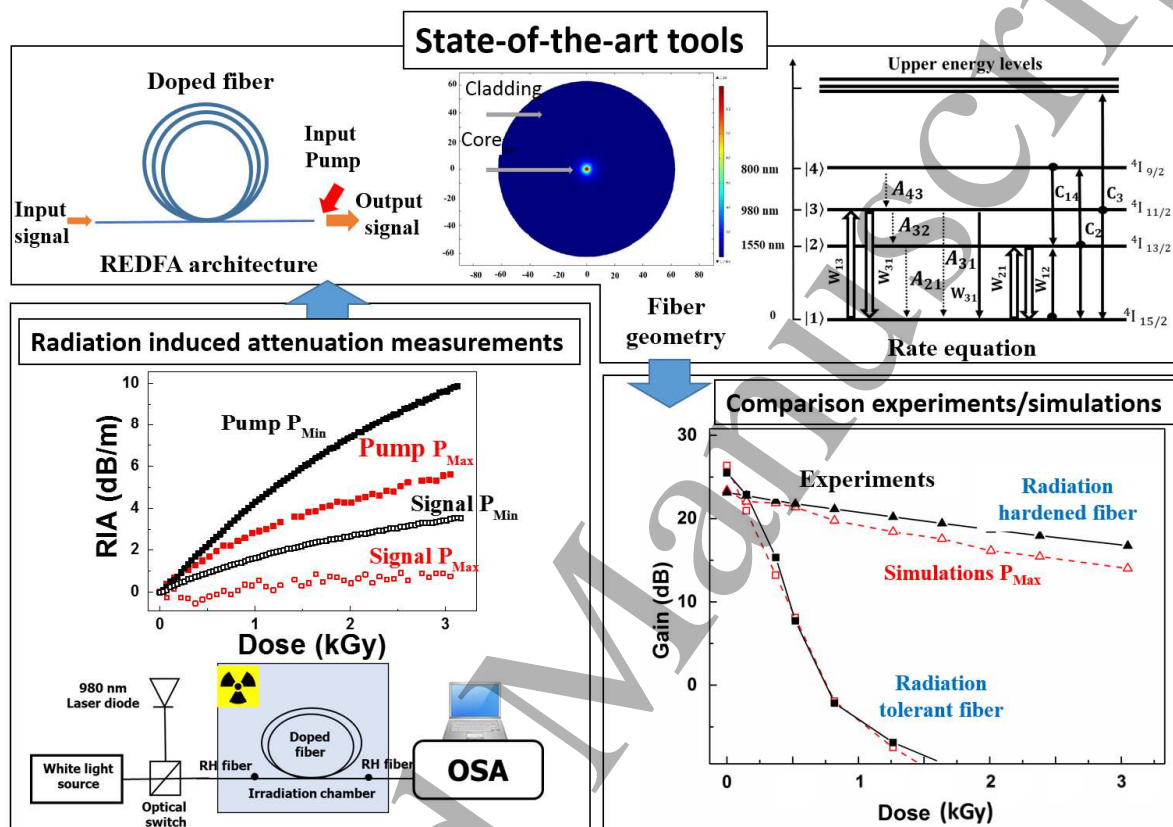
Figure 27 a) Illustration of the RIA measurement setup allowing to obtain the RIA levels at the pump and signal wavelengths in the P$_{MAX}$ and P$_{MIN}$ configurations. b) Illustration of the modelled architecture of EDFA and the considered model for the erbium ion spectroscopy c) Comparison between experimental and modelled EDFA gain degradations with dose when a rad-hard and a COTS fibers are used.

IV.5. Gyroscopes: recent advances

Four main mitigation strategies are followed to overcome radiation issues in commercial space FOGs. The first one remains the design of the targeted mission: adapting the orbit and optimizing the FOG localization inside the spacecraft are efficient mitigation mechanisms but are out of the scope of this topical review. Another way to decrease the radiation constraints is shielding (*as discussed in section I.2*): commercial FOGs indeed possess internal metallic shielding designed to decrease the level of TID dose on their sub-parts identified as the most radiation sensitive. Obviously, as it can be inferred from the results and discussion presented in section III.4, the third and most important mitigation approach

* Corresponding author: Sylvain Girard, sylvain.girard@univ-st-etienne.fr : Phone: +33 (0)477 915 812

consists in the identification and the use of radiation resistant optical fibers for both the optical source (REDFs) and for the Sagnac's coil (PSC PMF) [326,327]. Another less-studied phenomenon reducing the radiation impact is the photobleaching effect, able to recover partially the RIA in the FOG's REDF and PMF fibers. This positive effect combined with the low dose rate steady state irradiation and space temperature constraints remains difficult to quantify in orbit and its relative impact is also strongly fiber dependent then its contribution to the FOG response remains subject to speculation [328].

By combining all these approaches, it is possible to have high performance FOGs able to operate in space. This is today well demonstrated by the recent data analysis of several real in-orbit ageing of the commercial FOGs of the Astrix® family. The analysis of this huge amount of in-flight data reveals first no anomaly over 1720000 hours of operation and shows no detectable impact of the RIA on the performances of radiation hardened space FOGs after several years of navigation at LEO, MEO and GEO orbits [328]. These Astrix® FOGs cover a variety of space mission profiles (see Figure 28) and present excellent results (see Figure 29) with very limited degradation of the system in terms of scale factor and noise, easily mitigated in-flight. An important outcome of these in-flight data that are discussed in details in [328] is that the degradation predictions that were extrapolated from on-Ground radiation tests lead to an overestimation of the observed changes in space. To the best of the current knowledge, this may be explained by a positive impact of the lower dose rate in space than during in-lab tests and also a continuous in-orbit optical photobleaching more efficient than expected in real conditions (varying temperature,…). More studies on these effects will have to be performed in the future to understand more precisely the basic mechanisms at stake.

* Corresponding author: Sylvain Girard, sylvain.girard@univ-st-etienne.fr : Phone: +33 (0)477 915 812
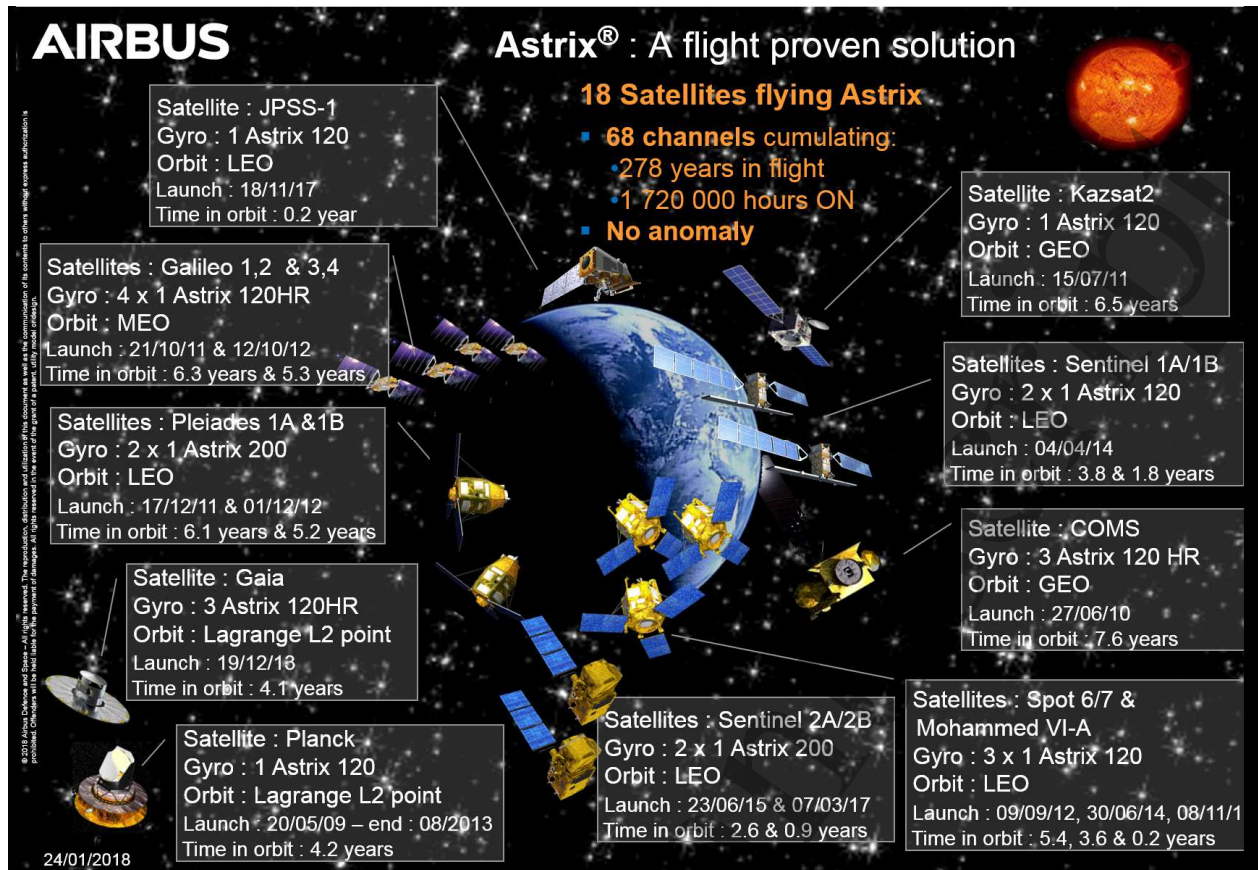
Figure 28. Astrix® Fiber Optic Gyro Space Fleet (Last Update: 01/24/18)

V. Conclusions and perspectives

In this article, we review the main fiber-related technologies that are today used or under evaluation for integration in harsh environments associated with low to extremely high levels of ionizing or non-ionizing radiations. After description of the operation principles of the main technologies, we described for each one its radiation response and if needed the identified solutions to enhance its radiation tolerance. Generally, for a large part of the targeted applications, optical fibers and fiber sensors (OFSs) present key advantages and even if they are not immune to radiation, adequate solutions for each application can be found using either commercial Telecom-grade fibers or commercially available radiation hardened optical fibers. Considering the numerous intrinsic and extrinsic parameters affecting the fiber radiation response, it remains mandatory, before the implementation of the fiber-based solutions to evaluate their vulnerability with respect to the environmental constraints: radiation, presence of gas, high operation temperature. Today the response of an optical fiber or OFS remains too complex to be predictable by multi-scale simulation and even if recent progresses have been done at the atomic scale [329], accelerated radiation test experiments are still mandatory, sometimes with facilities covering only partially the characteristics of the future environments (eg. For megajoule class

lasers). Considering the increasing interest of industries for radiation tolerant optical fibers, mitigation techniques (or radiation hardening techniques) of the radiation effects, mainly radiation induced attenuation (RIA) have been developed. Especially for space applications, very promising developments have been demonstrated, allowing to conceive radiation tolerant rare-earth doped optical fibers, EDFA, EYDFA for today's space missions. For the future missions, as JUICE missions, higher dose levels and larger operation temperature range are expected, pushing to the development and qualification of even more radiation tolerant devices and systems. In the future and driven by the increasing free space optical communication needs, studies will also have to be performed on the combined radiation and thermal effects in high power fiber-based amplifiers (>10W). In the recent years, distributed OFS performances strongly increase making these sensors very attractive candidates for integration in nuclear facilities, high energies physics facilities (CERN) or fusion related facilities (ITER, NIF, LMJ). For these on-Earth applications, recent studies show that most of these sensors can operate in radiation rich environments even if for some of them, such as RDTS, specific mitigation techniques have to be applied at the system levels to ensure the measurement precision. Before these technologies can be used in satellites, progresses are necessary on the integration and radiation hardening of the interrogation parts of these sensors. This should be facilitated in the next year by the increasing performances of integrated photonic technologies such as ASPICSs. As the fiber based applications are more and more implemented in radiation environments, future studies will also have to be devoted on the establishment of new guidelines and qualification procedures, considering the new generations of optical fibers and the diversity of fiber-related applications, to complete the existing reference documents [229].

VI. Acknowledgments

VII. References

* Corresponding author: Sylvain Girard, sylvain.girard@univ-st-etienne.fr : Phone: +33 (0)477 915 812

[1] J.L. Barth, "Space and atmospheric environments: from low earth orbits to deep space", In Proceedings of the 9th International Symposium on Materials in a Space Environment, 16-20 June 2003, Noordwijk, The Netherlands.

[2] J-L. Miquel, C. Lion and P. Vivini, "The Laser MegaJoule: LMJ & PETAL status and Program Overview", Journal of Physics: Conference Series, Volume 688, conference 1, 2016.

[3] G. H. Miller, E. I. Moses and C. R. Wuest, "The National Ignition Facility: enabling fusion ignition for the 21st century", Nuclear Fusion, Volume 44, Number 12, 2004.

[4] O. Motojima, "The ITER project construction status", Nuclear Fusion, Volume 55, Number 10, 2015.

[5] R.E. Sharp, and D.R. Garlick, "Radiation effects on electronic equipment, a designers'/users' guide for the nuclear power industry," AEA-D&W-0691, 1994.

[6] F. Ravotti, M. Glaser, A. B. Rosenfeld, M. L. F. Lerch, A. G. Holmes-Siedle and G. Sarrabayrouse, "Radiation Monitoring in Mixed Environments at CERN: From the IRRAD6 Facility to the LHC Experiments," in IEEE Transactions on Nuclear Science, vol. 54, no. 4, pp. 1170-1177, Aug. 2007.

[7] E. J. Friebele, "Optical Fiber Waveguides In Radiation Environments," Optical Engineering 18(6), 186552, 1979.

[8] J. E. Golob, P. B. Lyons and L. D. Looney, "Transient Radiation Effects in Low-Loss Optical Waveguides," in IEEE Transactions on Nuclear Science, vol. 24, no. 6, pp. 2164-2168, Dec. 1977.

[9] D.L. Griscom, "Nature of defects and defect generation in optical glasses," SPIE Vol. 541 - Radiation Effects in Optical Materials, P.W. Levy, Ed. (SPIE, Bellingham, WA), pp. 38-59, 1985.

[10] E.J. Friebele, C.G. Askins, M.E. Gingerich, M.J. Marrone, and D.L. Griscom, "Overview of radiation effects in fiber optics," SPIE Vol. 541 - Radiation effects in optical glasses, P.W. Levy, Ed. (SPIE, Bellingham, WA), pp. 70-80, 1985.

[11] D. L. Griscom. "Defect structure of glass: Some outstanding questions in regard to vitreous silica", Non-Crystalline solids 73 p. 61–77, 1985.

[12] D. L. Griscom, "Intrinsic and extrinsic point defects in a-SiO$_2$," in The Physics and Technology of Amorphous, R.A.B. Devine, Ed. New York: Plenum, pp. 125–134, 1988.

[13] J.A. Wall, J.F. Bryant, "Radiation Effects on Fiber Optics", AFCRl-TR-7 5-0190 Physical Sciences Research papers, n°627, 2 April 1975.

[14] S. Girard, J. Baggio, and J. Bisutti, "14-MeV Neutron, gamma-ray, and Pulsed X-Ray Radiation-Induced Effects on Multimode Silica-Based Optical Fibers", IEEE Transactions on Nuclear Science, vol. 53, n°6, pp. 3750-3757, 2006.

[15] M. Benabdesselam, F. Mady, S. Girard, Y. Mebrouk, J.B Duchez, M. Gaillardin, P. Paillet, "Performance of Ge-doped Optical Fiber as a Thermoluminescent Dosimeter", IEEE Transactions on Nuclear Science, vol.60, n°6, pp. 4251-4256, 2013.

[16] W. Primak, "Fast-neutron-induced changes in quartz and vitreous silica," Phys. Rev. B, vol. 110, no. 6, pp. 1240–1254, 1958.

[17] S. Rizzolo, A. Boukenter, E. Marin, T. Robin, M. Cannas, A. Morana, J. Perisse, J-R. Mace, Y. Ouerdane, B. Nacir, P. Paillet, C. Marcandella, M. Gaillardin, and S. Girard, "Evaluation of Distributed OFDR-based Sensing Performance in Mixed Neutron/Gamma Radiation Environments", IEEE Transactions on Nuclear Science, vol.64, n°1, pp. 61 – 67, 2017.

[18] G. Cheymol, H. Long, J. F. Villard, and B. Brichard, "High level gamma and neutron irradiation of silica optical fibers in CEA OSIRIS nuclear reactor," IEEE Transactions on Nuclear Science, vol. 55, no. 4, pp. 2252–2258, Aug. 2008.

[19] J. Barth, "Evolution of the Radiation Environments", in RADECS 2009 Short Course, Bruges, Belgium, 2009.

[20] J.L. Bourgade, R. Marmoret, S. Darbon, R. Rosch, P. Troussel, B. Villette, V. Glebov, W. Shmayda, J.C. Gommé, Y. Le Tonqueze, F. Aubard, J. Baggio, S. Bazzoli, F. Bonneau, J.Y. Boutin, T. Caillaud, C. Chollet, P. Combis, L. Disdier, J. Gazave, S. Girard, D. Gontier, P. Jaanimagi, H.P. Jacquet, J.P. Jadaud, O. Landoas, J. Legendre, J.L Leray, R. Maroni, D.D. Meyerhofer, J.L. Miquel, F.J. Marshall, I. Masclet-Gobin, G. Pien, J. Raimbourg, C. Reverdin, A. Richard, D. Rubins de Cervens, C.T. Sangster, J.P. Seaux,

* Corresponding author: Sylvain Girard, sylvain.girard@univ-st-etienne.fr : Phone: +33 (0)477 915 812

G. Soullie, C. Stoeckl, I. Thfoin, L. Videau, and C. Zuber, "Present LMJ Diagnostics Developments Integrating its Harsh environment", Review of Scientific Instruments, vol. 79 n°10, 10F301, 2008

[21] S. Delepine-Lesoille, S. Girard, M. Landolt, J. Bertrand, I. Planes, A. Boukenter, E. Marin, G. Humbert, S. Leparmentier, J-L. Auguste, Y. Ouerdane, "France's State of the Art Distributed Optical Fibre Sensors Qualified for the Monitoring of the French Underground Repository for High Level and Intermediate Level Long Lived Radioactive Wastes", Sensors, vol.17, 1377, 2017.

[22] J. Stone, "Interactions of hydrogen and deuterium with silica optical fibres: a review", J. Lightwave Technol., 5, 712–7331987.

[23] K. Røed, M. Brugger, G. Spiez, "An overview of the radiation environment at the LHC in light of R2E irradiation test activities", CERN-ATS-Note-2011-077 TECH, May 2012.

[24] S. Yamamoto, T. Shikama, V. Belyakov, E. Farnum, E. Hodgson, T. Nishitani, D. Orlinski, S. Zinkle, S. Kasai, P. Stott, K. Young, V. Zaveriaev, A. Costley, L. deKock, C. Walker, G. Janeschitz, "Impact of irradiation effects on design solutions for ITER diagnostics", In Journal of Nuclear Materials, Volumes 283–287, Part 1, pp. 60-69, 2000.

[25] L. Remy, G. Cheymol, A. Gusarov, A. Morana, E. Marin and S. Girard, "Compaction in optical fibres and fibre Bragg gratings under nuclear reactor high neutron and gamma fluence", IEEE Transactions on Nuclear Science, vol.63 (4), pp. 2317 - 2322, 2016.

[26] P. Ferdinand, S. Magne, G. Laffont, "Optical fiber sensors to improve the safety of nuclear power plants," Proc. SPIE 8924, Fourth Asia Pacific Optical Sensors Conference, 89242G (15 October 2013);

[27] S. O'Keeffe, "Optical Fibres for Radiation Dosimetry" in Fiber Optic Sensors: Current Status and Future Possibilities, Eds I. R. Matias, S. Ikezawa, J. Corres, Springer, 2017.

[28] G.P. Agrawal, "Fiber-Optic Communication Systems, Fourth Edition" John Wiley & Sons, Inc., 2010.

[29] J.L. Bourgade, A.E. Costley, R. Reichle, E.R. Hodgson, W. Hsing, V. Glebov, M. Decreton, R. Leeper, J.L. Leray, M. Dentan, T. Hutter, A. Morono, D. Eder, W. Shmayda, B. Brichard, J. Baggio, L. Bertalot, G. Vayakis, M. Moran, T.C. Sangster, L. Vermeeren, C. Stoeckl, S. Girard, and G. Pien, "Diagnostic components in harsh environments: possible overlap in R&D requirements of IC and MF systems", Review of Scientific Instruments, vol. 79 n°10, 10F304, 2008.

[30] C. Emslie, "Fiber-Optic Components: Harsh-environment optical fiber coatings: Beauty is only skin deep", Laser Focus World, August 2015.

[31] G. Santin, P. Truscott, R. Gaillard, R. G. Alia, "Radiation Environments: space, avionics ground and below", In RADECS 2017 short course notebook; 2017

[32] Spjeldvik and Rothwell, Handbook of Geophysics And The Space Environment, 1985.

[33] D. M. Sawyer and J. I. Vette, "AP-8 trapped proton environment for solar maximum and solar minimum," NASA TM-X-72605, 1976

[34] J. I. Vette, "The AE-8 trapped electron model environment," NSSDC/WDC-A-R&S 91-24, 1991.

[35] G. P. Ginet, T.P. O'Brien, S.L. Huston, W.R. Johnston, T.B. Guild, R. Friedel, C.D. Lindstrom, C.J. Roth, P. Whelan, R.A. Quinn, D. Madden, S. Morley, Yi-Jiun Su, "AE9, AP9 and SPM: New models for specifying the trapped energetic particle and space plasma environment," Space Sci. Rev., 179, 579-615, 2013.

[36] W. Robert Johnston T.P. O'Brien, G.P. Ginet,S.L. Huston, T. B.Guild, and J.A. Fennelly, "AE9/AP9/SPM: New Models for Radiation Belt and Space Plasma Specification", Proc. of SPIE Vol. 9085, 908508, 2014.

[37] P. O'Brien, "The AE9/AP9/SPM Next Generation Radiation Specification Models" -Progress Report, Proceedings of the Space Radiation Modelling and Data Analysis, Workshop 2016.

[38] AE9/AP9/SPM URL: https://www.vdl.afrl.af.mil/programs/ae9ap9/

[39] D. Boscher A. Sicard-Piet ; D. Lazaro ; T. Cayton, and G. Rolland, "A New Proton Model for Low Altitude High Energy Specification", IEEE Transactions On Nuclear Science, Vol. 61, No. 6, 2014.

[40] ECSS Standard, "ECSS E-10-04 Space Environment Standard," ESA/ESTEC, Tech. Rep., April 2008

[41] W. Fourcault, J-M. Léger, V. Costes, I. Fratter, and L. Mondin, "Athermal fiber laser for the swarm absolute scalar magnetometer", International Conference on Space Optics (ICSO), Rhose, Greece, 4-8 octobre 2010

* Corresponding author: Sylvain Girard, sylvain.girard@univ-st-etienne.fr : Phone: +33 (0)477 915 812

74

[42] S.M. Seltzer, "SHIELDOSE: A computer code for space-shielding radiation dose calculations," National Bureau of standards Technical Note 1116, 1980

[43] S.M Seltzer, "Electron, electron-bremsstrahlung and proton dose depth data for space-shielding applications," IEEE Trans Nucl Sci, NS-26, No 6, 4896-4904, 1979

[44] S.M Seltzer, "Updated calculations for routine space-shielding radiation dose estimates: SHIELDOSE2," National Institute of Standards and Technology report NISTIR 5477, December 1994.

[45] M. N. Ott, "Space Flight Applications of Optical Fiber: 30 Years of Space Flight Success", Invited Paper, TuA2, IEEE Photonics Society Avionics, Fiber-Optics and Photonics Technology Conference (AVFOP) Denver Colorado. September 21-23, 2010.

[46] A.Reutlinger, M. Glier, K-H. Zuknik, L. Hoffmann, M. Müller, S. Rapp, C. Kurvin, T. Ernst, I. McKenzie, N. Karafolas, "Fiber optic sensing for telecommunication satellites", Proc. SPIE 10566, International Conference on Space Optics — ICSO 2008, 105661C (21 November 2017)

[47] https://escies.org/download/webDocumentFile?id=1622

[48] https://spaceequipment.airbusdefenceandspace.com/avionics/fiber-optic-gyroscopes/astrix-120/

[49] COTS Fibre Optic Components in SMOS/MOHA – ESCIES, file:///D:/Utilisateurs/boutillierm/Downloads/1251367974174SMOS_Moha__ESA_ESTEC.pdf

[50] Ian McKenzie, "SMOS – The 1st Deployment of an Optical Harness on a Deployment of an Optical Harness on a Satellite", CCT CNES.

[51] NASA facts "Lunar Laser Communication Demonstration NASA's First Space Laser Communication System　　　　　　　　　　　　　Demonstration"　　　　　　　　　　　　　[Online] https://www.nasa.gov/sites/default/files/llcdfactsheet.final_.web_.pdf

[52] http://www.esa.int/Our_Activities/Telecommunications_Integrated_Applications/EDRS/Start_of_service_for_Europe_s_SpaceDataHighway

[53] Raman Kashyap, "Fiber Bragg Gratings (Second Edition)", Elsevier Inc., 2010.

[54] X. Bao and L. Chen, "Recent Progress in Distributed Fiber Optic Sensors", Sensors 2012, 12(7), 8601-8639, 2012.

[55] R.M. Measures, "Structural Monitoring with Fiber Optic Technology", Academic Press: San Diego, CA, USA, Chapter 2, 2001.

[56] A.H Hartog, A.P. Leach, M.P. Gold, "Distributed temperature sensing in solid-core fiber", Electron. Lett., vol.21, pp. 1061–1062, 1985.

[57] H. Henschel, M. Körfer, J. Kuhnhenn, U. Weinand et F. Wilf. "Fibre optic radiation sensor systems for particle accelerators" Nuclear instruments and methods in physics research A, vol. 526, p. 537–550 2004.

[58] I. Toccafondo, T. Nannipieri ; A. Signorini ; E. Guillermain ; J. Kuhnhenn ; M. Brugger, and F. Di Pasquale "Raman Distributed Temperature Sensing at CERN," in *IEEE Photonics Technology Letters*, vol. 27, no. 20, pp. 2182-2185, Oct.15, 15 2015.

[59] M.J.F. Digonnet, "Rare-Earth-Doped Fiber Lasers and Amplifiers, Revised and Expanded", CRC Press, 2001.

[60] H. Lefevre "The Fiber-Optic Gyroscope", Artech House, ISBN-13 978-1-60807-695-6,2014

[61] P. Stajanca, K. Krebber, "Radiation-Induced Attenuation of Perfluorinated Polymer Optical Fibers for Radiation Monitoring", Sensors, vol.17, 1959, 2017.

[62] S. O'Keeffe, A. Fernandez-Fernandez, C. Fitzpatrick, B. Brichard, E. Lewis, "Real-time gamma dosimetry using PMMA optical fibres for applications in the sterilization industry", Meas. Sci. Technol. 2007, 18, 3171–3176.

[63] H. Henschel, J. Kuhnhenn and U. Weinand, "High radiation hardness of a hollow core photonic bandgap fiber," 2005 8th European Conference on Radiation and Its Effects on Components and Systems, Cap d'Agde, 2005, pp. LN4-1-LN4-4.

[64] S. Girard, J. Baggio and J. L. Leray, "Radiation-induced effects in a new class of optical waveguides: the air-guiding photonic crystal fibers," in *IEEE Transactions on Nuclear Science*, vol. 52, no. 6, pp. 2683-2688, Dec. 2005.

* Corresponding author: Sylvain Girard, sylvain.girard@univ-st-etienne.fr : Phone: +33 (0)477 915 812

[65]L Olanterä, C Sigaud, J Troska, F Vasey, M N Petrovich, F Poletti, N V Wheeler, J P Wooler and D J Richardson, "Gamma irradiation of minimal latency Hollow-Core Photonic Bandgap Fibres", Journal of Instrumentation, Volume 8, December 2013.

[66] European Space Agency," Statement of Work ECI4: space validation of rad-hard erbium optical fibre amplifier at 1.55µm,"TEC-QTC/2013/ECI4-EEE41, March 18, 2013

[67] T.M. Monro and H. Ebendorff-Heidepriem, "Progress in microstructured optical fibers", Annual Review of Materials Research, vol.36:1, 467-495, 2006.

[68] P. Russell, "Photonic Crystal Fibers", Science, vol.17, 358-362, 2003.

[69] A. Fernandez-Fernandez, "Photonics for Nuclear Environments From Radiation Effects to Applications in Sensing and Data-Communication," Ph.D. dissertation, Faculté Polytechnique de Mons, Mons, 1997.

[70] E. J. Friebele, "Correlation of Single Mode Fiber Fabrication Factors and Radiation Response", Final Rep., NRL/MR/6505-92-6939, 1991.

[71] M. Ott, "Radiation effects data on commercially available optical fiber: Database summary," in Proc. IEEE NSREC Data Workshop, 2002, pp.24–31.

[72 J. Bisutti, "Etude de la transmission du signal sous irradiation transitoire dans les fibres optiques," Ph.D. dissertation, Université de Saint-Etienne, Saint-Etienne, France, 2010.

[73 M. Van Uffelen, "Modélisation de systèmes d'acquisition et de transmission à fibres optiques destinés à fonctionner en environnement nucléaire," Ph.D. dissertation, Université de Paris XI, Paris, 2001.

[74] S. Girard, "Analyse de la réponse des fibres optiques soumises à divers environnements radiatifs," Ph.D. dissertation, Université de Saint-Etienne, Saint-Etienne, France, 2003

[75] T. Wijnands, L. K. De Jonge, J. Kuhnhenn, S. K. Hoeffgen, and U. Weinand, "Optical absorption in commercial single mode optical fibers in a high energy physics radiation field," IEEE Transactions on Nuclear Science, vol.55, no. 4, pp. 2216–2222, Aug. 2008.

[76] E.J. Friebele, P. B. Lyons, J. Blackburn, H. Henschel, E. W. Taylor, G. T. Beauregard, R. H. West, P. Zagarino, and D. Smith, "Interlaboratory Comparison of Radiation-Induced Attenuation in Optical Fibers. Part III: Transient Exposures" Journal of Lightwave Technology, vol. 8, pp. 977-989, 1990.

[77] E.J. Friebele, E. W. Taylor, G. T. Beauregard, J. Wall, and C. Barnes, "Interlaboratory Comparison of Radiation-Induced Attenuation in Optical Fibers. Part I: SteadyState Exposures" Journal of Lightwave Technology, vol. 6, pp. 165-171, 1988.

[78] E.W. Taylor, E. J. Friebele, H. Henschel, R. H. West, C. Barnes, and J. A. Krinski, "Interlaboratory Comparison of Radiation-Induced Attenuation in Optical Fibers. Part II: SteadyState Exposures" Journal of Lightwave Technology, vol. 8, pp. 967-976, 1990.

[79] P. Borgermans, "Spectral and Kinetic Analysis of Radiation Induced Optical Attenuation in Silica: Towards Intrinsic Fiber Optic Dosimetry?," Ph.D. dissertation, Vrije Universiteit, Brussels, 2001.

[80] O. Deparis, "Etude physique et expérimentale de la tenue des fibres optiques aux radiations ionisantes par spectrométrie visible-infrarouge," Ph.D. dissertation, Faculté Polytechnique de Mons, Mons, 1997.

[81] B. Brichard, "Systèmes à fibres optiques pour infrastructures nucléaires: du durcissement aux radiations à l'application," Ph.D. dissertation, IES—Institut d'Electronique du Sud, Montpellier, 2008.

[82] Chiara Cangialosi, "Performances of Raman and Brillouin fiber-based sensing of temperature and strain in harsh environments", Ph.D. dissertation, University of Saint-Étienne, Saint-Etienne, 2016.

[83] Diego Di Francesca, "Roles of dopants, interstitial O_2 and temperature in the effects of irradiation on silica-based optical fibers", Ph.D. dissertation, University of Saint-Étienne, Saint-Etienne, 2015.

[84] Giusy Origlio, "Properties and Radiation Response of Optical Fibers: Role of Dopants" Ph.D. dissertation, University of Saint-Étienne, Saint-Etienne, 2009.

[85] Blandine Tortech, "Effets des radiations sur des fibres optiques dopées erbium," Ph.D. dissertation, University of Saint-Étienne, Saint-Etienne, 2008.

[86] K. V. Zotov, M. E. Likhachev, A. L. Tomashuk, M. L. Bubnov, M. V.Yashkov, A. N. Guryanov, and S. N. Klyamkin, "Radiation-resistant erbium-doped fiber for spacecraft applications," IEEE Trans. Nucl. Sci.,vol. 55, no. 4, pp. 2213–2215, Aug. 2008.

[87] A. Morana, "Gamma-rays and neutrons effects on optical fibers and Bragg gratings for temperature sensors", Ph.D. dissertation, University of Saint-Étienne, Saint-Etienne, 2013.

[88] B.P. Fox, "Investigation of Ionizing-Radiation-Induced Photodarkening in Rare-Earth-Doped Optical Fiber Amplifier Materials", Ph.D. dissertation, University of Arizona, 2013.

[89] Jérémie Thomas, "Impact de la nanostructuration des fibres dopées Erbium sur leurs performances : application aux contraintes du spatial" Ph.D. dissertation, University of Montpellier, 2013.

[90] Ayoub Ladaci, "Rare Earth Doped Optical Fibers and Amplifiers for Space Applications" ", Ph.D. dissertation, University of Saint-Étienne, 2017.

[91] M. E. Likhachev, M. M. Bubnov, K. V. Zotov, A.L. Tomashuk, D.S. Lipatov, M.V. Yashkov, and A.N. Guryanov, "Radiation Resistance of Er-Doped Silica Fibers: Effect of Host Glass Composition," in *Journal of Lightwave Technology*, vol. 31, no. 5, pp. 749-755, 2013.

[92] H. Henschel, O. Kohn, H. U. Schmidt, J. Kirchof, and S. Unger, "Radiation- induced loss of rare earth doped silica fibres," *IEEE Transactions on Nuclear Science*, vol. 45, no. 3, pp. 1552–1557, Jun. 1998.

[93] Jean-Bernard Duchez, "Étude du noircissement dans les fibres optiques dopées Ytterbium : interaction entre photo- et radio-noircissement", Ph.D. dissertation, University of Nice, 2015.

[94] M. Lezius, K. Predehl, W. Stower, A. Turler, M. Greiter, C. Hoeschen, P. Thirolf, W. Assmann, D. Habs, A. Prokofiev, C. Ekstrom, T. W. Hansch, and R. Holzwarth, "Radiation induced absorption in rare earth doped optical fibers," *IEEE Transactions on Nuclear Science* 59(2), 425–433 (2012).

[95] E. J. Friebele, L. A. Brambani, M. E. Gingerich, S. J. Hickey, and J. R. Onstott, "Radiation-induced attenuation in polarization maintaining fibers: Low dose rate response, stress, and materials effects," Appl. Opt., vol. 28, no. 23, pp. 5138–5143, 1989.

[96] Y. K. Chamorovskii, O. V. Butov, G. I. Ivanov, A. A. Kolosovskii, V.V. Voloshin, I. L. Vorob'ev, and K. M. Golant, "N-doped-silica-core polarization maintaining fibre for gyros and other sensors for application in space industry," in Proc. SPIE Vol 7503, 2009, pp.75036T-1–75036T-1.

[97] E. W. Taylor, V. R. Wilson, M. L. Vigil, R. A. Lemire, and E. E. Thompson, "Ionization-induced nonequivalent absorption in a birefringent silica fiber," IEEE Photon. Technol. Lett., vol. 1, pp. 248–249, 1989.

[98] S. Girard, A. Yahya, A. Boukenter, Y. Ouerdane, J.-P. Meunier, R. E. Kristiansen, and G. Vienne, "Gamma radiation-induced attenuation in photonic crystal fibre,"IEE Electron. Lett., vol. 38, no. 20, pp. 1169–1171, 2002.

[99] A. F. Kosolapov, I. V. Nikolin, A. L. Tomashuk, S. L. Semjonov, and M. O. Zabezhailov, "Optical losses in as prepared and gamma-irradiated microstructured silica-core optical fibers," Inorg. Mater., vol. 40, no. 11, pp. 1229–1232, 2004.

[100] S. Girard, Y. Ouerdane, M. Bouazaoui, C. Marcandella, A. Boukenter,L. Bigot, and A. Kudlinski, "Transient radiation-induced effects on solid core microstructured optical fibers," Opt. Exp., vol. 19, pp.21760–21767, 2011.

[101] G. Cheymol, H. Long, J. F. Villard, and B. Brichard, "High level gamma and neutron irradiation of silica optical fibers in CEA OSIRIS nuclear reactor," *IEEE Transactions on Nuclear Science*, vol. 55, no. 4, pp. 2252–2258, Aug. 2008.

[102] K. O. Hill and G. Meltz, "Fiber Bragg grating technology: Fundamentals and Overview", Journal of Lightwave Technology, 15 (8), pp. 1263-1276 (1997).

[103] K. O. Hill, Y. Fujii, D. C. Johnson and B.S. Kawasaki, "Photosensitivity in optical fiber waveguides: Application to reflection filter fabrication", Applied Physics Letters, 32 (10), pp. 647-649 (1978).

[104] B. Malo, K.O. Hill, F. Bilodeau, D.C. Johnson and J. Albert, "Point by point fabrication of micro-Bragg gratings in photosensitive fibre using single excimer pulse refractive index modification techniques", Electronics Letters, 29, pp. 1668-1669 (1993).

[105] K. O. Hill, B. Malo, F. Bilodeau, D. C. Johnson and J. Albert, "Bragg gratings fabricated in monomode photosensitive optical fiber by UV exposure through a phase mask", Applied Physics Letters, 62 (10), pp. 1035-1037 (1993).

[106] A. D. Kersey, M. A. Davis, H. J. Patrick, M. LeBlanc, K. P. Koo, C. G. Askins, M. A. Putnam, and E. J. Friebele, "Fiber Grating Sensors", Journal of Lightwave Technology, vol.15, n°8, 1997.

* Corresponding author: Sylvain Girard, sylvain.girard@univ-st-etienne.fr : Phone: +33 (0)477 915 812

[107] A. Morana, S. Girard, E. Marin, M. Lancry, C. Marcandella, P. Paillet, L. Lablonde, T. Robin, R. J. Williams, M. J. Withford, A. Boukenter and Y. Ouerdane, "Influence of photo-inscription conditions on the radiation-response of fiber Bragg gratings," Opt. Express, vol. 23, no. 7, pp. 8659-8669, 2015.

[108] A. Morana, S. Girard, E. Marin, C. Marcandella, P. Paillet, J. Périsse, J.-R. Macé, A. Boukenter, M. Cannas and Y. Ouerdane, "Radiation tolerant Fiber Bragg Gratings for high temperature monitoring at MGy dose levels," Opt. Lett., vol. 39, no. 18, pp. 5313-5316, 2014.

[109] T.T. Tam, D.Q. Trung, T.A. Vu, L.H. Minh and D.N. Chung, "Investigation of the embedded fiber bragg grating temperature sensor", VNU Journal of Science, Mathematics - Physics, 23, pp. 237-242 (2007).

[110] T. Erdogan, V. Mizrahi, P.J. Lemaire and D. Monroe, "Decay of ultraviolet-induced fiber Bragg gratings", Journal of Applied Physics, 76 (1), pp. 73-80 (1994).

[111] S.R. Baker, H.N. Rourke, V. Baker and D. Goodchild, "Thermal decay of fiber Bragg gratings written in boron and germanium codoped silica fiber", Journal of Lightwave Technology, 15 (8), pp. 1470-1477 (1997).

[112] D.A. Barber and N.H. Rizvi, Proc. SPIE 4941, "A practical study of the effects of exposure conditions on the quality of fibre Bragg gratings written with excimer and argon-ion lasers", Laser Micromachining for Optoelectronic Device Fabrication, 16 (2003).

[113] S.J. Mihailov, C.W. Smelser, P. Lu, R.B. Walker, D. Grobnic, H. Ding, G. Henderson and J. Unruh, "Fiber Bragg gratings made with a phase mask and 800-nm femtosecond radiation", Optics Letters, 28 (12), pp. 995-997, 2003.

[114] T.-E. Tsai, G.M. Williams and E.J. Friebele, "Index structure of fiber Bragg gratings in Ge-SiO$_2$ fibers", Optics Letters, 22 (4), pp. 224-226, 1997.

[115] S.J. Mihailov, C.W. Smelser, D. Grobnic, R.B. Walker, P. Lu, H. Ding, and J. Unruh, "Bragg Gratings written in All-SiO$_2$ and Ge-doped core fibers with 800-nm femtosecond radiation and a phase mask", Journal of Lightwave Technology, 22 (1), pp. 94-100^2, 2004.

[116] C.W. Smelser, S.J. Mihailov and D. Grobnic, "Hydrogen loading for fiber grating writing with a femtosecond laser and a phase mask", Optics Letters, 29 (18), pp. 2127-2129, 2004.

[117] J.-L. Archambault, L. Reekie and P.St.J. Russell, "100% Reflectivity Bragg reflectors produced in optical fibers by single excimer laser pulses", Electronics Letters, 29 (5), pp. 453-455, 1993.

[118] C.W. Smelser, S.J. Mihailov and D. Grobnic, "Formation of Type I-IR and Type II-IR gratings with an ultrafast IR laser and a phase mask", Optics Express, 13 (14), pp. 5377-5386, 2005.

[119] Y. Liu, J.A.R. Williams, L. Zhang and I. Bennion, "Abnormal spectral evolution of fiber Bragg gratings in hydrogenated fibers," Optic Letters, 27 (8), pp. 586-588, 2002.

[120] L. Dong, W. F. Liu and L. Reekie, "Negative-index gratings formed by a 193-nm excimer laser", Optics Letters, 21 (24), pp. 2032-2034, 1996.

[121] S. Pissadakis and M. Konstantaki, "Type IIA gratings recorded in B-Ge codoped optical fibre using 213nm Nd:YAG radiation", 31st European Conference on Optical Communication, 3, pp. 563-564, 2005.

[122] E. Lindner, J. Canning, C. Chojetzki, S. Bruckner, M. Becker, M. Rothhardt and H. Bartelt, "Thermal regenerated type IIa fiber Bragg gratings for ultra-high temperature operation", Optics Communications, 284, pp. 183-185, 2011.

[123] A. Martinez, M. Dubov, I. Khrushchev and I. Bennion, "Photo-induced modifications in fiber gratings inscribed directly by infrared femtosecond irradiation," IEEE Photonics Technology Letters, vol. 18 no. 21, pp. 2266-2268, 2006.

[124] A. Martinez, I. Khrushchev, and I. Bennion, "Thermal properties of fiber Bragg gratings inscribed point-by-point by an infrared femtosecond laser," Electron. Lett., vol. 41, pp. 176–177, 2005.

[125] G. P. Agrawal, Nonlinear Fiber Optics,5th ed. (Academic Press, 2012).

[126] S. Sakaguchi, S.-i. Todoroki, and S. Shibata, "Rayleigh Scattering in Silica Glasses", Journal of the American Ceramic Society, 79: 2821–2824, 1996.

[127] J.P. Dakin, "Distributed optical fiber sensors", Proc. SPIE 1797, Distributed and Multiplexed Fiber Optic Sensors II, Boston (USA), 76, 1993.

* Corresponding author: Sylvain Girard, sylvain.girard@univ-st-etienne.fr : Phone: +33 (0)477 915 812

78

[128] Y. Li, F. Zhang and T. Yoshino, "Wide temperature-range Brillouin and Rayleigh optical-time-domain reflectometry in a dispersion-shifted fiber", Applied Optics, 42 (19), pp. 3772-3775, 2003.

[129] D.K. Gifford, B.J. Soller, M.S. Wolfe and M.E. Froggatt, "Distributed fiber-optic temperature sensing using Rayleigh backscatter", 31st European Conference on Optical Communication (ECOC 2005), 3, pp. 511-512, 2005.

[130] L. Thévenaz, "Novel schemes for optical signal generation using laser injection locking with application to Brillouin sensing", Frontiers of Optoelectronics in China, 3 (1), pp. 13-21, 2010.

[131] T. Kurashima, T. Horiguchi and M. Tateda, "Distributed-temperature sensing using stimulated Brillouin scattering in optical silica fibers", Optics Letters, 15 (18), pp. 1038-1040, 1990.

[132] J. R. Ferraro, K. Namamoto, and C. W. Brown, "Introductory Raman Spectroscopy", Academic Press, 2003.

[133] A. Fernandez Fernandez, P. Rodeghiero, B. Brichard, F. Berghmans, A.H. Hartog, P. Hughes, K. Williams, A.P. Leach., "Radiation-tolerant Raman distributed temperature monitoring system for large nuclear infrastructures," in IEEE Transactions on Nuclear Science, vol. 52, no. 6, pp. 2689-2694, Dec. 2005.

[134] G. Failleau, O. Beaumont, R. Razouk, S. Delepine Lesoille, M. Landolt, B. Courthial, J.M. Hénault, F. Martinot, J. Bertrand, B. Hay, "A metrological comparison of Raman-distributed temperature sensors" Measurement, vol.116, Pages 18-24, 2018.

[135] S Delepine-Lesoille, I Planes, M Landolt, G Hermand, O Perrochon, "Compared performances of Rayleigh Raman and Brillouin distributed temperature measurements during concrete container fire test", Optical Fiber Sensors Conference (OFS) 25th, 1-4, 2017.

[136] S. Delepine-Lesoille, X. Phéron, J. Bertrand, G. Pilorget, G. Hermand, R. Farhoud, Y. Ouerdane, A. Boukenter, S. Girard, L. Lablonde, D. Sporea and V. Lanticq, "Industrial Qualification Process for Optical Fibers Distributed Strain and Temperature Sensing in Nuclear Waste Repositories," Journal of Sensors, vol. 2012, Article ID 369375, 2012.

[137] D. Cornwell: "Space-Based Laser Communications Break Threshold," Optics and Photonics News vol. 27, pp. 24-31, 2016.

[138] T. Dreischer, B. Thieme, M. Bacher, K. Buchheim, "OPTEL-μ: A compact system for optical downlink from LEO satellites", SpaceOps, vol. 1, pp. 789-798, 2012.

[139] S. Yamakawa, Y. Chishiki, Y. Sasaki, Y. Miyamoto, H. Kohata, "JAXA's Optical Data Relay Satellite Programme," ICSOS 2015.

[140] G. Muehlnikel, H. Kämpfner, F. Heine, H. Zech, D. Troendle, R. Meyer, S. Philipp-May, "The Alphasat GEO Laser Communication Terminal Flight Acceptance Tests," ICSOS 2012, 5-1, 2012.

[141] Y. Chishiki, S. Yamakawa, Y. Takano, Y. Miyamoto, T. Araki, H. Kohata, "Overview of optical data relay system in JAXA," Proc. of SPIE Vol. 9739, 97390D-1, 2016.

[142] Shen-En Qian: "Optical payload for space missions," Wiley, 2016

[143] E. Kehayas, L. Stampoulidis, P. Henderson, A. Robertson, F. Van Dijk, M. Achouche, A. Le Kernec, M. Sotom, F. Schuberts, T. Brabant, "The european project HIPPO high-power photonics for satellite laser communications and on-board optical processing," ICSO 2014.

[144] A. Ladaci, S. Girard, L. Mescia, T. Robin, A. Laurent, B. Cadier, M. Boutillier, Y. Ouerdane, A. Boukenter : "Optimization of rare-earth-doped amplifiers for space mission through a hardening-by-system strategy," Proc. SPIE 10096, 100960F-1, 2017.

[145] A. Ladaci, S. Girard, L. Mescia, T. Robin, A. Laurent, B. Cadier, M. Boutillier, Y. Ouerdane, A. Boukenter: "Optimized Radiation-Hardened Erbium Doped Fiber Amplifiers for Long Space Missions", J of Applied Physics, vol. 121, 163104, 2017.

[146] L. Mescia, S. Girard, P. Bia, T. Robin, A. Laurent, F. Prudenzano, A. Boukenter, Y. Ouerdane: "Optimization of the design of high power Er^{3+}/Yb^{3+}–codoped fiber amplifiers for space missions by means of particle swarm approach," IEEE J. Selected Topics in Quantum Electronics, vol. 20, Article 3100108, 2014.

[147] S. Girard, L. Mescia, M. Vivona, A. Laurent, Y. Ouerdane, C. Marcandella, F. Prudenzano, A. Boukenter, T. Robin, P. Paillet, V. Goiffon, M. Gaillardin, B. Cadier, E. Pinsard, M. Cannas, R. Boscaino:

* Corresponding author: Sylvain Girard, sylvain.girard@univ-st-etienne.fr : Phone: +33 (0)477 915 812

"Design of Radiation-Hardened Rare-Earth Doped Amplifiers through a Coupled Experiment/Simulation Approach," J. Lightwave Technology, vol. 31, pp. 1247-1254, 2013.

[148] L. Stampoulidis, J. Edmunds, M. Kechagias, G. Stevens, J. Farzana, M. Welch, E. Kehayas: "Radiation-resistant optical fiber amplifiers for satellite communications," Proc. of SPIE Vol. 10096, 100960H, 2017.

[149] D. Engin, F. Kimpel, J. Burton, H. Cao, B. McIntosh, M. Storm, S. Gupta, "Highly efficient and athermal 1550nm-fiber-MOPA-based high power down link laser transmitter for deep space communication", Proc. SPIE 8610, 86100G, 2013.

[150] L. Stampoulidis, E. Kehayas, M. Kehayas, G. Stevens, L Henwood-Moroney, P. Hosking, A. Robertson: "Radiation-hard mid-power booster optical fiber amplifiers for high-speed digital and analogue satellite laser communication links," ICSO 2014.

[151] Mi Li, W. Jiao, Y. Song, X. Zhang, L. Chang: "Self-Adaptive High Anti-Radiation EDFA for Space Optical Communication Systems," J. Lightwave Technol., vol. 33, pp.4513-4516, 2015.

[152] J. MacDougall, P. Henderson, P. Naylor, J. Elder, A. Norman, I. Turner, L. Stampoulidis, E. Kehayas: "Transmission and pump laser modules for space applications," Proc. of SPIE Vol. 10096 100960I-1, 2017.

[153] M. W. Wright, H. Yao, J. R. Marciante: "Resonant Pumping of Er-Doped Fiber Amplifiers for Improved Laser Efficiency in Free-Space Optical Communications," IPN Progress Report 42-189, 2012

[154] "The Fiber-Optic Gyroscope", Hervé Lefèvre, ISBN-13 978-1-60807-695-6,2014 Artech House

[155] "The Fiber Optic Gyroscope : Achievement and Perspective", Hervé Lefevre, ISSN 2075-1087, Gyroscopy and Navigation, Vol 3, No 4, pp 223-226, 2012.

[156] E.J.Post, "Sagnac effect", Review of Modern Physics, Vol. 39, 475-494, 1967.

[157] H.J Arditty and H.C. Lefèvre, "Sagnac effect in fiber gyroscopes", Optics Letters, Vol. 6, 401-403, 1981.

[158] G. Sagnac, Comptes rendus à l'Académie des Sciences, Vol. 95, 708-710, 1913.

[159] K.A.Fesler, R.F. Kalman, M.J.F. Digonnet, B.Y. Kim, and H.J. Shaw, "Behavior of Broadband Fiber Sources in a Fiber Gyroscope," SPIE Proceedings, Vol. 1171, pp. 346–352, 1989.

[160] P.F.Wysocki, R.F Kalman, M.J.F. Digonnet, B.Y. Kim, "1.55 µm broadband fiber sources pumped near 980 nm," SPIE Proceedings, Vol. 1373, pp. 66–77, 1990.

[161] P.R. Ashley, M.G. Temmen, M. Sanghadasa, "Applications of SLDs in fiber optical gyroscopes", Proc. SPIE 4648, Test and Measurement Applications of Optoelectronic Devices, 2002.

[162] S. Ezekiel, E. Udd, eds., "Fiber Optic Gyro: 15th Anniversary Conference," SPIE Proceedings, Vol. 1585, 1991.

[163] P.G. Suchosky, T.K. Findakly, T.K. and F.L. Leonberger, "LiNbO3 Integrated Optical Components for Fiber-Optic Gyroscopes," SPIE Proceedings, Vol. 993, 240–243, 1988.

[164] R. Ulrich, "Fiber-optic rotation sensing with low drift", *Opt. Lett.*, vol. 5, pp. 173-175, 1980

[165] H. Lefevre, P. Martin, J. Morisse, P. Simonpietri, P. Vivenot, H. Arditti, « High dynamic range fiber gyro with all-digital signal processing », Proc. Vol. 1367, Fiber Optic and Laser Sensors VIII (1991)

[166] S. Girard, C. Marcandella, "Transient and Steady State Radiation Responses of Solarization-Resistant Optical Fibers", IEEE Transactions on Nuclear Science, vol. 57, n°4, pp.2049-2055, 2010.

[167] L. Skuja, "Optically active oxygen-deficiency-related centers in amorphous silicon dioxide", Journal of Non-Crystalline Solids, vol. 239, pp.16-48, 1998.

[168] A. Johan, B. Azaïs, C. Malaval, G. Raboisson, and M. Roche, "ASTERIX, un nouveau moyen pour la simulation des effets de débit de dose sur l'électronique," Ann. Phys., vol. 14, pp. 379–393, 1989.

[169] B. Capoen, H. El Hamzaoui, M. Bouazaoui, Y. Ouerdane, A. Boukenter, S. Girard, C. Marcandella, O. Duhamel, "Sol-gel derived copper-doped silica glass as a sensitive material for X-ray beam dosimetry", Optical Materials, Volume 51, pp. 104–109, 2016.

[170] S. Girard; B. Capoen; H. El Hamzaoui; M. Bouazaoui; G. Bouwmans; A. Morana; D. Di Francesca; A. Boukenter; O. Duhamel; P. Paillet; M. Raine; M. Gaillardin; M. Trinczek; C. Hoehr; E. Blackmore; Y. Ouerdane, "Potential of Copper- and Cerium-doped Optical Fiber Materials for Proton Beam Monitoring", IEEE Transactions on Nuclear Science, vol.64, n°1, pp. 567 - 573, 2017.

* Corresponding author: Sylvain Girard, sylvain.girard@univ-st-etienne.fr : Phone: +33 (0)477 915 812

[171] W. Primak, "Fast-neutron-induced changes in quartz and vitreous silica," Phys. Rev. B, vol. 110, no. 6, pp. 1240–1254, 1958.

[172] E. Lell, N. J. Hensler, and J. R. Hensler, J. Burke, Ed., "Radiation effects in quartz, silica and glasses," in Progr. Ceramic Sci., New York, 1966, vol. 4, pp. 3–93, Pergamon.

[173] M. León, L. Giacomazzi ; S. Girard ; N. Richard ; P. Martín ; L. Martín-Samos ; A. Ibarra ; A. Boukenter ; Y. Ouerdane, "Neutron Irradiation Effects on the Structural Properties of KU1, KS-4V and I301 Silica Glasses," in IEEE Transactions on Nuclear Science, vol. 61, no. 4, pp. 1522-1530, 2014.

[174] L. Skuja, "Optical properties of defects in silica," in Defects in and Related Dielectrics: Science and Technology (NATO Science Series II), G. Pacchioni, L. Skuja, and D.L. Griscom, Eds. Dordrecht, The Netherlands: Kluwer, pp. 73–116, 2000.

[175] M. Cannas, "Point Defects in Amorphous SiO_2: Optical Activity in the Visible, UV and Vacuum-UV Spectral Regions," Ph.D. dissertation, Università di Palermo, Palermo, Italy, 1998.

[176] S. Agnello, "Gamma Ray Induced Processes of Point Defect Conversion in Silica," Ph.D. dissertation, Università di Palermo, Palermo, Italy, 2000.

[177] S. Girard, B. Vincent, J.-P. Meunier, Y. Ouerdane, A. Boukenter, and A. Boudrioua, "Spatial distribution of the red luminescence in pristine, gamma-rays and ultraviolet-irradiated multimode optical fibers", Applied Physics Letters, vol. 84, pp. 4215-4217, 2004.

[178] B. Tortech, S. Girard, E. Régnier, Y. Ouerdane, A. Boukenter, J-P. Meunier, M. Van Uffelen, A. Gusarov, F. Berghmans, and H. Thienpont, "Core versus cladding effects of proton irradiation on erbium-doped optical fiber: micro-luminescence study", IEEE Transactions on Nuclear Science, Vol. 55, pp. 2223-2228, 2008.

[179] I. Reghioua, S. Girard, A. Alessi, D. Di Francesca, L. Martin-Samos, M. Fanetti, N. Richard, M. Raine, M. Valant, A. Boukenter, Y. Ouerdane, "Cathodoluminescence investigation of Ge-point defects in silica-based optical fibers" Journal of Luminescence, vol.179, pp.1-7, 2016.

[180] I. Reghioua, S. Girard, M. Raine, A. Alessi, D. Di Francesca, M. Fanetti, L. Martin-Samos, N. Richard, M. Valant, A. Boukenter, and Y. Ouerdane, "Cathodoluminescence Characterization of Point Defects in Optical Fibers", IEEE Transactions on Nuclear Science, vol.64, n°8, pp. 2318 - 2324, 2017.

[181] S. Girard, J. Keurinck, A. Boukenter, J.-P. Meunier, Y. Ouerdane, B. Azaïs, P. Charre, and M. Vié, "Gamma-rays and pulsed X-ray radiation responses of nitrogen, germanium doped and pure silica core optical fibers", Nuclear Instruments and Methods in Physics Research B, vol. 215, pp. 187-195, 2004.

[182] Gwendal Beauvois, "Projet DROÏD : étude et développement d'un dosimètre distribué à fibre optique » Ph.D. dissertation, Université de Perpignan Via Domitia, Perpignan, 2017.

[183] S. Girard, J. Keurinck, Y. Ouerdane, J.-P. Meunier, and A. Boukenter, "gamma-Rays and Pulsed X-Ray Radiation Responses of Germanosilicate Single-Mode Optical Fibers: Influence of Cladding Codopants", IEEE/OSA Journal of Lightwave Technology, vol. 22, pp. 1915-1922, 2004.

[184] L. Skuja, K. Kajihara, K. Smits, A. Silins, H. Hosono, "Luminescence and Raman Detection of Molecular Cl_2 and ClClO Molecules in Amorphous SiO_2 Matrix", J. Phys. Chem. C, vol. 121, 5261–5266, 2017.

[185] K. Tanimura, C. Itoh, and N. Itoh, "Transient optical absorption and luminescence induced by band-to-band excitation in amorphous SiO_2," J. Phys. C: Solid State Phys, vol. 21, pp. 1869–1876, 1988.

[186] Y. Sasajima and K. Tanimura, "Optical transitions of self-trapped holes in amorphous SiO_2," Phys. Rev. B, vol. 68, pp. 014204–014204, 2003.

[187] A. L. Tomashuk, M.Y. Salgansky, P.F. Kashaykin, V.F. Khopin, A.I. Sultangulova, K.N. Nishchev, S.E. Borisovsky, A.N. Guryanov, and E.M. Dianov, "Enhanced Radiation Resistance of Silica Optical Fibers Fabricated in High O_2 Excess Conditions," in Journal of Lightwave Technology, vol. 32, no. 2, pp. 213-219, 2014.

[188] P. F. Kashaykin, A.L. Tomashuk, M. Yu. Salgansky, A.N. Guryanov, and E.M. Dianov, "Anomalies and peculiarities of radiation-induced light absorption in pure silica optical fibers at different temperatures", Journal of Applied Physics, vol. 121, 213104, 2017.

[189] G. Origlio, M. Cannas, S. Girard, R. Boscaino, A. Boukenter, and Y. Ouerdane, "Influence of the drawing process on the defect generation in multistep-index germanium-doped optical fibers", Optics Letters, vol. 34, n°15, pp. 2282-2284, 2009.

[190] S. Girard, C. Marcandella, A. Alessi, A. Boukenter, Y. Ouerdane,N. Richard, P. Paillet, M. Gaillardin, and M. Raine, "Transient Radiation Responses of Optical Fibers: Influence of MCVD Process Parameters", IEEE Transactions on Nuclear Science, vol.59, issue n°6, pp. 2894 – 2901, 2012.

[191] Y. Watanabe, H. Kawazoe, K. Shibuya and K. Muta, "Structure and Mechanism of Formation of Drawing- or Radiation-Induced Defects in SiO_2:GeO_2 Optical Fiber", Japanese Journal of Applied Physics, Volume 25, Part 1, Number 3, 1986.

[192] A. Alessi, S. Girard, M. Cannas, S. Agnello, A. Boukenter and Y. Ouerdane, "Influence of Drawing Conditions on the Properties and Radiation Sensitivities of Pure-Silica-Core Optical Fibers," in Journal of Lightwave Technology, vol. 30, no. 11, pp. 1726-1732, June1, 2012.

[193] B. Brichard, P. Borgermans, A. F. Fernandez, K. Lammens and A. Decreton, "Radiation effect in silica optical fiber exposed to intense mixed neutron-gamma radiation field," in IEEE Transactions on Nuclear Science, vol. 48, no. 6, pp. 2069-2073, 2001.

[194] D. L. Griscom, M. E. Gingerich, and E. J. Friebele, "Model for the dose, dose-rate and temperature dependence of radiation-induced loss in optical fibers," IEEE Trans. Nucl. Sci., vol. 41, no. 3, pp. 523–526, 1994.

[195] D. L. Griscom, "Fractal kinetics of radiation-induced point-defect formation and decay in amorphous insulators: Application to color centers in silica-based optical fibers," Phys. Rev. B, vol. 64, no. Doc. ID 174201, 2001.

[196] H. Henschel, O. Köhn, and H. U. Schmidt, "Influence of dose rate on radiation induced loss in optical fibres," in Proc. SPIE Ser. 1399, pp. 49–63, 1991.

[197] E. J. Friebele, C. G. Askins, and M. E. Gingerich, "Effect of low dose rate irradiation on doped silica core optical fibers," Appl. Opt., vol. 23, no. 23, pp. 4202–4208, 1984.

[198] F. Mady, M. Benabdesselam, J-B. Duchez,Y. Mebrouk, and S. Girard, "Global View on Dose Rate Effects in Silica-Based Fibers and Devices Damaged by Radiation-Induced Carrier Trapping", ", IEEE Transactions on Nuclear Science, vol.60, n°6, pp. 4241-4348, 2013

[199] S. Girard, C. Marcandella, A. Morana, J. Perisse, D. Di Francesca, P. Paillet, J-R. Macé, A. Boukenter, M. Léon, M. Gaillardin, N. Richard, M. Raine, S. Agnello, M. Cannas and Y. Ouerdane, "Combined High Dose and Temperature Radiation Effects on Multimode Silica-based Optical Fibers", IEEE Transactions on Nuclear Science, vol.60, n°6, pp. 4305 - 4313, 2013.

[200] T. Blue, "Testing of Performance of Optical Fibers Under Irradiation in Intense Radiation Fields When Subjected to High Temperature", Reactors Concept RD&D, Project No. 09-81, 2012.

[201] E. Regnier, I. Flammer, S. Girard, F. Gooijer, F. Achten, G. Kuyt, "Low-dose radiation-induced attenuation at infrared wavelengths for P-doped, Ge-doped and pure silica-core optical fibres", IEEE Transactions on Nuclear Science, vol.54, n°4, pp. 1115-1119, 2007.

[202] H. Henschel and O. Kohn, "Regeneration of irradiated optical fibres by photobleaching?," IEEE Trans. Nucl. Sci., vol. 47, no. 3, pp. 699–704, Jun. 2000.

[203] H. Mori, Y. Suzuki, and M. Hirai, "Selective photobleaching of radiation-induced absorption in a-SiO_2 ," Nucl. Instrum. Meth. Phys. Res.B, vol. 91, pp. 391–394, 1994.

[204] E.J. Friebele, M.E. Gingerich, « Photobleaching Effects in optical waveguide », Applied Optics 1981.

[205] K. Nagasawa, Y. Hoshi, Y. Ohki, and K. Yahagi, "Improvement of radiation resistance of pure silica core fibers by hydrogen treatment," Jpn. J. Appl. Phys., vol. 24, pp. 1224–1228, 1985.

[206] J. E. Shelby, "Radiation effects in hydrogen impregnated vitreous silica," J. Appl. Phys., vol. 50, no. 5, pp. 3702–3706, 1979.

[207] B. Brichard, A. L. Tomashuk, H. Ooms, V. A. Bogatyrjov, S. N. Klyamkin, A. F. Fernandez, F. Berghmans, and M. Decréton, "Radiation assessment of hydrogen-loaded aluminium-coated pure silica core fibres for ITER plasma diagnostic applications," Fusion Eng. Des., vol. 82, pp. 2451–2455, 2007.

[208] D. L. Griscom, "Radiation hardening of pure-silica-core optical fibers: Reduction of induced absorption bands associated with self-trapped holes," Appl. Phys. Lett., vol. 71, pp. 175–177, 1997

[209] D.L. Griscom, "Radiation hardening of pure silica core optical fibers and their method of making by ultra-high-dose gamma ray pre-irradiation", Patent US 5574820 A, 1995.

* Corresponding author: Sylvain Girard, sylvain.girard@univ-st-etienne.fr : Phone: +33 (0)477 915 812

[210] T. Shikama, T. Kakuta, N. Shamoto, M. Narui, T. Sagawa, "Behavior of developed radiation-resistant silica-core optical fibers under fission reactor irradiation", Fusion Engineering and Design, vol. 51 – 52, pp. 179 – 183, 2000.

[211] T. Wijnands, K. Aikawa, J. Kuhnhenn, D. Ricci, and U. Weinand, "Radiation tolerant optical fibers: From sample testing to large series production,"J. Lightw. Technol., vol. 29, no. 22, pp. 3393–3400, 2011.

[212] E.M. Dianov, K. M. Golant, R. R. Khrapko, A. S. Kurkov, and A. L. Tomashuk, "Low-hydrogen silicon oxynitride optical fibers prepared by SPCVD," J. Lightw. Technol., vol. 13, no. 7, pp. 1471–1474, 1995.

[213] A. L. Tomashuk, E. M. Dianov, K. M. Golant, R. R. Khrapko, and D. E. Spinov, "Performance of special radiation-hardened optical fibers intended for use in the telecom spectral windows at a megagray level," IEEE Trans. Nucl. Sci., vol. 45, no. 3, pp. 1566–1569, Jun. 1998

[214] M. Lancry, B. Hari Babu, N. Ollier, B. Poumellec, "Radiation hardening of silica glass through fictive temperature reduction", Int J Appl Glass Sci., vol.8, pp.285-290, 2017.

[215] https://www.fujikura.co.uk/products/medical-industrial-optical-fibre/radiation-resistant-fibre/radiation-resistant-fibre/

[216] https://photonics.ixblue.com/products-list-detail/rad-hard-harsh-environment-custom-passive-fibers

[217] https://www.prysmiangroup.com/en/en_fibre_speciality-drakaelite_radhard_radhard2.html

[218] G. Origlio, M. Cannas, S. Girard, R. Boscaino, A. Boukenter, and Y. Ouerdane, "Influence of the drawing process on the defect generation in multistep-index germanium-doped optical fibers", Optics Letters, vol. 34, n°15, pp. 2282-2284,2009.

[219] A. Alessi, S. Girard, C. Marcandella, S. Agnello, M. Cannas, A. Boukenter and Y. Ouerdane, "X-ray irradiation effects on a multistep Ge-doped fiber produced using different drawing conditions", Journal of Non-Crystalline Solids, vol.357(8-9), pp. 1966-1970, 2011.

[220] A. Alessi, S. Girard, M. Cannas, S. Agnello, A. Boukenter and Y. Ouerdane, "Influence of drawing conditions on the properties and radiation sensitivities of pure-silica-core optical fibers", Journal of Lightwave Technology, Vol. 30, Issue 11, pp. 1726-1732, 2012.

[221] H. Henschel, S. K. Hoeffgen, K. Krebber, J. Kuhnhenn, and U. Weinand, "Influence of Fiber Composition and Grating Fabrication on the Radiation Sensitivity of Fiber Bragg Gratings," IEEE Trans. Nucl. Sci, vol. 55, no. 4, pp. 2235–2242, Aug. 2008

[222] T. Blanchet, A. Morana, T. Allanche, C. Sabatier, I. Reghioua, E. Marin, A. Boukenter, Y. Ouerdane, P. Paillet, M. Gaillardin, O. Duhamel, C. Marcandella, M. Trinczek, G. Assaillit, G. Auriel, D. Aubert, G. Laffont, and S. Girard, "X-rays, Protons and Electrons Radiation Effects on Type I Fiber Bragg Gratings", IEEE Trans. Nucl. Sci, submitted to, 2017.

[223] S. Rizzolo, E. Marin, A. Morana, A. Boukenter, Y. Ouerdane, M. Cannas, J. Perisse, S. Bauer, J-R. Mace and S. Girard, "Investigation of Coating Impact on OFDR Optical remote Fiber-based Sensors Performances for Their Integration in High Temperature and Radiation Environments", Journal of Lightwave Technology, Volume: 34, Issue: 19, pp. 4460 - 4465, 2016.

[224] O. Gilard, M. Caussanel, H. Duval, G. Quadri, and F. Reynaud, "New model for assessing dose, dose rate, and temperature sensitivity of radiation-induced absorption in glasses," J. Appl. Phys., vol. 108, pp.093115–093115, 2010.

[225] V. A. Mashkov, W. R. Austin, L. Zhang, and R. G. Leisure, "Fundamental role of creation and activation in radiation-induced defect production in high-purity amorphous SiO_2," Phys. Rev. Lett., vol. 76, pp.2926–2929, 1996.

[226] D. L. Griscom, "γ-Ray-induced visible/infrared optical absorption bands in pure and F-doped silica-core fibers: Are they due to self-trapped holes?," J. Non-Cryst. Solids, vol. 349, pp. 139–147, 2004.

[227] D. L. Griscom, "Self-trapped holes in pure-silica glass: A history of their discovery and characterization and an example of their critical significance to industry," J. Non-Cryst. Solids, vol. 352, pp. 2601–2617, 2006.

[228] Y. Sasajima and K. Tanimura, "Optical transitions of self-trapped holes in amorphous SiO_2 ," Phys. Rev. B, vol. 68, pp. 014204–014204, 2003.

* Corresponding author: Sylvain Girard, sylvain.girard@univ-st-etienne.fr : Phone: +33 (0)477 915 812

[229] FOTP-64 Procedure for Measuring Radiation-Induced Attenuation in Optical Fibers and Optical Cables, TIA-455-64 1998 Edition, 1998.

[230] IEC 60793-1-54:2018: "Optical fibres - Part 1-54: Measurement methods and test procedures - Gamma irradiation", January 12, 2018.

[231] M. J. Lu Valle, E. J. Friebele, F. V. Dimarcello, G. A. Miller, E. M. Monberg, L. R. Wasserman, Patrick W. Wisk, Man F. Yan, Elizabeth M. Birtch, "Radiation-induced loss predictions for pure silica core polarization-maintaining fibers", Proc. SPIE 6193, Reliability of Optical Fiber Components, Devices, Systems, and Networks III, 61930J (24 May 2006);

[232] G. M. Williams, B. M. Wright, W. D. Mack, E. J. Friebele, "Projecting the performance of erbium-doped fiber devices in a space radiation environment", Proc. SPIE 3848, Optical Fiber Reliability and Testing, 1999.

[233] L. Mescia ; P. Bia ; S. Girard ; A. Ladaci ; M. A. Chiapperino ; T. Robin ; A. Laurent ; B. Cadier ; M. Boutillier; Y. Ouerdane, A. Boukenter, "Temperature dependent modelling of cladding–pumped Er3+/Yb3+-codoped fiber amplifiers for space applications", IEEE Journal of Lightwave Technology, in press, 2018 (DOI: 10.1109/JLT.2018.2841799).

[234] E. J. Friebele and D. L. Griscom, "Radiation effects in glass," inTreatise on Materials Science and Technology, M. T. Doremus, Ed. New York: Academic, 1979

[235] R. A. B. Devine, "On the physical models of annealing of radiation induced defects in amorphous SiO_2," Nucl Instrum. Meth. Phys. Res.B, vol. 46, no. 1–4, pp. 261–264, 1990

[236] D. T. H. Liu and A. R. Johnston, "Theory of radiation-induced absorption in opticalfibers,"Opt. Lett., vol. 19, no. 8, pp. 548–550, 1994

[237] M. Kyoto, Y. Chigusa, M. Ohe, H. Go, M. Watanabe, T. Matsubara, T. Yamamoto, and S. Okamoto, "Gamma-Ray radiation hardened properties of Pure silica core single-modefiber and its data link system in radioactive environments," J. Lightw. Technol., vol. 10, no. 3, pp.289–294, 1992.

[238] P. W. Levy, "Overview of nuclear radiation damage processes phenomenological features of radiation damage in crystals and glasses,"Proc. SPIE, vol. 541, pp. 2–24, 1985

[239] O. Gilard, J. Thomas, L. Troussellier, M. Myara, P. Signoret, E. Burov, and M. Sotom, "Theoretical explanation of enhanced low dose rate sensitivity in erbium-doped opticalfibers,"Appl. Opt., vol. 51, no. 13, pp.2230–2235, 2012.

[240] E. J. Friebele, M. E. Gingerich, and D. L. Griscom, "Survivability of opticalfibers in space," in Proc. SPIE, 1992, vol. 1791, pp. 177–188.

[241] S. A. Vasiliev, E. M. Dianov, K. M. Golant, O. I. Medvedkov, A. L. Tomashuk, V. I. Karpov, M. V. Grekov, A. S. Kurkov, B. Leconte, and P.Niay, "Performance of Bragg and long-period gratings written in N- and Ge-doped silica fibers under γ-radiation", IEEE Trans. Nucl. Sci., vol. 45, no. 3, pp. 1580-1583, June 1998.

[242] P. Niay, P. Bernage, M. Douay, F. Fertein, F. Lahoreau, J. F. Bayon, T. Georges, M. Monerie, P. Ferdinand, S. Rougeault, and P. Cetier, "Behavior of Bragg gratings, written in germanosilicate fibers, against γ ray exposure at low dose rate", IEEE Photon. Technol. Lett., vol. 6, no. 11, pp. 1350-1352, Nov. 1994.

[243] A. I. Gusarov, and S. K. Hoeffgen, "Radiation Effects on Fiber Gratings", IEEE Trans. Nucl. Sci., vol. 60, no. 3, pp. 2037-2053, 2013.

[244] A.I. Gusarov, B. Brichard and D.N. Nikogosyan, "Gamma-radiation effects on Bragg gratings written by femtosecond UV laser in Ge-doped fibers", IEEE Transactions on Nuclear Science, 57 (4), pp. 2024-2028, 2010.

[245] A.I. Gusarov, and D.B. Doyle, "Modeling of gamma-radiation impact on transmission characteristics of optical glasses", Proc. SPIE 4547, Photonics for Space and Radiation Environment II, Toulouse, France, pp. 78-85, 2001.

[246] S. Lin, N. Song, J. Jin, X. Wang and G. Yang, "Effect of grating fabrication on radiation sensitivity of fiber Bragg gratings in gamma radiation field", IEEE Transactions on Nuclear Science, 58 (4), pp. 2111-2117 (2011).

* Corresponding author: Sylvain Girard, sylvain.girard@univ-st-etienne.fr : Phone: +33 (0)477 915 812

[247] A.I. Gusarov, F. Berghmans, A. Fernandez Fernandez, O. Deparis, Y. Defosse, D.Starodubov, M. Décreton, P. Mégret and M. Blondel, "Behavior of fibre Bragg gratings under high total dose gamma radiation", IEEE Transactions on Nuclear Science, 47 (3), pp. 688-692, 2000.

[248] A. Fernandez Fernandez, B. Brichard, F. Berghmans and M. Décreton, « Dose-rate dependencies in gamma-irradiated fiber Bragg grating filters", IEEE Transactions on Nuclear Science, 49 (6), pp. 2874-2877, 2002.

[249] A. Morana ; S. Girard; E. Marin ; M. Lancry ; J. Grelin ; C. Marcandella ; P. Paillet ; A. Boukenter ; Y. Ouerdane., "Dependence of the voids-fiber Bragg grating radiation response on temperature, dose and dose-rate," in IEEE Transactions on Nuclear Science, Early Access doi: 10.1109/TNS.2017.2778882

[250] H. Henschel, S.K. Hoeffgen, J. Kuhnhenn and U. Weinand, "Influence of manufacturing parameters and temperature on the radiation sensitivity of fiber Bragg gratings", IEEE Transactions on Nuclear Science, 57 (4), pp. 2029-2034, 2010.

[251] A. Faustov, P. Safari, C. Koutsides, A. Gusarov, M. Wuilpart, P. Mégret, K. Kalli and L. Zhang, "Highly radiation sensitive type IA FBGs for future dosimetry applications", IEEE Transactions on Nuclear Science, 59 (4), pp. 1180-1185, 2012.

[252] D. Di Francesca ; G. Li Vecchi ; S. Girard; A. Alessi ; I. Reghioua ; A. Boukenter ; Y. Ouerdane ; Y. Kadi ; M. Brugger "Radiation Induced Attenuation in Single-Mode Phosphosilicate Optical Fibers for Radiation Detection," in IEEE Transactions on Nuclear Science, Early Access doi: 10.1109/TNS.2017.2778314.

[253] F. B. H. Jensen, E. Takada, M. Nakazawa, T. Kakuta and S. Yamamoto, "Consequences of radiation effects on pure-silica-core optical fibers used for Raman-scattering-based temperature measurements," in IEEE Transactions on Nuclear Science, vol. 45, no. 1, pp. 50-58, Feb 1998.

[254] C. Cangialosi, S. Girard, A. Boukenter, M. Cannas, S. Delepine-Lesoille, J. Bertrand, P. Paillet, and Y. Ouerdane." Effects of Radiation and Hydrogen-Loading on the Performances of Raman Distributed Temperature Fiber Sensors", IEEE/OSA Journal of Lightwave Technology, vol.33, n°12, pp. 2432-2438, 2015.

[255] C. Cangialosi, S. Girard, M. Cannas, A. Boukenter, E. Marin, S. Agnello, S. Delepine-Lesoille, C. Marcandella, P. Paillet, and Y. Ouerdane, "On-line Characterization of Gamma Radiation Effects on Single-Ended Raman Based Distributed Fiber Optic Sensor", IEEE Transactions on Nuclear Science, vol.63 (4), pp. 2051 - 2057, 2016.

[256] P. Lecomte, "Mesure haute température en environnement irradié par fibre optique utilisant l'effet Raman", Thèse de Doctorat, Université de Perpignan via Domitia, 2017.

[257] D. Alasia, A. F. Fernandez, L. Abrardi, B. Brichard, and L. Thévenaz, "The effects of gamma-radiation on the properties of Brillouin scattering in standard Ge-doped optical fibres," Meas. Sci. Technol. 17(5), 1091–1094, 2006.

[258] X. Phéron, S. Girard, A. Boukenter, B. Brichard, S. Delepine-Lesoille, J. Bertrand, and Y. Ouerdane, "High γ-ray dose radiation effects on the performances of Brillouin scattering based optical fiber sensors," Opt. Express 20, 26978-26985, 2012.

[259] Alexey Faustov, "Advanced fibre optics temperature and radiation sensing in harsh environments", PhD Thesis, University of Mons, Belgium, 2014.

[260] S. Rizzolo, A. Boukenter, E. Marin, M. Cannas, J. Perisse, S. Bauer, J-R. Macé, Y. Ouerdane, S. Girard, "Vulnerability of OFDR-based distributed sensors to high γ-ray doses", Optics Express, 23 (15), pp.18997-19009, 2015.

[261] S. Rizzolo, E. Marin, M. Cannas, A. Boukenter, Y. Ouerdane, J. Perisse, J-R. Macé, S. Bauer, S. Girard, "Radiation Effects on Optical Frequency Domain Reflectometry fiber-based Sensor", Optics Letters, vol.40 (20), pp.4571-4574, 2015.

[262] S. Rizzolo, E. Marin, A. Boukenter, Y. Ouerdane, M. Cannas, J. Périsse, S. Bauer, J-R. Macé, C. Marcandella, P. Paillet, and S. Girard, "Radiation Hardened Optical Frequency Domain Reflectometry Distributed Temperature Fiber-based sensors", IEEE Transactions on Nuclear Science, vol.62 (6), pp. 2988 - 2994, 2015.

[263] A. Faustov, A. Gusarov, P. Mégret, M. Wuilpart, Zhukov A., S.G. Novikov, V.V. Svetuhin, A. A. Fotiadi, 'The Use of Optical Frequency-Domain Reflectometry in Remote Distributed Measurements of the Gamma-Radiation Dose', Technical Physics Letters, vol. 41, n. 5, pp. 412-415, 2015.

[264] A. Faustov, A. Gusarov, P. Mégret, M. Wuilpart, Zhukov A., S.G. Novikov, V.V. Svetuhin, A. A. Fotiadi, 'Application of phosphate doped fibers for OFDR dosimetry', Results in Physics, vol. 6, pp. 86-87, 2016.

[265] M. A. S. Zaghloul, A. Yan, R. Chen, M.-J. Li ; R. Flammang, M. Heibel, and K. P. Chen, "High Spatial Resolution Radiation Detection Using Distributed Fiber Sensing Technique," in *IEEE Transactions on Nuclear Science*, vol. 64, no. 9, pp. 2569-2577, 2017.

[266] H. Henschel, M. Körfer, K. Wittenburg, F. Wulf, "Fiber Optic Radiation Sensing Systems for TESLA", TESLA Report No. 2000-26, September 2000.

[267] I. Toccafondo, Y.E. Marin, E. Guillermain, J. Kuhnhenn, J. Mekki, M. Brugger, and F. Di Pasquale, "Distributed Optical Fiber Radiation Sensing in a Mixed-Field Radiation Environment at CERN," J. Lightwave Technol. 35, 3303-3310, 2017.

[268] S. Rizzolo, A. Boukenter, T. Allanche, J. Périsse, G. Bouwmans, H. El Hamzaoui, L. Bigot, Y. Ourdane, M. Cannas, M. Bouazaoui, J-R Macé, S. Bauer and S. Girard, "Optical Frequency Domain Reflectometer Distributed Sensing Using Microstructured Pure Silica Optical Fibers under Radiations", IEEE Transactions on Nuclear Science , vol.63 (4), pp. 2038 - 2045, 2016.

[269] S. Rizzolo, J. Périsse, A. Boukenter, Y. Ourdane, E. Marin, J-R. Macé, M. Cannas and S. Girard, "Real time monitoring of water level and temperature in storage fuel pools through optical fibre sensors", Scientific Reports 7, Article number: 8766, 2017.

[270] G.M. Williams,M. A. Putnam, C.G. Askins,M. E. Gingerich, and E. J. Friebele, "Radiation effects in erbium-doped optical fibres," Electron. Lett., vol. 28, no. 19, pp. 1816–1818, 1992.

[271] S. Girard, Y. Ourdane, B. Tortech, C. Marcandella, T. Robin, B. Cadier, J. Baggio, P. Paillet, V. Ferlet-Cavrois, A. Boukenter, J.-P. Meunier, J. R. Schwank, M. R. Shaneyfelt, P. E. Dodd, and E.W. Blackmore, "Radiation effects on Ytterbium-and Ytterbium/Erbium-doped double-clad optical fibers," IEEE Trans. Nucl. Sci., vol.56, no. 6, pp. 3293–3299, Dec. 2009.

[272] B. P. Fox, K. Simmons-Potter, W. J. Thomes, and D. A. V. Kliner, "Gamma-radiation-induced photodarkening in unpumped optical fibers doped with rare-earth constituents," IEEE Trans. Nucl. Sci., vol.57, no. 3, pp. 1618–1625, Jun. 2010.

[273] S. Girard, B. Tortech, E. Regnier,M.Van Uffelen, A. Gusarov, Y. Ourdane, J. Baggio, P. Paillet, V. Ferlet-Cavrois, A. Boukenter, J.-P.Meunier, F. Berghmans, J. R. Schwank,M. R. Shaneyfelt, J. A. Felix, E. W. Blackmore, and H. Thienpont, "Proton- and gamma-induced effects on erbium- doped optical fibers," IEEE Trans. Nucl. Sci., vol. 54, no. 6,pp. 2426–2434, Dec. 2007.

[274] G. M. Williams and E. J. Friebele, "Space radiation effects on erbium doped fiber devices: Sources, amplifiers, and passive measurements," IEEE Trans. Nucl. Sci., vol. 45, no. 3, pp. 1531–1536, 1998.

[275] M. Ott, Radiation effects expected for fiber laser/amplifier and rare earth-doped optical fibers, 2004, NASA GSFC , Parts, Packaging and Assembly Technologies Office Survey Report.

[276] Y. Xing, N. Zhao, L. Liao, Y. Wang, H. Li, J. Peng, L. Yang, N. Dai, and J. Li, "Active radiation hardening of Tm-doped silica fiber based on pump bleaching," Opt. Express 23, 24236-24245, 2015.

[277] A. Gusarov, M. Van Uffelen, M. Hotoleanu, H. Thienpont, and F. Berghmans, "Radiation sensitivity of EDFAs based on highly Er-doped fibers," J. Lightw. Technol., vol. 27, no. 11, pp. 1540–1545, 2009.

[278] J. Ma, M. Li, L. Tan, Y. Zhou, S. Yu, and Q. Ran, "Experimental investigation of radiation effect on erbium-ytterbium co-doped fiber amplifier for space optical communication in low-dose radiation environment," Opt. Exp., vol. 17, no. 18, pp. 15571–15577, 2009.

[279] T. S. Rose, D. Gunn, and G. C. Valley, "Gamma and proton radiation effects in erbium-doped fiber amplifiers: Active and passive measurements," J. Lightw.Technol., vol. 19, no. 12, pp. 1918–1923, 2001.

[280] M. Li, J. Ma, L. Y. Tan, Y. P. Zhou, S. Y. Yu, J. J. Yu, and C. Che, "Investigation of the irradiation effect on erbium-doped fiber amplifiers composed by different density erbium-doped fibers," Laser Phys., vol.19, no. 1, pp. 138–142, 2009.

[281] B. J. Ainslie, "A review of the fabrication and properties of erbium-doped fibers for optical amplifiers," in Journal of Lightwave Technology, vol. 9, no. 2, pp. 220-227, Feb 1991.

* Corresponding author: Sylvain Girard, sylvain.girard@univ-st-etienne.fr : Phone: +33 (0)477 915 812

[282] D. L. Griscom, E. J. Friebele and K. J. Long, "Fundamental defect centers in glass: Electron spin resonance and optical absorption studies of irradiated phosphorus-doped silica glass and optical fibers", J. Appl. Phys., vol. 54, pp. 3743-3762, 1983

[283] T. Deschamps, H. Vezin, C. Gonnet, and N. Ollier, "Evidence of AlOHC responsible for the radiation-induced darkening in Yb doped fiber," Opt. Express 21, 8382-8392, 2013.

[284] V. Pukhkaya, P. Goldner, A.Ferrier, and N. Ollier, "Impact of rare earth element clusters on the excited state lifetime evolution under irradiation in oxide glasses," Opt. Express 23, 3270-3281, 2015.

[285] A. Ladaci, S. Girard, L. Mescia, T. Robin, A. Laurent, B. Cadier, M. Boutillier, A. Morana, D.Di Francesca, Y. Ouerdane, A. Boukenter "X-rays, γ-rays, electrons and protons radiation-induced changes on the lifetimes of Er^{3+} and Yb^{3+} ions in silica-based optical fibers", In Journal of Luminescence, 2017, ISSN 0022-2313, https://doi.org/10.1016/j.jlumin.2017.11.061.

[286] K. V. Zotov, M. E. Likhachev ; A. L. Tomashuk ; A. F. Kosolapov ; M. M. Bubnov ; M. V. Yashkov ; A. N. Guryanov and E. M. Dianov, "Radiation Resistant Er-Doped Fibers: Optimization of Pump Wavelength," in IEEE Photonics Technology Letters, vol. 20, no. 17, pp. 1476-1478, 2008.

[287] A. Gusarov, M. V. Uffelen, M. Hotoleanu, M. Thienpont, and F. Berghmans, "Radiation sensitivity of EDFAs based on highly Er-doped fibers," IEEE Journal of Lightwave Technology, vol. 27, no. 11, pp. 1540–1545, 2009.

[288] R. Dardaillon, J. Thomas, M. Myara ; S. Blin ; A. Pastouret ; C. Gonnet ; P. Signoret "Broadband Radiation-Resistant Erbium-Doped Optical Fibers for Space Applications," in IEEE Transactions on Nuclear *Science*, vol. 64, no. 6, pp. 1540-1548, 2017.

[289] J-B. Duchez, F. Mady, Y. Mebrouk, N. Ollier, and M. Benabdesselam, "Interplay between photo- and radiation-induced darkening in ytterbium-doped fibers," Opt. Lett., vol. 39, pp. 5969-5972, 2014.

[290] A. Johnston, "Radiations Effect in Light-Emitting and Laser Diodes", IEEE Transaction on Nuclear Science, Vol 50, No 3, 2003.

[291] T. Buret, "Fibre Optic Gyroscopes for Space Application", OFS Proceedings (2006)

[292] W.J Thomes, "Investigation of hermetically sealed commercial $LiNbO_3$ optical modulator for use in laser/LIDAR space-flight applications", Proc. SPIE 6713, Nanophotonics and Macrophotonics for Space Environments, 67130T, 2007.

[293] E.W. Taylor, "Radiation effects in $LiNbO_3$", Properties of Lithium Niobate, K.K. Wong, 359-371, INSPEC, London, 2002.

[294] H. Henschel, O. Kohn, and H. Schmidt, "Radiation sensitivity of fiber optic couplers," Proc. SPIE, vol. 1791, pp. 151–163, 1992

[295] R. Gutierez, G. Swift, S. Dubovitsky, R. Bartman, C. Barnes, and L.Dorsky, "Radiation effects on fused biconical paper wavelength division multiplexer," IEEE Trans. Nucl. Sci. , vol. 41, pp. 1950–1957, 1994

[296] B. Brichard, A. Fernandez Fernandez,H. Ooms, F. Berghmans, M. Decréton, A.Tomashuk, S. Klyamkin, M. Zabezhailov, I.Nikolin, V. Bogatyrjov, E. Hodgson, T.Kakuta, T. Shikama, T. Nishitani, ACostley, G.Vayakis, "Radiation-hardening techniques of dedicated optical fibres used in plasma diagnostic systems in ITER", Journal of Nuclear Materials, vol. 329–333, Part B, pp. 1456-1460, 2004.

[297] I.A. Alvanov, S.N. Tugarinov, Yu.A. Kaschuck, A.V. Krasilnikov, S.E. Bender, "In situ radiation testing of KU and KS-4V optical fibers in a reactor environment", Fusion Engineering and Design, vol. 51–52, pp. 973-978, 2000.

[298] T. Shikama, T. Kakuta, N. Shamoto,M. Narui, T.Sagawa, "Behavior of developed radiation-resistant silica-core optical fibers under fission reactor irradiation", Fusion Engineering and Design, vol. 51–52, pp. 179-183, 2000.

[299] S. P. Faile, J. J. Schmidt, and D. M. Roy, "Irradiation effects in glasses: Suppression by synthesis under high pressure hydrogen," Science, vol.156, pp. 1593–1595, 1967.

[300] J. E. Shelby, "Radiation effects in hydrogen impregnated vitreous silica,"J. Appl. Phys., vol. 50, no. 5, pp. 3702–3706, 1979.

[301] B. Brichard, A.L. Tomashuk, H. Ooms, V.A. Bogatyrjov, S.N. Klyamkin, A. F. Fernandez, F. Berghmans, and M. Decréton, "Radiation assessment of hydrogen-loaded aluminum-coated pure silica core fibres for ITER plasma diagnostic applications," Fusion Eng. Des.,vol. 82, pp. 2451–2455, 2007.

* Corresponding author: Sylvain Girard, sylvain.girard@univ-st-etienne.fr : Phone: +33 (0)477 915 812

[302] D. Di Francesca, S. Agnello, S. Girard, C. Marcandella, P. Paillet, A. Boukenter, Y. Ouerdane, F.M. Gelardi, "Influence of O_2 loading pre-treatment on the radiation response of pure and fluorine doped silica-based optical fibers", IEEE Transactions on Nuclear Science, vol.61 (6), pp. 3302-3308, 2014.

[303] D. Grobnic, H. Henschel, S.K. Hoeffgen, J. Kuhnhenn, S.J. Mihailov and U. Weinand, "Radiation sensitivity of Bragg gratings written with femtosecond IR lasers", Fiber Optic Sensors and Application VI, Orlando (US), E. Udd, H.H. Du and A. Wang Eds., Proc. SPIE 7316, pp. 7316-11, 2009.

[304] AREVA and Laboratoire Hubert Curien, "Procédé de fabrication d'une fibre optique traitée pour capteur de température résistant aux radiations;" France Brevet 13 62691, 16 December 2013.

[305] A. Morana, S. Girard, E. Marin, J. Périsse, J.S. Genot, J. Kuhnhenn, J. Grelin, L Hutter, G. Mélin, L. Lablonde, T. Robin, B. Cadier, J.-R. Macé, A. Boukenter, and Y. Ouerdane, "Radiation-Hardened Fiber Bragg Grating Based Sensors for Harsh Environments," IEEE Transactions on Nuclear Science, 64 (1), pp. 68-73, 2016.

[306] J. Kuhnhenn, U. Weinand, A. Morana, S. Girard, E. Marin, J. Périsse, J.S. Genot, J. Grelin, L Hutter, G. Mélin, L. Lablonde, T. Robin, B. Cadier, J.-R. Macé, A. Boukenter, and Y. Ouerdane, "Gamma Radiation Tests of Radiation-Hardened Fiber Bragg Grating Based Sensors for Radiation Environments," IEEE Transactions on Nuclear Science, 64 (8), pp. 2307-2311, 2017.

[307] A. Morana, S. Girard, E. Marin, M. Trinczek, C. Hoehr, E. Blackmore, J. Périsse, P. Paillet, C. Marcandella, O. Duhamel, L. Lablonde, J.-R. Macé, A. Boukenter and Y. Ouerdane, "Radiation-hardened fiber Bragg gratings for space Missions," Photonics and Fiber Technology 2016 (ACOFT, BGPP, NP) OSA 2016, paper JT4A.25, 2016.

[308] M. Ams, A. Pal, R. J. Williams, R. Sen, M. J. Withford, T. Sun and K. T. V. Grattan, "Fibre Bragg grating sensors for radiation insensitive measurements," OECC/ACOFT 2014, Melbourne (Australia), 2014.

[309] R. Evenblij, J.A.P. Leijtens, " Space gator: a giant leap for fiber sensing", presented at International Conference on Space Optics, ICSO 2014, 7 -10 October 2014, Tenerife, Spain.

[310] Serena Rizzolo, "Advantages and Limitations of Distributed Optical Frequency-Domain-Reflectometry for Optical Fiber based Sensors in Harsh Environments", PhD Dissertation, Université de Saint-Etienne, Saint-Etienne,2016.

[311] FBGS website: http://www.fbgs.com/

[312] A. Morana; I. Planes; S. Girard; C. Cangialosi; S. Delepine-Lesoille; E. Marin; A. Boukenter; Y. Ouerdane, "Steady-State Radiation-Induced Effects on the performances of BOTDA and BOTDR Optical Fiber Sensors", IEEE Transactions on Nuclear Science, in press, 2017 (DOI: 10.1109/TNS.2017.2772333).

[313] D. Di Francesca, S. Girard, I. Planes, A. Cebollada, G. Li Vecchi, A. Alessi, I. Reghioua, C. Cangialosi, A. Ladaci, S. Rizzolo, V. Lecoeuche, A. Boukenter, A. Champavère, Y. Ouerdane, "Radiation Hardened Architecture of a Single-Ended Raman-based Distributed Temperature Sensor", IEEE Transactions on Nuclear Science, vol.64, n°1, pp. 54 – 60, 2017.

[314] S. Girard, A. Laurent, E. Pinsard, M. Raine, T. Robin, B. Cadier, D. Di Francesca, P. Paillet, M. Gaillardin, O. Duhamel, C. Marcandella, M. Boutillier, A. Ladaci, A. Boukenter and Y. Ouerdane, "Proton irradiation response of Hole-Assisted Carbon Coated Erbium-Doped Fiber Amplifiers", IEEE Transactions on Nuclear Science, vol.61 (6), pp. 3309-3315, 2014.

[315] S. Girard, M. Vivona, A. Laurent, B. Cadier, C. Marcandella, T. Robin, E. Pinsard, A. Boukenter, and Y. Ouerdane, "Radiation hardening techniques for Er/Yb doped optical fibers and amplifiers for space application," Opt. Express 20, 8457-8465, 2012.

[316] J. Thomas, M. Myara, L. Troussellier, E. Burov, A. Pastouret, Da. Boivin, G. Mélin, O. Gilard, M. Sotom, and P. Signoret, "Radiation-resistant erbium-doped-nanoparticles optical fiber for space applications," Opt. Express 20, 2435-2444, 2012.

[317] A. Pastouret, C. Gonnet, and E. Burov, "Amplifying optical fiber and production method," (2010). Patent US 2010135627

[318] D. Boivin, T. Fohn, E. Burov, A. Pastouret, C. Gonnet, O. Cavani, C. Collet, and S. Lempereur, "Quenching investigation on new erbium doped fibers using MCVD nanoparticle doping process," in Proc. SPIE , 7580 , 75802B–1, 2010.

* Corresponding author: Sylvain Girard, sylvain.girard@univ-st-etienne.fr : Phone: +33 (0)477 915 812

88

[319] S. Girard, A. Laurent, E. Pinsard, T. Robin, B. Cadier, M. Boutillier, C. Marcandella, A. Boukenter, and Y. Ouerdane, "Radiation-hard erbium optical fiber and fiber amplifier for both low- and high-dose space missions", Opt. Lett. 39(9) 2541-2544, 2014.

[320] Benoit Cadier, Arnaud Laurent, Thierry Robin, Sylvain Girard, Claude Marcandella, Radiation-resistant rare-earth-doped optical fiber and method of radiation-hardening a rare-earth-doped optical fiber US Patent 20130101261 A1, 2013.

[321] M. Vivona, S. Girard, T. Robin, B. Cadier, L. Vaccaro, M. Cannas, A. Boukenter, and Y. Ouerdane, "Influence of Ce3+ codoping on the photoluminescence excitation channels of phosphosilicate Er/Yb doped glasses," IEEE Photonics Technology Letters (Volume: 24, Issue: 6, March15, 2012.

[322] J. S. Stroud, "Color-Center Kinetics in Cerium-Containing Glass," J. Chem. Phys. 43(7), 2442–2450, 1965.

[323] J. S. Stroud, "Color Centers in a Cerium-Containing Silicate Glass," J. Chem. Phys. 37(4), 836–841, 1962.

[324] K V Zotov, M E Likhachev, A L Tomashuk, M M Bubnov, M V Yashkov and A N Gur'yanov, "Radiation-resistant erbium-doped silica fibre", Quantum Electronics, Volume 37, Number 10, pp.946-949, 2007.

[325] Saeed Rehman, and Lars Norin "Specialty optical fibers for harsh environments", Photonics Spectra, October issue, 2010.

[326] E. Pinsard, A. Laurent, T. Robin, B. Cadier, S. Ferrand, J-J. Bonnefois, C. Moluçon and M. Boutillier, Radiation Resistant Erbium Doped Fiber for ASE Source and Fiber Gyroscope Application, 9th International Conference on Space Optics (ICSO), Ajaccio, France, 2012.

[327] D. Di Francesca, S. Girard ; S. Agnello ; A. Alessi ; C. Marcandella ; P. Paillet ; N. Richard ; A. Boukenter ; Y. Ouerdane and F. Gelardi; "Radiation Response of Ce-Codoped Germanosilicate and Phosphosilicate Optical Fibers", IEEE Transaction on Nuclear Vol 63, issue 4, 2016.

[328] A. Paveau, G. Cros, R. Mangeret, S. Mariojouls, JJ. Bonnefois, "Robustness of Astrix Fiber optic gyros in space radiative environment", Proceedings of American Astronautical Society 2017 Guidance Navigation and Control conference, Breckenridge, AAS-17-111

[329] N. Richard, S. Girard, L. Giacomazzi, L. Martin-Samos, D. Di Francesca, C. Marcandella, A. Alessi, P. Paillet, S. Agnello, A. Boukenter, Y. Ouerdane, M. Cannas, and R. Boscaino, « Coupled theoretical and experimental studies for the radiation hardening of silica-based optical fibers", IEEE Transactions on Nuclear Science, vol.61(4), pp 1819 - 1825, 2014.